Technische Universität München
TUM School of Engineering and Design

Energy-Based Numerical Models for Simulation and Control of Flexible Mechanical Systems

Tobias Elmar Thoma

Vollständiger Abdruck der von der TUM School of Engineering and Design der Technischen Universität München zur Erlangung des akademischen Grades eines

Doktors der Ingenieurwissenschaften (Dr.-Ing.)

genehmigten Dissertation.

Vorsitz:		Prof. Dr. ir. Daniel J. Rixen
Prüfer der Dissertation:	1.	Prof. Dr.-Ing. habil. Paul Kotyczka
	2.	Prof. Dr.-Ing. habil. Peter Betsch

Die Dissertation wurde am 26.09.2025 bei der Technischen Universität München eingereicht und durch die TUM School of Engineering and Design am 22.01.2026 angenommen.

To my family.

Abstract

Increasing efficiency of mechatronic devices is often achieved through lightweight design using flexible mechanical structures like beams, strings, plates, and so on. The gain in flexibility usually requires a more complex modeling procedure often relying on the theory of nonlinear continuum mechanics. In addition, due to the limited number of actuators, these flexible structures are highly underactuated, which makes their analysis and control design challenging. In this thesis, we focus on numerical methods for efficient simulations and control designs of flexible mechanical systems.

Therefore, we discuss port- and energy-based formulations, which are favorable for modular and structured modeling of large-scale interconnected and coupled multi-physics phenomena. The port-Hamiltonian approach emphasizes the interconnection or energy exchange mechanisms and the interactions of subsystems through their (boundary) ports, i.e., interfaces of dual power variables. Numerical methods that conserve important geometric properties are well-known in their corresponding engineering disciplines, e.g., mixed finite elements for velocity-stress formulations of nonlinear elastodynamics. For example, we considered geometrically exact strings, and the general setting of geometrically nonlinear continua from the perspective of boundary control systems, their structure-preserving discretization in space and time, retaining the underlying port-Hamiltonian structure.

In addition to numerical advantages, energy-based formulations might lead to intuitive feed-back controller designs. Moreover, structure-preserving higher order time integration schemes can be used to generate discrete-time control systems covering the sampling process in a digital control loop. This reduces the increasing mismatch at low sampling rates between the underlying model and a time-continuous model (neglecting the sampling process) leading to deteriorating effects in a digital control loop. Since in a modern control structure, the feed-back controller is usually supported by a feed-forward part, this thesis also includes an optimal trajectory feed-forward controller for geometrically exact strings.

All concepts applied in this thesis are application-oriented approaches enabling practicable implementation using common software packages.

Acknowledgments

First of all, I would like to express my deepest gratitude to Prof. Dr.-Ing. habil. Paul Kotyczka for his professional and personal guidance, as well as for the encouragement and opportunities he has given me. I would also like to thank Prof. Dr.-Ing. habil. Boris Lohmann for making this thesis possible and for always ensuring a great working environment at the chair of automatic control. In addition, I want to thank Prof. Dr.-Ing. habil. Peter Betsch for the successful collaboration and his participation in the examination board. I also thank Prof. Dr. ir. Daniel Rixen for his mentorship and for serving as a chairman of the examination committee. I gratefully appreciate the support by the DFH-UFA French-German doctoral college "Port-Hamiltonian Systems: Modeling, Numerics and Control".

I want to thank Philipp Lothar Kinon for a fruitful cooperation and inspiring discussions. I also want to thank all my former colleges for filling my time at the chair of automatic control with moments of joy and friendship. I am grateful to Raphael Weber, Maximilian Mogler, Maximilian Herrmann, and Philipp Lothar Kinon for proofreading this thesis.

Last but not least, I would like to thank my loving family and friends for their support and encouragement. I am deeply grateful to my parents for giving me the opportunity and love to follow this path and write this thesis. And dear Franziska, thank you for being by my side and believing in me. Without your loving support I would not have been able to undertake this journey and those that will follow.

Munich, March 14, 2026
Tobias Thoma

Contents

1 Introduction

1.1 Motivation and context

The term *simulation* comes from the Latin word *simulatio*, which means "deception" or "hypocrisy". For example, Cicero used the word to describe Odysseus' ruse of pretending to be a madman to avoid having to take part in the Trojan War [144]. Accordingly, the word had a negative meaning and described something morally reprehensible. The current use of the word simulation is much more positive and has only developed in the 20th century. Nowadays, the term is associated with Latin words such as *simulacrum* in the sense of "imitation" or the verb *simulo* meaning "to reproduce". These translations indicate that a simulation is used to create something based on something that already exists [143]. However, more often, simulation denotes a method of predicting future results by approximating real-world systems, processes or events. Accordingly, the core of a simulation is to provide a model, which reflects the relevant characteristics of an original system.

Before the computer age, we speak of traditional simulation technologies, which refer to the use of mathematical models and analytical tools to compute the behavior or evolution of systems [100]. For example, solving Lancester's ordinary differential equations represents a military application, where the attrition of combat troops of two opposing sides is computed [90]. The benefits of traditional simulation methods include the simplicity of models and efficient analytical calculations. Consequently, traditional simulation tools are limited to simple systems. To overcome this, modern simulation technologies go hand in hand with the use of computer models and numerical tools to analyze complex systems and their interactions [100]. In the following, we focus only on computer-aided simulations, whose origin can be traced back to World War II. In the 1940s, during the Manhatten project, Monte-Carlo simulations were carried out for the development of nuclear weapons [134]. Naturally, the U.S. Department of Defense recognized the potential of military simulations and established the Defense Modeling and Simulation Office in 1991 [154]. However, simulations are not only used for military purposes. Nowadays, simulations are often used as a tool for the development of a wide variety of products. E.g., market research companies use agent-based simulation soft-

ware to analyze consumer behavior and to predict market responses [59]. Simulation models are also increasingly being used in medicine, for example to analyze aneurysms [58] or stent implantation [47]. In the engineering sector, simulations represent a cost saving option to verify the function or performance of technical systems. For example, finite element simulations play a key role in the development of aircraft, automobiles, buildings, machine tools, etc., where engineers often use the finite element method for thermal, structural and vibration analyses [98]. Another common engineering tool is a multi-body simulation, which is heavily applied in the field of robotics [151].

As the above engineering examples show, modern technical products are mostly mechatronic systems. Mechatronics is a combination of mechanics, electrics and informatics and, in conjunction with sensors and actuators for control, represents a fundamental interdisciplinary engineering science [46]. Figure 1.1 provides an overview of the principle of mechatronic systems. Although this cross-domain combination of different disciplines increases the performance of technical systems, it also requires large scale, multi-domain simulation models, which are still the subject of active research [100].

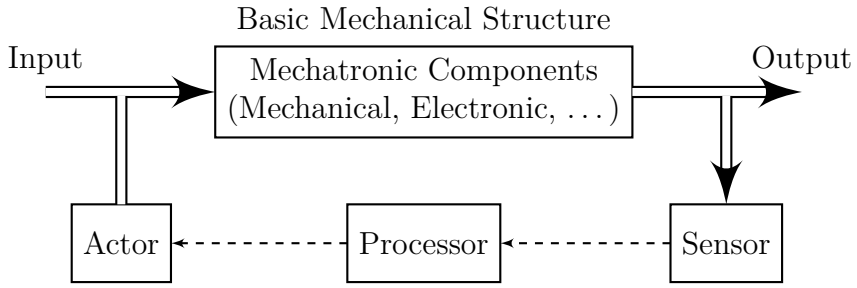

Figure 1.1: Principle of a mechatronic system. It has an underlying basic mechanical structure interconnected with mechanical, electronic, magnetic, thermal, optical and other functional components. Sensors determine functionally relevant measured variables and feed them to processors. The processors generate control input variables for the actuators, thus ensuring the functionality of the system [46] (image mainly reproduced from [46]).

It is to be highlighted that this thesis focuses on the mechanical components of a technical system and the corresponding control design. Since increasing efficiency of mechatronic devices is often achieved through a lightweight design, mechanical structures like beams, strings, plates become more flexible [164]. Accordingly, nonlinear phenomena occur due to geometrical changes, material behavior or external conditions. This leads to a more complex modeling procedure often relying on the theory of nonlinear continuum mechanics. Due to the limited number of actuators, the considered

systems are highly underactuated, which makes their analysis and control design challenging. In this work, we focus on efficient simulation and control methods to overcome the challenges associated with this system class.

1.2 Literature review

A brief literature review of the topics considered in this thesis is given here. This literature review mainly repeats and extends the literature reviews from [A3, A2, A5, A1, A4]. Throughout the chapters, some articles might be referenced again.

1.2.1 Velocity-stress formulation and its finite element approximation

Models of elastodynamics are extensively used in structural analysis and engineering design, which has motivated the development of efficient finite element methods for simulation. Starting in 1941 with the birth of the finite element method, Hrennikoff [74] published a paper about solving elasticity problems using a mesh of lattice structure to approximate a computational domain. Two years later, Courant [44] presented a variational method to solve a seconder-order partial differential equation (PDE) based on the Rayleigh-Ritz principle applied to sub-domains. Based on these early concepts several articles of variational formulations and discretization have been published, see [98] for a precise historical overview. Finally, the phrase *finite element method* was first introduced in 1960 by Clough [42]. In the 1960s, Pian [127] used mixed variational formulations, e.g., the Hellinger–Reissner principle [135] with the displacement and stress field as primary unknowns to invent the assumed stress finite element method. Several researchers followed Pian's idea and invented novel mixed finite element formulations, e.g., [69, 78]. Nonetheless, the construction of mixed finite elements is quite delicate and can lead to numerical instability [7]. Babuska and Brezzi analyzed this problem and developed the so-called inf-sup condition, a guide for choosing mixed-finite element spaces [19, 23, 158]. As can be seen from the above literature, the finite element method has its origins in elastostatics, and in the 1970s engineers began to use it for elastodynamic problems as well. Consequently, several time integration methods for structural mechanics have been developed, e.g., the Hilber-Hughes-Taylor method [71].

In 1992, Makridakis [103] investigated mixed finite elements for the *displacement-stress* and *velocity-stress* formulation of linear elastodynamics. The results are partly based on corresponding results for the wave equation [60]. The construction and analysis of variational numerical schemes for time-dependent wave propagation problems

have been heavily discussed in the literature, see [43, 77] for an overview including primal-dual and dual-primal velocity-stress formulations for linear elastodynamics as an example, and stability and energy conservation on the semi- and fully-discrete level. In [14], a new family of mixed finite elements for linear elastodynamics and mass lumping is given. The velocity-stress formulation is also a common tool for seismological simulations [54]. Since the inclusion of the symmetry of the stress tensor into a finite element space is not trivial, Arnold and Lee [8] analyzed mixed finite element methods for linear elastodynamics with weakly imposed symmetry for the stresses. In addition, the velocity-stress formulation is frequently used as a basis for other Galerkin approximations. Another efficient stabilized nodal finite element method based on a space-time variational statement of the velocity-stress formulation was introduced in [146]. The virtual finite element approach for a velocity-stress formulation with weakly imposed symmetry was discussed in [168]. In order to simulate a coupled system of linear thermoelasticity in a power-preserving way, a mixed finite element method based on a port-Hamiltonian formulation was used in [24].

1.2.2 Port-Hamiltonian (PH) systems

The PH formulation provides a general framework for modeling, analysis, and control of complex multi-physical dynamical systems [50]. It originates from the theory of port-based modeling, a formalism for multi-physical systems pioneered by Paynter [124] in 1961. His framework introducing energy as the link between physical domains offered a graphical representation, the so called *bond graph* [61, 140]. In *geometric mechanics* [9], the second origin of the PH framework, the Hamiltonian dynamics are represented in a geometric, coordinate-free way using a symplectic or Poisson structure [142]. Finally, electrical network synthesis theory and some groundbreaking works [45, 106, 137] made PH systems an essential topic of *systems and control theory*.

Since then, the research field of PH systems has grown considerably. E.g., the framework has been used to develop energy-based control design approaches like Interconnection and Damping Assignment Passivity-Based Control (IDA-PBC) [118] and Control by Interconnection (CbI) [120]. Furthermore, PH systems motivated several structure-preserving model order reduction techniques in which a given large-scale PH model is approximated by a PH state space model of smaller dimension [111]. In addition, the past two decades brought important progress in the development of the theory for infinite-dimensional or distributed PH systems. Therefore several PDEs from different physical domains have been rewritten in PH form, including structural mechanics, see

e.g. [76, 96, 102, 138] and the review article [133]. The intrinsic geometrical structure of nonlinear elasticity is discussed in the framework of exterior calculus in [132]. In addition to the theoretical considerations concerning geometrical aspects of PH-models, the structure-preserving numerical approximation has been a major field of interest, too. Therefore, the PH community developed and analyzed several discretization methods preserving the PH character on the semi-discrete level, see [53, 62, 84, 89, A6]. Cardoso-Ribeiro et al. [38, 39] demonstrated the compatibility of mixed finite elements with the PH framework, see also [15, 37, 149, 150] and, in particular, [24, 26–28, 163] for applications in linear elastodynamics. Recent contributions to the modeling and structure-preserving discretization of the nonlinear equations of elastodynamics have been presented in [32, 35, 81]. In order to preserve major characteristics (e.g. stability, passivity, ...) of finite-dimensional systems on the fully-discrete level, symplectic integration [85], discrete gradients [52], Petrov-Galerkin [51], and projection methods [112] have been proposed for the structure-preserving time discretization. These methods were partially combined with the above control design approaches to obtain discrete-time controllers, which are the subject of the next section.

1.2.3 Discrete-time energy-based feed-back control

Energy-based methods are a common tool for the feed-back control design of mechanical systems, see e.g. [117, 119, 139, 156, 167]. Most of these methods including IDA-PBC and CbI were initially introduced to continuous-time systems. Therefore, most of the literature addressing control theory of mechanical systems does not cover the sampling process [2] in a digital control loop. Nevertheless, nowadays, control laws are mainly implemented digitally and deteriorating effects of quasi-continuous control laws (direct implementation) in digital control loops with low sampling rates are well-known [41]. Additionally, large effective stiffness or high dynamic performance also requires high sampling rates [80], which is associated with the use of expensive sensors. In order to circumvent this performance degradation or even destabilization, several discrete-time control methods have been developed [1, 130]. The implementation of a discrete-time control law is based either on a controller design using discrete-time state space models [101, 115] or a continuous-time controller designed using well-known continuous-time control theory methods [73].

In [114], discrete-time feed-back linearizing control laws for robotic manipulators based on the discretization of the action integral are proposed. Discrete-time control algorithms for a thin piezoelectric structure are presented in [21]. Bloch et al. [18]

presented a discrete-time *Controlled Lagrangian* approach using a midpoint approximation of the Lagrangian. The design of nonlinear control under explicit consideration of the sampling process is described in [109] based on series expansions. In [95], separable Hamiltonian systems are controlled by a discrete-time IDA-PBC approach based on the explicit Euler integration scheme. Discrete gradients have also been used for generating discrete-time controllers, see [64], and in particular, Aoues et al. [6] applying a midpoint discrete gradient to IDA-PBC of linear mechanical systems. In [86], a systematic procedure for discrete-time eigenvalue assignment based on the symplectic integration is given. Structure-preserving discretization methods, like variational or symplectic integration, have also been used for optimal control approaches, see [116, 125].

1.2.4 Feed-forward control of complex mechanical systems

So far, we only considered feed-back controllers, whose design might be burdensome for large-scale complex systems, e.g., finite element models. Therefore, a two degree of freedom control structure containing a feed-forward and a feed-back part represents a common strategy to handle such systems, see Figure 1.2 and [110, 162] for recent examples. While an advanced feed-forward part is responsible for highly accurate tracking of a given reference trajectory, a simple feed-back controller reacts to unexpected disturbances.

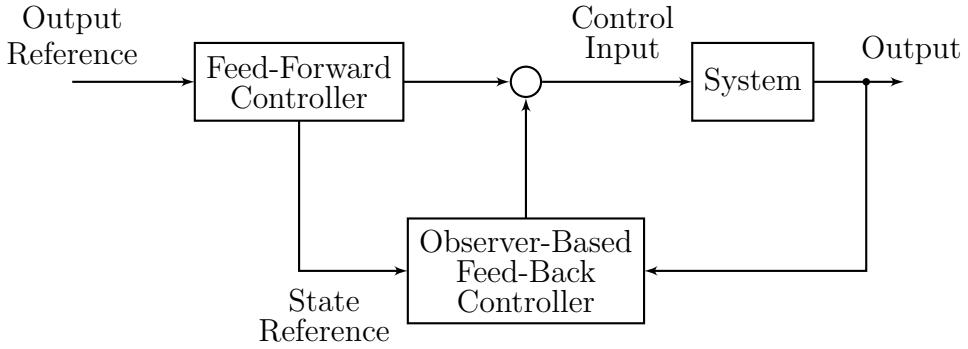

Figure 1.2: Block diagram of a two degree of freedom control structure. In case of a large-scale system or missing sensors an observer-based feed-back controller might be required.

Starting in 1995, Fliess et al. [55] coined the concept of flatness, leading to a new milestone for the feed-forward control design of nonlinear systems. Flat systems offer the possibility of a purely algebraic inversion-based control design [67, 136]. The concept of differential flatness has been extended for infinite-dimensional systems including several

mechanical structures, see [126], and in particular, [83] for a feed-forward control design for a nonlinear string based on the theory of flatness and the method of characteristics. However, the feed-forward control design of non-flat systems is much more difficult and one has to distinguish between minimum and non-minimum phase systems [79]. Due to the internal dynamics of non-minimum phase systems, their inversion usually involves solving a two-point boundary value problem. A stable inversion of nonlinear non-minimum phase systems generating a bounded solution for the system state and the control input is presented in [40], where a desired output trajectory with pre- and post-actuation phases is required. In 2002, Taylor and Li [157] introduced finite difference methods for the stable inversion of nonlinear systems. Graichen et al. [66] modified the boundary value problem, i.e., the output trajectory, to obtain a stable inversion without pre- and post-actuation phases. So far, we only mentioned inversion-based feed-forward control approaches. Alternatively, one can also design an optimal trajectory tracking controller, see [131] for a survey on numerical methods for optimal control.

In 2004, Blajer and Kołodziejczyk [17] introduced the servo-constraint framework forming a set of differential algebraic equations for under-actuated mechanical systems. Their work had a huge influence on the multibody system dynamics community and motivated several research articles [49] focusing either on flat, minimum or non-minimum phase systems. E.g., Otto and Seifried [121] designed a real-time trajectory controller for a flat crane system using the servo-constraint framework. In addition, they discussed the challenges of servo-constraints for systems with a high differential index [122]. Brüls et al. [36] extended the approach of Chen and Paden [40] to the servo-constraint framework. Drücker and Seifried [48] approximated the original boundary value problem to simplify the control design for non-minimum phase systems. Bastos et al. [12] combined optimal control and servo-constraints for solving the inverse dynamics. Additionally, in [13], the authors demonstrated that their optimization problem converges to the original two-point boundary value problem of Brüls et al. [36] as the pre- and post-actuation phases go to infinity. An analysis of different cost functionals is given in [4]. Ströhle and Betsch [155] solved the inverse dynamics of geometrically exact strings using servo-constraints and a space-time finite element discretization. Further flatness-based control design approaches for strings based on infinite-dimensional or lumped mass systems are given in [83, 113, 155].

1.3 Contributions

In this thesis, we want to extend on the above literature from a control engineering perspective to handle the complex system class of nonlinear elastodynamics. In addition, it is desired to make the systems of nonlinear elastodynamics more suitable for control engineers and close the gap between numerical mechanics and automatic control. This is achieved by analyzing different formulations and compatible discretization methods. In summary, the contributions of this thesis are as follows:

- We discuss and develop efficient energy-based formulations of nonlinear elastodynamical systems. Our non-canonical formulation for the general equations of geometrically nonlinear elastodynamics can be easily adapted to structures such as beams and strings. Moreover, we use structure-preserving discretization methods to retain the structure or underlying PH character of the systems on the semi-discrete level. These semi-discrete models therefore contain properties that might facilitate a subsequent controller design.

- Furthermore, we study time-integration methods that preserve momentum and energy balance on the fully-discrete level. These integration methods align with our symplectic discrete-time feed-back control design approach to capture the sampling process in a digital control loop. The resulting controller preserves the structure of its continuous counterpart and is compatible with lower sampling rates than a quasi-continuous (direct) controller implementation. In this thesis, we apply the approach to a robot with flexible joints and discuss its practical use.

- Additionally, we combine well-known optimal control theory with standard finite element software to obtain an optimal feed-forward tracking controller for geometrically exact strings. The approach is based on a space-time finite element method and can be applied to large scale structural mechanical (non-minimum phase) systems. Moreover, we do not require the explicit analysis of a semi-discrete system and its internal dynamics.

- Finally, it should be mentioned that the methods in this thesis represent application-oriented approaches that enable practical implementation with common software tools, e.g., FEniCS [91, 99] and FEniCSx [3, 11, 147, 148].

1.4 Outline

The remainder of this thesis is organized as follows: In Chapter 2, we recall some basic concepts of modeling and simulation of mechanical systems. Chapter 3 represents the methodological chapter, where we recapitulate relevant methods building the foundation of our main results in Chapter 4. More precisely, Section 3.1 recalls the PH formulation and its benefits from an engineering perspective. Section 3.2 focuses on the simulation aspect, where we illustrate the spatial Galerkin approximation, temporal discretization schemes, and their structure-preserving properties. In Section 3.3, we mention control strategies that fit to the considered system class. Chapter 4 summarizes our main achievements and scientific results. In Chapter 5, we discuss our main results with respect to the current literature and conclude with a brief outlook on future research objectives.

2 Preliminaries

In this chapter, we recall the theoretical background for our work. If the reader is already familiar with the theoretical fundamentals of modeling and simulation of mechanical systems, the chapter can be skipped.

2.1 Modeling of mechanical systems

In order to analyze, simulate, optimize or control a mechanical system an accurate mathematical model is mandatory.

2.1.1 Multibody system dynamics

The dynamics of a simple[1], finite-dimensional mechanical system [72] can be described by a second-order differential equation[2],

$$M(q(t))\ddot{q}(t) + C(q(t), \dot{q}(t))\dot{q}(t) + \partial_q V(q(t)) = u(t). \tag{2.1}$$

As usual, $q \in \mathbb{R}^n$ denotes the vector of generalized coordinates, $\dot{q} \in \mathbb{R}^n$ the (angular) velocities, $M : \mathbb{R}^n \to \mathbb{R}^{n\times n}$ the symmetric, positive definite mass matrix, $C : \mathbb{R}^n \times \mathbb{R}^n \to \mathbb{R}^{n\times n}$ the Coriolis matrix[3], and $u \in \mathbb{R}^n$ non-conservative forces or torques. The equations of motion (2.1) result from the Euler-Lagrange equations with the Lagrangian,

$$L(q, \dot{q}) = \frac{1}{2}\dot{q}^\top M(q)\dot{q} - V(q), \tag{2.2}$$

where the first term represents the kinetic (co:-)energy $T : \mathbb{R}^n \times \mathbb{R}^n \to \mathbb{R}$, expressed by the generalized velocities $\dot{q} \in \mathbb{R}^n$, and the second one $V : \mathbb{R}^n \to \mathbb{R}$ the potential energy.

[1] The total energy is split in a kinetic and potential part.

[2] The operator $\partial_a b = \frac{\partial b}{\partial a}$ represents the partial derivative with respect to a, where we consider the numerator layout.

[3] The Coriolis matrix and the mass matrix are related via the property that $\dot{M} - 2C$ is skew-symmetric.

The Lagrangian and equivalent Hamiltonian formulation are coupled via the Legendre transform $H(p,q) + L(q,\dot{q}) = p^\top \dot{q}$ with the Hamiltonian or total energy,

$$H(p,q) = \frac{1}{2} p^\top M^{-1}(q) p + V(q). \tag{2.3}$$

The vector $p := M(q)\dot{q} \in \mathbb{R}^n$ represents the generalized momenta. Consequently, we can derive the standard canonical Hamiltonian form,

$$\begin{bmatrix} \dot{q} \\ \dot{p} \end{bmatrix} = \begin{bmatrix} 0 & I \\ -I & 0 \end{bmatrix} \begin{bmatrix} \partial_q H \\ \partial_p H \end{bmatrix} + \begin{bmatrix} 0 \\ I \end{bmatrix} u, \tag{2.4}$$

where the energy balance,

$$\dot{H} = \underbrace{\partial_p H^\top}_{\dot{q}^\top} u, \tag{2.5}$$

follows immediately. The pairs of variables on the right side of (2.5) form the power transferred to the system. In other words, the pairs of power variables can be seen as ports to the system and its environment. A detailed discussion on the concept of *ports* is given in Section 3.1.

2.1.2 Elastodynamics

This section recalls the basic equations of nonlinear continuum mechanics. The interested reader is referred to [5, 22, 56] for more information. Since we focus on structural mechanical systems, we only recall major equations in material coordinates. Consequently, all fields depend on the spatial coordinate X and time t, which we mostly omit for brevity. The coordinate X denotes each material point of a reference configuration $\Omega \subset \mathbb{R}^d$, $d = 1, 2, 3$, $\varphi(X,t) : \Omega \times \mathbb{R}^{\geq 0} \to \mathbb{R}^d$ the motion of a continuum, and $q = \varphi - X$ the displacement field, see also Figure 2.1. The linear momentum balance of the system is given by

$$\rho(X)\ddot{\varphi}(X,t) = \mathrm{Div}(F(X,t) \cdot S(X,t)) + b(X,t) \quad \text{in } \Omega, \tag{2.6}$$

where $\rho \in \mathbb{R}$ denotes the material density, and $F = \mathrm{Grad}(\varphi) : \mathbb{R} \to \mathbb{R}^{d \times d}$ the deformation gradient[4]. Furthermore, the vector $b \in \mathbb{R}^d$ represents the volume forces, which might result from a potential (e.g., gravity) or other exogenous loads. The conservation of mass follows by the fact that $\dot{\rho} = 0$. Since we consider a Boltzmann continuum[5], the

[4] The operator $\mathrm{Div}(a) = \partial_X a : I$ represents the divergence and $\mathrm{Grad}(a) = \partial_X a$ the gradient of a tensor a with respect to the material coordinates.

[5] Infinitesimal volume elements do not contain rotational inertia.

angular momentum balance is automatically fulfilled due to the symmetry of the second Piola-Kirchhoff stress tensor, $S = S^\top$. In case of hyperelastic (completely reversible) materials, $S \in \mathbb{R}^{d\times d}_{\text{sym}}$ is characterized by

$$S = \partial_E W(E), \tag{2.7}$$

where $W : \mathbb{R}^{d\times d}_{\text{sym}} \to \mathbb{R}$ represents the strain energy density function. $C = F^\top \cdot F$ is the right Cauchy-Green deformation tensor and $E \in \mathbb{R}^{d\times d}_{\text{sym}}$ the nonlinear Green strain tensor,

$$E = \frac{1}{2}(C - I). \tag{2.8}$$

In order to close the system description, we consider an appropriate decomposition of the boundary into a Dirichlet and Neumann part, $\partial\Omega = \partial\Omega_D \cup \partial\Omega_N$, which leads to the mixed boundary conditions (BCs),

$$\varphi = \varphi_D \quad \text{on } \partial\Omega_D, \tag{2.9}$$

$$F \cdot S \cdot N = \tau_N \quad \text{on } \partial\Omega_N, \tag{2.10}$$

where N denotes the outer oriented normal vector on $\partial\Omega$, and φ_D, τ_N the given boundary data.

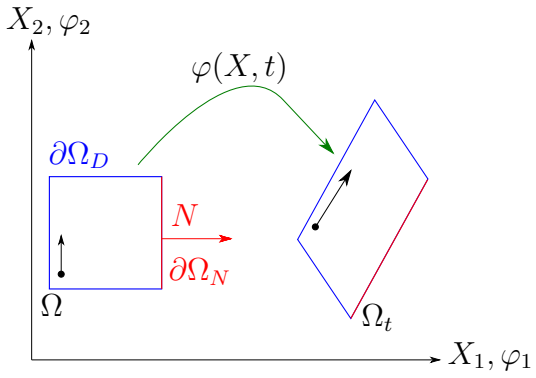

Figure 2.1: The motion φ maps the material (undeformed) configuration ($\Omega \subset \mathbb{R}^2$) to the spatial (deformed) one ($\Omega_t \subset \mathbb{R}^2$).

Introducing the momentum density $p := \rho\dot{\varphi}$, the Hamiltonian can be expressed as

$$H(\varphi, p) = \int_\Omega \mathcal{H}(\varphi, p)\, \mathrm{d}X = \int_\Omega \left(\frac{1}{2}\rho^{-1} p \cdot p + W(F_\varphi)\right)\, \mathrm{d}X, \tag{2.11}$$

where F_φ is computed by means of φ. Accordingly, the variational derivatives of H yield the expressions

$$\delta_\varphi H = \partial_\varphi \mathcal{H} - \mathrm{Div}(\partial_F \mathcal{H}), \tag{2.12a}$$

$$\delta_p H = \partial_p \mathcal{H}, \tag{2.12b}$$

and we can formulate the canonical Hamiltonian representation,

$$\begin{bmatrix} \dot{\varphi} \\ \dot{p} \end{bmatrix} = \begin{bmatrix} 0 & I \\ -I & 0 \end{bmatrix} \begin{bmatrix} \delta_\varphi H \\ \delta_p H \end{bmatrix} + \begin{bmatrix} 0 \\ I \end{bmatrix} b, \tag{2.13}$$

which reveals the analogy to (2.4).

By means of further assumptions on the above equations of nonlinear elastodynamics, special system classes, such as shells, beams, and strings can be derived.

Example 2.1. In case of small displacements q, one can use the well-known equations of linear elastodynamics [65],

$$\rho(X)\ddot{q}(X,t) = \mathrm{Div}(\sigma(X,t)) + b(X,t) \quad \text{in } \Omega, \tag{2.14}$$

where $\sigma \in \mathbb{R}^{d\times d}_{\mathrm{sym}}$ denotes the Cauchy stresses. These are related to the strains[6],

$$\varepsilon = \mathrm{sym}(\mathrm{Grad}(q)) \ \in \mathbb{R}^{d\times d}_{\mathrm{sym}}, \tag{2.15}$$

by the linear material law,

$$\sigma = \mathbb{C} : \varepsilon, \tag{2.16}$$

where $\mathbb{C}$ represents the fourth-order tensor of Hooke's law elastic coefficients. The system dynamics are completed by the BCs,

$$q = q_D \quad \text{on } \partial\Omega_D, \tag{2.17}$$

$$\sigma \cdot N = \tau_N \quad \text{on } \partial\Omega_N. \tag{2.18}$$

Among many other things, the above model can be used for active vibration control to suppress unwanted oscillations [163].

Example 2.2. Let us briefly introduce another example, the geometrically exact strings [94, 105, 155, 165], whose simulation and control have been discussed in [A8, A7, A2, A5]. In summary, we consider the one-dimensional reference configuration $\Omega = [0, L] \subset$

[6] $\mathrm{sym}(a) = \frac{1}{2}(a + a^\top) : \mathbb{R}^{d\times d} \to \mathbb{R}^{d\times d}_{\mathrm{sym}}$ denotes the symmetrization operator.

$\mathbb{R}^d$ of length L. The arc length coordinate $s = X_1 \subset \mathbb{R}$ describes the position of each particle in the reference configuration. The momentum balance is given by

$$A(s)\rho(s)\ddot{\varphi}(s,t) = \partial_s n(s,t) + b(s,t) \quad \text{in } \Omega, \tag{2.19}$$

where the position vector $\varphi(s,t) : \Omega \times \mathbb{R}^{\geq 0} \to \mathbb{R}^d$ describes the actual configuration (or motion) of the string, see also Figure 2.2. As usual, $\rho \in \mathbb{R}$ represents the density, $A \in \mathbb{R}$ the cross-sectional area, $b \in \mathbb{R}^d$ the body forces per unit length, and $n \in \mathbb{R}^d$ the contact force given by the relationship,

$$n = \hat{N}\frac{\partial_s \varphi}{\nu}. \tag{2.20}$$

The tension $\hat{N} \in \mathbb{R}$ is determined by the constitutive equation,

$$\hat{N} = \partial_\nu W(\nu), \tag{2.21}$$

where $W : \mathbb{R} \to \mathbb{R}$ denotes the strain energy density and $\nu = ||\partial_s \varphi|| : \mathbb{R}^d \to \mathbb{R}$ the stretch. Let us apply the BCs,

$$n(0,t) = -\tau_N(t), \tag{2.22}$$

$$n(L,t) = 0, \tag{2.23}$$

where τ_N denotes the control input or actuating force vector. A control problem could now consist of finding τ_N, such that the end of the string $y(t) = \varphi(L,t)$ follows a desired trajectory $y_d(t)$.

2.2 Numerical aspects of simulation

The general numerical analysis cycle of a simulation includes several steps [161]: The first step is the *preprocessing*, which includes modeling, data collection, specification of constraints, and so on. The second step *solution processing* focuses on the computational effort. In numerical mechanics, this might include a spatial discretization with finite elements and a subsequent time integration, which are the topics of this section. *Postprocessing* represents the step of analysis and visualization of the computed results.

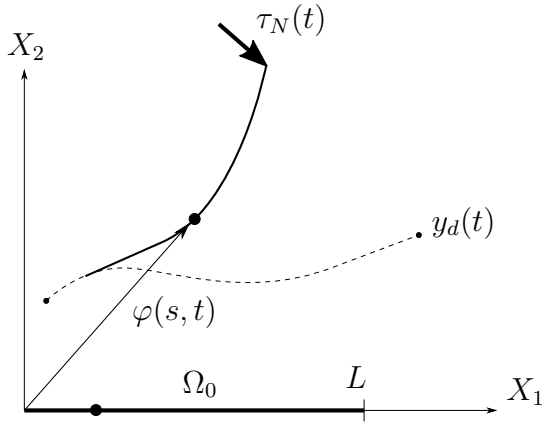

Figure 2.2: Illustration of a geometrically exact string, its reference configuration and the corresponding control problem: The end of the string is supposed to follow y_d with τ_N as control input.

2.2.1 Recall on finite elements

Let us start with the spatial discretization, which is mandatory to obtain a finite-dimensional (semi-discrete) system from a set of PDEs and BCs. In structural mechanics, many researchers including the PH community have mainly focused on Galerkin approximations with finite elements [170]. Let us briefly mention some key advantages of Galerkin approximations with finite elements: The process is compatible with complex geometries and can easily be extended to higher order methods. Moreover, the method offers a systematic approach and a wide range of implementation tools. In order to repeat the systematic finite element approach, we use the following example.

Example 2.3. Assume $q \in \mathscr{Q} = \{q \in \mathscr{H}^1(\Omega;\mathbb{R}^d) : q = q_D \text{ on } \partial\Omega_D\}$ being a solution of (2.14)-(2.18) with $b = 0$, then the weak formulation[7]

$$\langle w, \rho\ddot{q}\rangle_\Omega + \langle \varepsilon(w), \mathbb{C} : \varepsilon(q)\rangle_\Omega - \langle w, \tau_N\rangle_{\partial\Omega_N} = 0, \tag{2.24}$$

holds for all test functions[8] $w \in \mathscr{W} = \{w \in \mathscr{H}^1(\Omega;\mathbb{R}^d) : w = 0 \text{ on } \partial\Omega_D\}$, and all $t \geq 0$. This weak form is obtained by testing (2.14), applying integration by parts (IbP), and inserting the given Neumann (natural) BCs. As long as we allow an infinite number of test functions, the weak form is equivalent to the strong form (2.14). Since we can

[7] For ease of notation, we introduce

$$\langle a, b\rangle_M = \int_M a \odot b \, \mathrm{d}X$$

for the integration of inner products of scalar and tensor valued functions over some domain M.

[8] $\mathscr{H}^1$ denotes the Sobolev space of weakly differentiable functions and $\mathscr{L}^2$ the space of square-integrable functions.

not handle an infinite number of infinite-dimensional functions, we restrict the spaces of trial and test function to a finite-dimensional basis, i.e.

$$\mathscr{Q} \supset \mathscr{Q}_h = \{q_h \in \mathscr{H}^1(\Omega;\mathbb{R}^d) : q_h = q_D \text{ on } \partial\Omega_D,\ q_h^{(e)}(X,t) = \psi(X)\mathrm{q}^{(e)}(t) \text{ in } \mathcal{T}_h^{(e)}\ \forall\ (e)\},$$
$$\mathscr{W} \supset \mathscr{W}_h = \{w_h \in \mathscr{H}^1(\Omega;\mathbb{R}^d) : w_h = 0 \text{ on } \partial\Omega_D,\ w_h^{(e)}(X) = \psi(X)\mathrm{w}^{(e)} \text{ in } \mathcal{T}_h^{(e)}\ \forall\ (e)\},$$

with the nodal displacements $\mathrm{q}^{(e)}$ and weighting values $\mathrm{w}^{(e)}$ for each element (e) of the computational mesh $\mathcal{T}_h$. Now find $q_h \in \mathscr{Q}_h$ such that

$$\langle w_h, \rho\ddot{q}_h\rangle_\Omega + \langle \varepsilon(w_h), \mathbb{C} : \varepsilon(q_h)\rangle_\Omega - \langle w_h, \tau_N\rangle_{\partial\Omega_N} = 0 \quad \forall w_h \in \mathscr{W}_h. \tag{2.25}$$

Accordingly, we obtain the mass $\mathrm{M}^{(e)}$, stiffness $\mathrm{K}^{(e)}$, and input matrix $\mathrm{B}^{(e)}$ of each element,

$$\sum_{e=1}^{N} \left[\mathrm{w}^{(e)\top}\left(\mathrm{M}^{(e)}\ddot{\mathrm{q}}^{(e)} + \mathrm{K}^{(e)}\mathrm{q}^{(e)} - \mathrm{B}^{(e)}\tau_N^{(e)}\right)\right] = 0 \tag{2.26}$$

which can be assembled to

$$\mathrm{w}^\top\left(\mathrm{M}\ddot{\mathrm{q}} + \mathrm{K}\mathrm{q} - \mathrm{B}\tau_N\right) = 0. \tag{2.27}$$

Because w is arbitrary, we obtain the system of ordinary differential equations,

$$\mathrm{M}\ddot{\mathrm{q}}(t) + \mathrm{K}\mathrm{q}(t) = \mathrm{B}\tau_N(t). \tag{2.28}$$

We now illustrate the process of direct assignment of inhomogeneous Dirichlet BCs to the corresponding boundary degrees of freedom. Therefore, we split the vector of degrees of freedom $\mathrm{q}^\top = [\mathrm{q}_r^\top\ \mathrm{q}_D^\top]$ and generate the reduced system[9] of the form

$$\mathrm{M}_r\ddot{\mathrm{q}}_r + \mathrm{K}_r\mathrm{q}_r = \mathrm{B}_r\tau_N - \mathrm{M}_D\ddot{\mathrm{q}}_D - \mathrm{K}_D\mathrm{q}_D. \tag{2.29}$$

For more information on the assignment of Dirichlet boundary conditions in finite element models, the reader is referred to [16].

Example 2.4. Generating the finite element model of the geometrically exact string given in Example 2.2, we assume $\varphi_h \subset \mathscr{H}^1(\Omega;\mathbb{R}^d)$ being a solution of

$$\langle w_h, A\rho\ddot{\varphi}_h\rangle_\Omega + \langle \partial_s w_h, n(\varphi_h)\rangle_\Omega - \langle w_h, \tau_N\rangle_{\partial\Omega_N} = 0, \tag{2.30}$$

[9] The subscript r denotes the reduced matrices/vectors, without the Dirichlet degrees of freedom, and the subscript D the columns of the matrices/vectors corresponding to Dirichlet degrees of freedom.

for all $w_h \subset \mathscr{H}^1(\Omega;\mathbb{R}^d)$, and $t \geq 0$. Therefore, we obtain nonlinear semi-discrete equations of motion,

$$\mathrm{M}\ddot{\varphi} + \mathrm{k}(\varphi) = \mathrm{B}\tau_N, \tag{2.31}$$

where the nonlinearity results from the nonlinear geometry or contact force (2.20), see also [155, A5].

In the above examples, the displacement field is the primary unknown and all other fields are calculated from these displacements. Therefore, the above weak formulation is called a displacement-based single-field formulation. The downside of single-field finite element formulations are possible locking effects, i.e. unphysical stiffening. Therefore, selective reduced integration or mixed finite element methods [20] are preferred. In addition, it has been shown that well-known mixed finite element formulations have an underlying PH character, see also Section 3.2, and in particular [25, A1].

2.2.2 Recall on time integration

In contrast to an analytical solution, the semi-discrete system can also be solved with time discretization methods. Commonly, time integration methods [57] are based on finite differences, whose idea can be expressed as

$$\dot{x} \approx d_\tau x = \tfrac{1}{\tau}(x^{k+1} - x^k), \tag{2.32}$$

where $\tau = t^{k+1} - t^k$ is the time step size, and $x^k \approx x(t^k)$ the approximation at the discrete time step t^k. Consequently, solutions are obtained sequentially at every time step t^k starting with the initial condition $x^0 = x(t^0)$. Depending on the numerical integration of the evolution equation, the methods are usually categorized as explicit, implicit, single-step or multi-step methods. In addition, these techniques are classified by their order of accuracy or stability [68].

In summary, numerical integration methods start with an initial condition and transport the system state in a direction defined by the evolution equations. However, several approaches do not account for the underlying geometric structure of the system and hence may lead to inaccurate results due to spurious effects [68]. In order to provide physically accurate numerical results, geometric numerical integrators (GNIs) have been developed [152]. More information on GNIs is given in Section 3.2.

3 Methodology

In this chapter, we mention the theoretical methods and concepts, which had a major influence on the development of our articles summarized in Chapter 4.

3.1 Port-Hamiltonian framework

3.1.1 Finite-dimensional setting

The PH framework results from a combination of Hamiltonian mechanics and the concept of *ports*. For more details, we refer to [142].

Port-based modeling The so-called ports represent power interfaces of power conjugated variables, e.g., pairs of velocities and forces, which allow for a description of energy-consistent or power-preserving interconnections of subsystems to compose models in a modular way, see [160] for an impressive multi-physical example. Consequently, an overall model might be an interconnection of the following elements, through which the system engages with its environment. In general, every element is described by a pair of power or port variables (e, f) with the *effort* e and the *flow* f, whose product forms the power extracted from the element:

$$e^\top f = \text{extracted power} \tag{3.1}$$

Finite-dimensional (or lumped[1]) energy storage elements are described by the dynamics,

$$\dot{x} = -f_S, \tag{3.2}$$

where $x \in \mathscr{X} \subset \mathbb{R}^n$ denotes the vector of state or energy variables. Energy storage is expressed by the Hamiltonian $H : \mathscr{X} \to \mathbb{R}$ defining the co-energy variables

$$e_S = \partial_x H(x). \tag{3.3}$$

[1] In this context, *lumped* means that energy is concentrated in elements whose spatial extension is negligible.

This leads to

$$\dot{H} = \partial_x H(x)^\top \dot{x} = -e_S^\top f_S, \tag{3.4}$$

showing that the product of effort and flow refers to the power taken from the element.

Example 3.1. Let us consider the mass in Figure 3.1a. The total (kinetic) energy of the mass is given by

$$H_m(p) = \frac{p^2}{2m}, \tag{3.5}$$

where $p = mv_m$ denotes its momentum and $v_m = \partial_p H_m$ the velocity. Its dynamics is described by the momentum balance,

$$\dot{p} = F_m. \tag{3.6}$$

Consequently, we obtain the power balance

$$\dot{H}_m = \partial_p H_m \dot{p} = \underbrace{v_m}_{e_m} \underbrace{F_m}_{-f_m}, \tag{3.7}$$

with the corresponding flow f_m and effort e_m.

Example 3.2. Let us consider the spring in Figure 3.1b. The total (potential) energy of the spring is given by

$$H_s(\Delta q) = \frac{c\Delta q^2}{2}, \tag{3.8}$$

where Δq denotes its compression and $F_s = \partial_{\Delta q} H_s$ the corresponding force. Its dynamics is described by the kinematic equation,

$$\Delta\dot{q} = v_s. \tag{3.9}$$

Consequently, we obtain the power balance,

$$\dot{H}_s = \partial_{\Delta q} H_s \Delta\dot{q} = \underbrace{F_s}_{e_s} \underbrace{v_s}_{-f_s}, \tag{3.10}$$

with the corresponding flow f_s and effort e_s.

Since resistive elements only take power from their environment, they are characterized by

$$e_R^\top f_R \leq 0. \tag{3.11}$$

This energetic flow might result from $e_R = -Sf_R$ or $e_R = -Sf_R$ with $S \geq 0$, which is referred to as impedance or admittance relation.

Example 3.3. Let us consider the damper in Figure 3.1c and the linear relation $F_d = dv_d$. The power entering the damper is given by

$$\underbrace{v_d}_{-f_d}\underbrace{F_d}_{e_d} = dv_d^2 \geq 0, \tag{3.12}$$

where $e_d = -df_d$ represents an impedance relation.

In order to model the interaction of a system with its environment, external port variables (e_P, f_P) are required. These ports might be accessible for controllers, interactions or other sources. Typically, external port variables are assigned the role of in- and outputs in the sense of control theory.

Example 3.4. Let us consider the actuator in Figure 3.1d. The actuator force F_a might be the control input u and the velocity the corresponding output y. Consequently, the power that the actuator can deliver to its environment is given by

$$f_a e_a = v_a F_a. \tag{3.13}$$

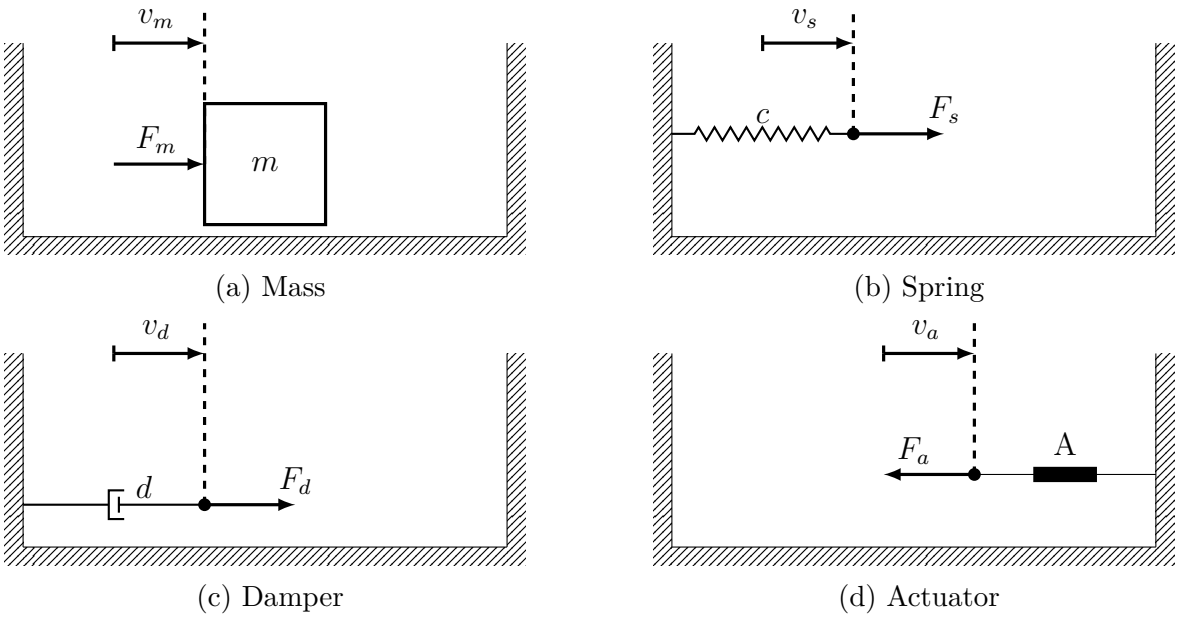

(a) Mass (b) Spring

(c) Damper (d) Actuator

Figure 3.1: Illustration of elements with the corresponding velocities v and forces F.

In the following, we interconnect the elements to generate an overall system.

Dirac structures Due to a geometric description using Dirac structures, a generalization of the symplectic or Possion structure, the above elements can be interconnected

in an algebraic and power-preserving way. Therefore, a Dirac structure represents a power-preserving subspace of efforts and flows.

Definition 3.1 (Dirac structure [141])**.** Consider a vector space of flows $\mathscr{F} = \mathbb{R}^k$ and its dual space $\mathscr{E} = \mathbb{R}^k$. A subspace $\mathscr{D} \subset \mathscr{F} \times \mathscr{E}$ is called a Dirac structure if $e^\top f = 0 \; \forall (e, f) \in \mathscr{D}$, where $\dim \mathscr{D} = \dim \mathscr{F}$.

The specific Dirac structure, (kernel representation [139]),

$$\mathscr{D} = \{(f, e) \in \mathscr{F} \times \mathscr{E} \mid Ff + Ee = 0\}, \tag{3.14}$$

$$F = I, \quad E = \begin{bmatrix} J & G & B \\ -G^\top & 0 & 0 \\ -B^\top & 0 & 0 \end{bmatrix}, \quad J = -J^\top, \tag{3.15}$$

with the above flows $f = (f_S, f_R, f_P) \in \mathbb{R}^k$ and efforts $e = (e_S, e_R, e_P) \in \mathbb{R}^k$ forms the so-called input–state–output PH system,

$$\dot{x} = (J - R)\partial_x H(x) + Bu, \tag{3.16a}$$

$$y = B^\top \partial_x H(x), \tag{3.16b}$$

with the input $u = e_P$, output $y = f_P$, and $R = GSG^\top$. This represents a generalization of the canonical Hamiltonian equations.

Example 3.5. In order to interconnect the elements of Figure 3.1, we use the following Dirac structure, which simply describes the equilibrium of forces and kinematic constraints on velocity level between the interconnected elements:

$$\left.\begin{array}{ll} F_m & = -F_s - F_d + F_a \\ v_s & = v_m \\ v_d & = v_m \\ -v_a & = -v_m \end{array}\right\} \Rightarrow - \begin{bmatrix} f_m \\ f_s \\ f_d \\ f_a \end{bmatrix} = \begin{bmatrix} 0 & -1 & -1 & 1 \\ 1 & 0 & 0 & 0 \\ 1 & 0 & 0 & 0 \\ -1 & 0 & 0 & 0 \end{bmatrix} \begin{bmatrix} e_m \\ e_s \\ e_d \\ e_a \end{bmatrix} \tag{3.17}$$

Accordingly, we obtain after substitution of $e_d = -df_d$ the state space model,

$$\begin{bmatrix} \dot{p} \\ \Delta\dot{q} \end{bmatrix} = \left(\begin{bmatrix} 0 & -1 \\ 1 & 0 \end{bmatrix} - \begin{bmatrix} d & 0 \\ 0 & 0 \end{bmatrix} \right) \begin{bmatrix} \frac{p}{m} \\ c\Delta q \end{bmatrix} + \begin{bmatrix} 1 \\ 0 \end{bmatrix} \underbrace{F_a}_{u}, \tag{3.18}$$

$$y = \begin{bmatrix} 1 & 0 \end{bmatrix} \begin{bmatrix} \frac{p}{m} \\ c\Delta q \end{bmatrix}, \tag{3.19}$$

with the total energy being the sum of all energies of the storage elements,

$$H(p, \Delta q) = H_m(p) + H_s(\Delta q) = \frac{p^2}{2m} + \frac{c\Delta q^2}{2}, \tag{3.20}$$

leading to the energy balance,

$$\dot{H} = -d\left(\frac{p}{m}\right)^2 + yu. \tag{3.21}$$

Note that (3.21) is equivalent to $e^\top f = 0$ as required by the definition of the Dirac structure. A graphical illustration of the connected system is given in Figure 3.2.

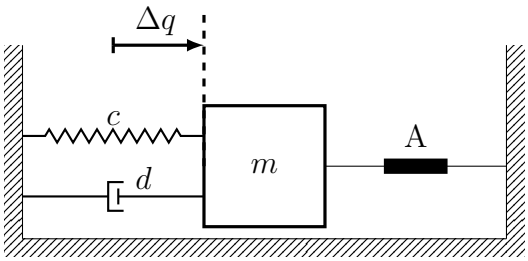

Figure 3.2: Overall system representing an interconnection of several elements.

In the following, we give a precise definition of a PH state space model.

Dynamical system representation As demonstrated above, PH systems can be described via Dirac structures. In the following, we only consider the dynamical system representation similar to (3.16), which is more common from a simulation or control engineering perspective.

Definition 3.2 (Finite-dimensional PH system)**.** A time-invariant state space model of the form,

$$E(x)\dot{x} = (J(x) - R(x))e(x) + B(x)u, \tag{3.22a}$$

$$y = B^\top(x)e(x), \tag{3.22b}$$

with the state $x \in \mathbb{R}^n$, input $u \in \mathbb{R}^m$, output $y \in \mathbb{R}^m$, where E, J, $R : \mathbb{R}^n \to \mathbb{R}^{n\times n}$, co-state $e : \mathbb{R}^n \to \mathbb{R}^n$, and input matrix $B : \mathbb{R}^n \to \mathbb{R}^{n\times m}$, is called a finite-dimensional port-Hamiltonian system, if the following properties are satisfied:

I The Hamiltonian $H(x) : \mathbb{R}^n \to \mathbb{R}$ is bounded from below and satisfies $E^\top e = \partial_x H$.

II The dissipation matrix R is symmetric and positive semi-definite, i.e., $R = R^\top \geq 0$.

III The structure matrix J is skew-symmetric, i.e., $J = -J^\top$.

A more general definition including time-varying systems with a feed-through term is given in [107]. We obtain the classical PH state space model (3.16), as presented in [141], if $E = I$. However, the matrix E leads to a greater diversity regarding the choice of state variables and covers the representation of differential algebraic PH systems.

Example 3.6. Introducing the velocity vector $v := \dot{q}$, the well-known first order representation of (2.1) can be rewritten in the form (3.22). In case of a holonomic constraint,

$$g(q) = 0 \quad \Rightarrow \quad \underbrace{\partial_q g^\top(q)}_{G^\top(q)} v = 0,$$

we obtain the port-Hamiltonian state equations,

$$\begin{bmatrix} I & 0 & 0 \\ 0 & M(q) & 0 \\ 0 & 0 & 0 \end{bmatrix} \begin{bmatrix} \dot{q} \\ \dot{v} \\ \dot{\lambda} \end{bmatrix} = \begin{bmatrix} 0 & I & 0 \\ -I & F(q,v) & G(q) \\ 0 & -G^\top(q) & 0 \end{bmatrix} \begin{bmatrix} e_q \\ e_v \\ e_\lambda \end{bmatrix} + \begin{bmatrix} 0 \\ I \\ 0 \end{bmatrix} u \tag{3.23}$$

with the Hamiltonian $H(q,v) = \frac{1}{2} v^\top M(q) v + V(q)$, and $F = \dot{M} - 2C$ being skew-symmetric. The vector $e_\lambda := \lambda$ corresponds to a Lagrange multiplier or reaction force, enforcing the constraint.

Due to their structure, PH systems exhibit certain characteristics.

Properties of PH systems A key property of PH systems is passivity, which represents a generalization of energy balance.

Definition 3.3 (Passivity)**.** A dynamical system of the form

$$\dot{x}(t) = f(x(t), u(t)), \tag{3.24a}$$
$$y(t) = c(x(t), u(t)), \tag{3.24b}$$

with the state vector $x \in \mathscr{X} \subset \mathbb{R}^n$, in- and output $u \in \mathscr{U} \subset \mathbb{R}^m, y \in \mathscr{Y} \subset \mathbb{R}^m$ is passive if a positive semi-definite storage function $H : \mathscr{X} \to \mathbb{R}$ exists such that

$$\dot{H}(x) \leq y^\top u \tag{3.25}$$

holds for all times.

Regarding PH systems, the Hamiltonian serves as a storage function and the power-conjugated in- and outputs guarantee passivity,

$$\dot{H} = -\underbrace{e^\top R e}_{\geq 0} + \underbrace{e^\top B}_{y^\top} u \leq y^\top u. \tag{3.26}$$

In the 1970s, researchers discovered the link between energy, dissipation and Lyapunov's theory [75]. Following this idea, Willems [166] published a paper about dissipative systems. Since then, the concept of dissipativity and passivity became an important tool for the analysis of dynamical systems. Due to its strong connection to Lyapunov's stability theory, the concept of passivity motivated several (energy-based) control concepts tailored to PH systems, see [117–120]. In general, a passivity-based controller contains a state feed-back part transferring the control system to a passive one and an additional damping injection stabilizing a desired equilibrium. For more information on passivity the reader is referred to [92, 93].

Example 3.7. Illustrating the concept of passivity-based control, we assume the state equations (2.4) with the Hamiltonian (2.3). Using the control law,

$$u = -\partial_q H_d + \partial_q H + u_{\mathrm{di}} = \underbrace{-\partial_q V_d + \partial_q V}_{u_{\mathrm{es}}} + u_{\mathrm{di}}, \tag{3.27}$$

we obtain the passive state space model

$$\begin{bmatrix} \dot{q} \\ \dot{p} \end{bmatrix} = \begin{bmatrix} 0 & I \\ -I & 0 \end{bmatrix} \begin{bmatrix} \partial_q H_d \\ \partial_p H_d \end{bmatrix} + \begin{bmatrix} 0 \\ I \end{bmatrix} u_{\mathrm{di}}, \qquad y = \partial_p H_d, \tag{3.28}$$

with the desired Hamiltonian $H_d(q,p) = \frac{1}{2} p^\top M^{-1}(q) p + V_d(q)$. Since H_d serves as a Lyapunov function, $u_{\mathrm{di}} := -D\partial_p H_d$ with $D > 0$ can stabilize the system asymptotically. In summary, u_{es} shapes the energy of the control system and u_{di} injects damping [118].

Another major characteristic is the compositionality of PH systems, which states that PH systems coupled through any interconnection Dirac structure form again a PH system. Accordingly, the total Hamiltonian of N interconnected PH subsystems with the Hamiltonian H_i is given by $H = \sum_{i=1}^{N} H_i$ [139]. This characteristic enables a modular modeling of complex systems. Since mechanical structures are usually submodules of an overall system and are accordingly interconnected to their environment, it makes the PH framework an ideal choice for them.

Regarding infinite-dimensional (or distributed) PH systems, the above characteristics are transferred to the infinite-dimensional setting.

3.1.2 Infinite-dimensional setting

Strictly speaking, the definition of infinite-dimensional PH systems is not univocal and two approaches are commonly used in the literature: Regarding jet-bundle formulations, PH systems are derived from the Euler-Lagrange equations and the Legendre transform, see (2.13) and [31]. However, deducing the boundary port variables might be challenging. E.g., the boundary ports stem from the variational derivatives of the Hamiltonian. In case of (Stokes-)Dirac structures, energy variables[2] are chosen as states and the boundary ports stem from a differential operator via IbP [104]. Consequently, boundary conditions are defined by co-energy variables. In contrast to the jet bundle formulation, there is no recipe for the systematic construction of PH-systems via Stokes-Dirac structures due to the larger selection of state variables. For an overview of the two approaches using a mechanical example, the reader is referred to [145]. For simplicity, we define an infinite-dimensional PH system in the (Stokes-)Dirac structure framework in a compact form based on [37, 171], which is compatible with several elastodynamical models, e.g., [26, 27, 32, 35, 163].

Definition 3.4 (Infinite-dimensional PH system)**.** We consider a spatial domain $\Omega \subset \mathbb{R}^d$, $d \geq 1$, defined by the spatial coordinate X and the boundary $\partial\Omega$. Additionally, we denote by $\mathscr{X}$ the space of state variables, i.e. $x(X,t) \in \mathscr{X}$, and by

$$H = \int_\Omega \mathcal{H}(x)\, \mathrm{d}X \tag{3.29}$$

the Hamiltonian with its density $\mathcal{H} : \mathscr{X} \to \mathscr{L}^1(\Omega, \mathbb{R})$. The set of PDEs and boundary port-variables,

$$\begin{bmatrix} \mathcal{E}\dot{x} \\ -y_\Omega \end{bmatrix} = \begin{bmatrix} \mathcal{J}_x - \mathcal{R} & \mathcal{B} \\ -\mathcal{B}^* & 0 \end{bmatrix} \begin{bmatrix} e \\ u_\Omega \end{bmatrix} \quad \text{in } \Omega, \tag{3.30}$$

$$\begin{pmatrix} y_\partial \\ u_\partial \end{pmatrix} = \begin{pmatrix} \mathcal{C}_\partial e \\ \mathcal{B}_\partial e \end{pmatrix} \quad \text{on } \partial\Omega, \tag{3.31}$$

with the co-state e, input data u_Ω, u_∂ and outputs y_Ω, y_∂ represents an infinite-dimensional PH system, if the following characteristics hold:

I $\mathcal{E}^*$ denotes the adjoint[3] of the positive semi-definite operator $\mathcal{E}$, which is related to the partial derivative of the Hamiltonian density by $\mathcal{E}^* e = \partial_x \mathcal{H}$.

[2] If the Hamiltonian does not depend on the spatial derivatives of the dependent state variables, we call these variables energy variables [145]. Consequently, the variational derivative of the Hamiltonian coincides with the partial derivative of the Hamiltonian density, i.e., $\delta_x H = \partial_x \mathcal{H}$.

[3] The adjoint operator $\mathcal{A}^*$ is defined by the relation $\langle a, \mathcal{A}b\rangle_\Omega = \langle \mathcal{A}^* a, b\rangle_\Omega$.

II The (resistive) operator $\mathcal{R}$ is composed of a differential operator $\mathcal{G}$ and a non-negative bounded matrix operator $\mathcal{S} \geq 0$, $\mathcal{R} = \mathcal{G}\mathcal{S}\mathcal{G}^*$.

III The differential (structure) operator $\mathcal{J}_x$ might be modulated by the state x and is formally skew-adjoint in a sense that $\langle a, \mathcal{J}_x b\rangle_\Omega = -\langle \mathcal{J}_x a, b\rangle_\Omega$ holds for homogeneous boundary conditions. Additionally, we assume that one can find a differential operator $\mathcal{A}_x$ such that

$$\langle a, \mathcal{J}_x b\rangle_\Omega - \langle a, \mathcal{R} b\rangle_\Omega = \langle a, \mathcal{A}_x b\rangle_\Omega - \langle \mathcal{A}_x a, b\rangle_\Omega - \langle \mathcal{G}^* a, \mathcal{S}\mathcal{G}^* b\rangle_\Omega + \langle \mathcal{C}_\partial b, \mathcal{B}_\partial a\rangle_{\partial\Omega},$$

follows by IbP or the appropriate Stokes formula to make the boundary term with the operators $\mathcal{B}_\partial$, $\mathcal{C}_\partial$ appear.

Remark 3.1. In addition to $\mathcal{J}_x$, the remaining differential operators might also be modulated by the state x. For the sake of clarity, this is not explicitly considered below and is not relevant for our systems of nonlinear elastodynamics [A8, A7, A2, A1].

Theorem 3.1. *Let (x, e) be a sufficiently regular solution of the above system of Definition 3.4. Then the passivity inequality due to the power balance,*

$$\dot{H} = -\mathcal{D}(e) + \langle y_\Omega, u_\Omega\rangle_\Omega + \langle y_\partial, u_\partial\rangle_{\partial\Omega} \leq \langle y_\Omega, u_\Omega\rangle_\Omega + \langle y_\partial, u_\partial\rangle_{\partial\Omega}, \tag{3.32}$$

with the rate of dissipated energy $\mathcal{D} \geq 0$ holds.

Proof. By testing the evolution $\mathcal{E}\dot{x} = (\mathcal{J} - \mathcal{R})e$ and constitutive equation $\mathcal{E}^* e = \partial_x \mathcal{H}$, applying an appropriate IbP, and substituting the corresponding boundary data, we obtain

$$\begin{aligned} \langle w, \mathcal{E}\dot{x}\rangle_\Omega = \langle w, \mathcal{A}_x e\rangle_\Omega - \langle \mathcal{A}_x w, e\rangle_\Omega - \langle \mathcal{G}^* w, \mathcal{S}\mathcal{G}^* e\rangle_\Omega \\ + \langle w, \mathcal{B} u_\Omega\rangle_\Omega + \langle \mathcal{C}_\partial w, u_\partial\rangle_{\partial\Omega}, \end{aligned} \tag{3.33}$$

$$\langle \tilde{w}, \mathcal{E}^* e\rangle_\Omega = \langle \tilde{w}, \partial_x \mathcal{H}\rangle_\Omega, \tag{3.34}$$

which hold for all regular test functions $(w, \tilde{w})$, and all $t \geq 0$. Testing (3.33) with $w = e$, it follows

$$\begin{aligned} \underbrace{\langle e, \mathcal{E}\dot{x}\rangle_\Omega}_{\langle \mathcal{E}^* e, \dot{x}\rangle_\Omega} = \underbrace{\langle e, \mathcal{A}_x e\rangle_\Omega - \langle \mathcal{A}_x e, e\rangle_\Omega}_{0} - \underbrace{\langle \mathcal{G}^* e, \mathcal{S}\mathcal{G}^* e\rangle_\Omega}_{\mathcal{D}\geq 0} \\ + \underbrace{\langle e, \mathcal{B} u_\Omega\rangle_\Omega}_{\langle \mathcal{B}^* e, u_\Omega\rangle_\Omega} + \langle \mathcal{C}_\partial e, u_\partial\rangle_{\partial\Omega}. \end{aligned} \tag{3.35}$$

Using $\langle \mathcal{E}^* e, \dot{x} \rangle_\Omega = \langle \partial_x \mathcal{H}, \dot{x} \rangle_\Omega$, and considering the above output variables, we obtain the given power balance, what completes the proof. □

Example 3.8. Let us consider the equations of linear elastodynamics (2.14)-(2.18) with $b = 0$ and pure Neumann BCs. In addition, we introduce the velocity field $v := \dot{q}$, so we can now define the total energy or Hamiltonian,

$$H(v, \sigma) = \frac{1}{2}\langle v, \rho v \rangle_\Omega + \frac{1}{2}\langle \sigma, \mathbb{C}^{-1} : \sigma \rangle_\Omega, \tag{3.36}$$

and use the mixed (velocity-stress) formulation,

$$\underbrace{\begin{bmatrix} \mathbb{C}^{-1} & 0 \\ 0 & \rho \end{bmatrix}}_{\mathcal{E}} \underbrace{\begin{bmatrix} \dot{\sigma} \\ \dot{v} \end{bmatrix}}_{\dot{x}} = \underbrace{\begin{bmatrix} 0 & \mathrm{sym}(\mathrm{Grad}(\square)) \\ \mathrm{Div}(\square) & 0 \end{bmatrix}}_{\mathcal{J}} \underbrace{\begin{bmatrix} e_\sigma \\ e_v \end{bmatrix}}_{e} \quad \text{in } \Omega, \tag{3.37}$$

$$\begin{pmatrix} y_\partial \\ u_\partial \end{pmatrix} = \begin{pmatrix} e_v \\ N \cdot e_\sigma \end{pmatrix} \quad \text{on } \partial\Omega. \tag{3.38}$$

Due to the quadratic Hamiltonian we obtain $(e_v, e_\sigma) = (v, \sigma)$. Now, let (v, σ) be a sufficiently regular solution of (3.37) and the BCs. Then, the variational identities[4]

$$\langle w_\sigma, \mathbb{C}^{-1}\dot{\sigma} \rangle_\Omega = \langle w_\sigma, \mathrm{sym}(\mathrm{Grad}(v)) \rangle_\Omega, \tag{3.39a}$$

$$\langle w_v, \rho \dot{v} \rangle_\Omega = -\langle \mathrm{sym}(\mathrm{Grad}(w_v)), \sigma \rangle_\Omega + \langle w_v, \underbrace{N \cdot \sigma}_{u_\partial} \rangle_{\partial\Omega} \tag{3.39b}$$

hold for all regular test functions (w_v, w_σ), and all $t \geq 0$. By testing (3.39a) with $w_\sigma = \sigma$ and (3.39b) with $w_v = v$, we obtain the power balance,

$$\begin{aligned} \dot{H}(v, \sigma) &= \langle \partial_v \mathcal{H}, \dot{v} \rangle_\Omega + \langle \partial_\sigma \mathcal{H}, \dot{\sigma} \rangle_\Omega \\ &= \langle v, N \cdot \sigma \rangle_{\partial\Omega} \\ &= \langle y_\partial, u_\partial \rangle_{\partial\Omega}. \end{aligned} \tag{3.40}$$

Since an analytical approach is not possible for most models of our above system class, the following chapters will deal with numerical methods that are suitable for accurate simulations or efficient controller designs.

[4] It follows, $\mathcal{A}_x = \begin{bmatrix} 0 & \mathrm{sym}(\mathrm{Grad}(\square)) \\ 0 & 0 \end{bmatrix}$.

3.2 Fundamentals of structure-preserving discretization

The discretization corresponds to a process, in which a continuous model is converted into its finite-dimensional counterpart. Naturally, the discrete model should retain the main properties of the original model. An algorithm that is capable of transferring the main characteristics or structure of the continuous model to the discrete level is called structure-preserving. In this section, we recall some fundamental concepts of discretization methods, which retain some characteristics of our continuous systems on the semi-discrete or fully-discrete level.

3.2.1 Spatial Galerkin approximation

In the following, we want to demonstrate a structure-preserving Galerkin approximation process with respect to our above model class, which can be summarized by the following steps: Test the evolution equations and apply an appropriate Stokes (Green) identity to obtain a weak formulation, where the corresponding boundary input data appear naturally. Project the formulation on an appropriate finite-element subspace. In other words, find $(x_h, e_h) \in (\mathscr{X}_h \times \mathscr{E}_h) \subset (\mathscr{X} \times \mathscr{E})$ such that

$$\begin{aligned}\langle w_h, \mathcal{E}\dot{x}_h\rangle_\Omega = \langle w_h, \mathcal{A}_{x_h} e_h\rangle_\Omega - \langle \mathcal{A}_{x_h} w_h, e_h\rangle_\Omega - \langle \mathcal{G}^* w_h, \mathcal{S}\mathcal{G}^* e_h\rangle_\Omega \\ + \langle w_h, \mathcal{B}u_\Omega\rangle_\Omega + \langle \mathcal{C}_\partial w_h, u_\partial\rangle_{\partial\Omega}\end{aligned} \tag{3.41}$$

$$\langle \tilde{w}_h, \mathcal{E}^* e_h\rangle_\Omega = \langle \tilde{w}_h, \partial_{x_h}\mathcal{H}\rangle_\Omega \tag{3.42}$$

hold for all $(w_h, \tilde{w}_h) \in (\mathscr{X}_h \times \mathscr{E}_h)$, where $(\mathscr{X}_h \times \mathscr{E}_h)$ denotes appropriate finite-dimensional subspaces. By choosing some basis for the approximation spaces, the above variational identities can be converted to the state equations of a finite-dimensional PH system (3.22) of the form,

$$\mathrm{E}\dot{\mathrm{x}} = (\mathrm{J}(\mathrm{x}) - \mathrm{R})\mathrm{e} + \mathrm{B}_\Omega \mathrm{u}_\Omega + \mathrm{B}_\partial \mathrm{u}_\partial, \tag{3.43a}$$

$$\mathrm{E}^\top \mathrm{e} = \partial_{\mathrm{x}} H_d, \tag{3.43b}$$

where x, e, and so on, represent the vector representations of the ansatz functions and H_d is the discrete Hamiltonian,

$$H_d = \int_\Omega \mathcal{H}(x_h)\, \mathrm{d}X. \tag{3.44}$$

Theorem 3.2. *Using the discrete outputs* $\mathrm{y}_\Omega = \mathrm{B}_\Omega^\top \partial_\mathrm{x} H_d$, $\mathrm{y}_\partial = \mathrm{B}_\partial^\top \partial_\mathrm{x} H_d$, *the above finite-dimensional system satisfies the passivity inequality due to the discrete power balance,*

$$\dot{H}_d = -\mathrm{e}^\top \mathrm{Re} + \mathrm{y}_\Omega^\top \mathrm{u}_\Omega + \mathrm{y}_\partial^\top \mathrm{u}_\partial \leq \mathrm{y}_\Omega^\top \mathrm{u}_\Omega + \mathrm{y}_\partial^\top \mathrm{u}_\partial. \tag{3.45}$$

Proof. The discrete power balance can be derived from the approximated weak formulation analogously to the continuous one or taking the time derivative of the discrete Hamiltonian. □

Remark 3.2. In case of $e = x$, it directly follows $e_h = x_h$. This makes the Galerkin approximation of the constitutive equation obsolete.

Example 3.9. In the context of linear elastodynamics, generating the semi-discrete system from (3.39), we can use standard finite element spaces, e.g., continuous Lagrange polynomials and discontinuous piecewise polynomials,

$$v_h \in [P_1(\mathcal{T}_h) \cap \mathscr{H}^1(\Omega)]^d \subset \mathscr{H}^1(\Omega; \mathbb{R}^d), \qquad \sigma_h \in P_0(\mathcal{T}_h; \mathbb{R}^{d\times d}_{\mathrm{sym}}) \subset \mathscr{L}^2(\Omega; \mathbb{R}^{d\times d}_{\mathrm{sym}}).$$

Following the mixed finite element discretization process, we obtain

$$\begin{bmatrix} \mathrm{M}_{\mathbb{C}^{-1}} & 0 \\ 0 & \mathrm{M}_\rho \end{bmatrix} \begin{bmatrix} \dot{\sigma} \\ \dot{\mathrm{v}} \end{bmatrix} = \begin{bmatrix} 0 & \mathrm{P} \\ -\mathrm{P}^\top & 0 \end{bmatrix} \begin{bmatrix} \sigma \\ \mathrm{v} \end{bmatrix} + \begin{bmatrix} 0 \\ \mathrm{B} \end{bmatrix} \mathrm{u}_\partial, \tag{3.46}$$

and the discrete Hamiltonian,

$$H_d = \frac{1}{2} \mathrm{v}^\top \mathrm{M}_\rho \mathrm{v} + \frac{1}{2} \sigma^\top \mathrm{M}_{\mathbb{C}^{-1}} \sigma. \tag{3.47}$$

So far, we only considered the structure-preserving discretization process with uniform BCs, which appear naturally in the weak formulation due to IbP. From a mechanical point of view, the type of BC is either on a velocity or traction level depending on the conservation law (balance or kinematics equation), which is integrated by parts. Enforcing non-homogeneous Dirichlet BCs in the ansatz and test spaces leads to a reduced system, which might not be compatible with the PH framework[5], see also (2.29). Therefore, discretization methods for mixed BCs have been discussed by the PH community, e.g. [29, A3]. In [29], the authors showed that the well-known Lagrange multiplier approach fits perfectly into the PH framework, see also Example 3.6 and [A2, A1].

[5] A state transformation for the reduced system similar to the split mass matrix lifting described in [16] can generate a PH state space model. Nevertheless, this new model might not preserve the original power balance.

3.2.2 Geometric numerical time integration

Now, we move on with the time integration of the semi-discrete system. In contrast to some traditional integrators, geometric numerical integrators (GNIs) respect the fundamental physics of the dynamical system. Therefore, GNIs preserve the underlying geometric structure and transfer physical properties of the continuous-time system to the discrete-time domain. Since we focus on mechanical systems, a GNI should preserve some invariants, such as, energy, momentum, or the symplectic geometry [152].

Symplectic integrators In simple words, symplecticity describes the preservation of a phase space area defined by the initial conditions. Although, symplectic methods do not conserve the system energy exactly, they have an excellent long-time behavior due to a bounded energy error [85]. It has been shown that certain Runge-Kutta schemes preserve the symplecticity. In addition, symplectic Runge-Kutta methods preserve the momentum of Hamiltonian problems [68, A1].

Variational integrators The most common GNIs are energy-momentum and variational ones. When it comes to variational integrators, one does not discretize the evolution equations but the underlying variational principle. In case of a fixed time-step size, variational integrators are symplectic and momentum-conserving. Although fixed time step variational integration methods do not preserve energy exactly, the energy error remains bounded due to their symplectic character [70, 97].

Energy-momentum integrators Energy-momentum integrators are designed in such a way that the momentum and energy of the system are conserved simultaneously. The design of energy-momentum integrators is often related to the concept of discrete gradients [63]. For Hamiltonian equations $\dot{x} = J(x)\nabla H(x)$ with $J = -J^\top$, discrete gradient methods are of the form,

$$d_\tau x = \bar{J}(x^{k+1}, x^k)\bar{\nabla} H(x^{k+1}, x^k), \tag{3.48}$$

with $\bar{J} = -\bar{J}^\top$, where the discrete gradient $\bar{\nabla} H$ satisfies consistency and directionality,

$$\bar{\nabla} H(x^k, x^k) = \nabla H(x^k), \qquad \bar{\nabla} H^\top (x^{k+1} - x^k) = H^{k+1} - H^k. \tag{3.49}$$

Although discrete gradients are not symplectic, they are very popular in the multibody and PH community [A8, 82, A9, A7].

3.3 Numerical methods for control

Due to the complexity of our mechanical systems, an analytical controller design, where we explicitly derive the control law, is hardly possible anymore. Consequently, numerical methods have became a major part of modern control design approaches. In the following, we want to highlight key concepts, which become relevant in Chapter 4.

3.3.1 Symplectic discrete-time feed-back control

In this section, we focus on a discrete-time control design strategy of finite-dimensional systems and its associated time integration. Therefore, we recapitulate the controller discretization process presented in [A10]. The main interest of this article is a systematic discrete-time energy-based control design of fully actuated mechanical systems to cover the sampling process. In summary, the approach is based on a description of the sampled control system with zero-order hold mechanism using the implicit midpoint rule, which is a second-order accurate sypmplectic integration method. Correspondingly, the discrete-time target dynamics are generated by the same scheme. In order to convert the control system into the target dynamics, an implicit controller with the same structure as the continuous one is required.

Example 3.10. To demonstrate the process clearly, let us consider Example 3.7 with the finite-dimensional control system (2.4) and the input $u = u_{\mathrm{es}}(q) + u_{\mathrm{di}}(q,p)$, which converts the control system to the target dynamics,

$$\begin{bmatrix} \dot{q} \\ \dot{p} \end{bmatrix} = \begin{bmatrix} 0 & I \\ -I & -D \end{bmatrix} \begin{bmatrix} \partial_q H_d(q,p) \\ \partial_p H_d(q,p) \end{bmatrix}. \tag{3.50}$$

Applying the implicit midpoint[6] rule to (2.4), we obtain[7]

$$\begin{bmatrix} d_\tau q \\ d_\tau p \end{bmatrix} = \begin{bmatrix} 0 & I \\ -I & 0 \end{bmatrix} \begin{bmatrix} \partial_q H(q^{k+\frac{1}{2}}, p^{k+\frac{1}{2}}) \\ \partial_p H(q^{k+\frac{1}{2}}, p^{k+\frac{1}{2}}) \end{bmatrix} + \begin{bmatrix} 0 \\ I \end{bmatrix} u^k. \tag{3.51}$$

Matching (3.51) with the implicit midpoint rule discretization of the target dynamics given by

$$\begin{bmatrix} d_\tau q \\ d_\tau p \end{bmatrix} = \begin{bmatrix} 0 & I \\ -I & 0 \end{bmatrix} \begin{bmatrix} \partial_q H_d(q^{k+\frac{1}{2}}, p^{k+\frac{1}{2}}) \\ \partial_p H_d(q^{k+\frac{1}{2}}, p^{k+\frac{1}{2}}) \end{bmatrix}, \tag{3.52}$$

[6] We use the notation $x^{k+\frac{1}{2}} := \frac{1}{2}(x^{k+1} + x^k)$.

[7] We use $u^{k+\frac{1}{2}} = u^k$ to approximate the zero-order hold mechanism.

yields the implicit control law,

$$u^k = u_{\mathrm{es}}(q^{k+\frac{1}{2}}) + u_{\mathrm{di}}(q^{k+\frac{1}{2}}, p^{k+\frac{1}{2}}), \tag{3.53}$$

which retains the structure of its continuous counterpart. In order to obtain a causal controller, (3.52) is solved for $(q^{k+\frac{1}{2}}, p^{k+\frac{1}{2}})$, where (q^k, p^k) denotes the corresponding measurement at the current time-step. Inserting the result into (3.53) yields a causal control law. Compared to a quasi-continuous control law $u^k = u_{\mathrm{es}}(q^k) + u_{\mathrm{di}}(q^k, p^k)$, the above controller (3.53) can be implemented in a digital control-loop with lower sampling rates.

The validation of the control concept using an experimental light-weight robot is given in [A4].

3.3.2 Optimal feed-forward control

In the following, we briefly mention the basics of (open-loop) optimal control. The term *optimal control* corresponds to a problem, where one has to find an input function of a control system that minimizes a given cost functional [131]. In other words, among all states $x(t) \in \mathbb{R}^n$ and input vectors $u(t) \in \mathbb{R}^m$, that fulfill

$$\dot{x} = f(x, u) \quad \text{and} \quad x(t_i) = x_i,\ x(t_e) = x_e, \tag{3.54}$$

find those that minimize the cost functional,

$$J = \frac{1}{2} \int_{t_i}^{t_e} g(x, u)\ \mathrm{d}t. \tag{3.55}$$

Solving these problems[8] usually requires numerical methods. Indirect and direct methods are the two major classes for solving optimal control problems numerically. In a direct approach the state and input is discretized leading to a nonlinear optimization problem, which can be solved using standard optimization techniques. In other words, the infinite-dimensional optimization problem is transferred to a finite-dimensional one. Indirect methods are based on optimality conditions derived from the Euler-Lagrange equations. Accordingly, they convert the optimal control problem to a multiple-boundary value problem, which can be solved using discretization methods like finite differences [123, 131]. In the following, we only consider the indirect approach. This is motivated by the fact that our finite element models have constant mass matrices, which facili-

[8] More complex optimal control problems are given in the literature, e.g., [10].

tates the derivation of optimality conditions, see Example 3.11. In order to derive the optimality conditions, we use the Lagrange functional,

$$L = J + \int_{t_i}^{t_e} \lambda^\top (f(x,u) - \dot{x}) \, \mathrm{d}t \tag{3.56}$$

with the Lagrange multiplier $\lambda \in \mathbb{R}^n$. Following the standard variational approach using the Euler-Lagrange equations, we obtain the optimality conditions,

$$\dot{x} = f(x,u), \tag{3.57}$$
$$\dot{\lambda} = -\partial_x g(x,u) - \partial_x f(x,u)\lambda, \tag{3.58}$$
$$0 = \partial_u g(x,u) + \partial_u f(x,u)\lambda, \tag{3.59}$$

which, together with the given initial and final conditions, formulate the multiple-boundary value problem.

Example 3.11. Let us consider the finite element model,

$$M\ddot{\varphi} + k(\varphi) = Bu, \tag{3.60}$$

of a geometrically exact string, see also Example 2.2 and 2.4. In order to generate a trajectory tracking controller for the above model, we can minimize the cost functional,

$$J = \frac{1}{2} \int_{t_i}^{t_e} (y - y_d)^\top Q (y - y_d) + u^\top u \, \mathrm{d}t, \quad Q \geq 0, \tag{3.61}$$

where $y = C\varphi$ denotes the output and y_d its reference [4]. The corresponding optimality conditions[9],

$$M\ddot{\varphi} + k(\varphi) = Bu, \tag{3.62}$$
$$M^\top \ddot{\lambda} + \partial_q k(\varphi)\lambda = C^\top Q(C\varphi - y_d), \tag{3.63}$$
$$-B^\top \lambda = u, \tag{3.64}$$

and the initial, and final conditions,

$$\varphi(t_i) = \varphi_i, \quad \dot{\varphi}(t_i) = v_i, \quad \varphi(t_e) = \varphi_e, \quad \dot{\varphi}(t_e) = v_e, \tag{3.65}$$

define the multiple-boundary value problem. Solving this multiple-boundary value problem with space-time finite elements is demonstrated in [A5].

[9] Note that the second-order control system (3.62) leads to a second-order adjoint system (3.63).

4 Summary of publications

In this chapter, we summarize the main results of the publications [A3, A2, A5, A1, A4], which are given in Appendix A.

On the velocity-stress formulation for geometrically nonlinear elastodynamics and its structure-preserving discretization

This paper [A1] is motivated by the PH representation and structure-preserving discretization of linear elastodynamics using a velocity-stress formulation. We extend the formulation to the general equations of geometrically nonlinear elastodynamics and demonstrate how a systematic structure-preserving approximation preserves characteristics on the semi- and fully-discrete level.

Therefore, we consider the St. Venant–Kirchhoff material, which represents a geometrically nonlinear generalization of Hooke's law and is characterized by a linear stress-strain relation, $S = \mathbb{C} : E$, with the fourth order stiffness tensor $\mathbb{C}$. This enables a velocity-stress formulation describing the essential system dynamics,

$$\begin{bmatrix} \mathbb{C}^{-1}\dot{S} \\ \rho\dot{v} \end{bmatrix} = \begin{bmatrix} 0 & \operatorname{sym}(F^\top(q) \cdot \operatorname{Grad}(\square)) \\ \operatorname{Div}(F(q) \cdot \square) & 0 \end{bmatrix} \begin{bmatrix} S \\ v \end{bmatrix} + \begin{bmatrix} 0 \\ I \end{bmatrix} b, \qquad \dot{q} = v. \tag{4.1}$$

Similar to the well-studied linear setting[1], the formulation has an underlying PH structure with the state variables (v, S, q). Due to the choice of state variables, the Hamiltonian

$$H(v, S) = \frac{1}{2}\langle v, \rho v\rangle_\Omega + \frac{1}{2}\langle S, \mathbb{C}^{-1} : S\rangle_\Omega \tag{4.2}$$

has a quadratic form and yields linear constitutive equations. The nonlinearity is shifted to the structural operator, which is modulated by the displacement field. The evolution equations of velocity and stress can be expressed in terms of a weak formulation, where Dirichlet BCs are incorporated via Lagrange multipliers and Neumann ones naturally.

[1] Substituting $F(q)$ with the identity matrix I leads to the velocity-stress formulation of linear elastodynamics, which is governed by the Cauchy stress σ instead of S, see Example 3.8.

The variational identities are satisfied by smooth solutions and encode the balance of energy and momentum.

Following a Galerkin projection in space the basic system structure and characteristics are preserved automatically. Due to the Lagrange multiplier enforcing the Dirichlet BCs, the semi-discrete system has differential-algebraic structure of index $\nu \geq 2$, see also Example 3.6. Additionally, the geometric structure and corresponding energy balance can be preserved on the fully-discrete level by appropriate time discretization methods. E.g., applying the implicit midpoint rule to the velocity and stress field, and approximating the discrete displacements on a staggered grid, we obtain the discrete-time energy balance, where only a single linear system has to be solved in every time iteration. This might be helpful for real-time capable application. A fully implicit midpoint rule has an additional computational effort but leads to an improved angular momentum balance.

The paper concludes with a simulation of a rubber-type body, which can be implemented efficiently using open software, e.g., FEniCS [91, 99]. The numerical experiment confirms the above statements.

Port-Hamiltonian FE models for filaments

Adding additional model assumptions to the general equations of geometrically nonlinear elastodynamics, several models, e.g., plates, beams, and strings, can be derived [165]. Solving the initial value problems of these models requires less computational effort than solving the general equations. In [A2], we present the PH formulation and structure-preserving discretization of an elastic string. The strings of this paper are classified as geometrically nonlinear mechanical systems. Therefore, the system description includes a linear relationship between normal force and nonlinear strain.

The original PH representation of the string is expressed in terms of linear momenta, positions, and the strain. Due to the choice of state variables, we obtain a quadratic Hamiltonian and correspondingly linear constitutive equations. The linear relationship between energy and co-energy variables enables a port-Hamiltonian representation with the new state vector including velocities, positions, and the normal force. Therefore, we obtain a velocity-stress formulation with a formally skew-adjoint structure operator modulated by the positions.

Using a spatial Galerkin approximation with mixed finite elements, the semi-discrete model preserves its PH character. Furthermore, the discrete Hamiltonian is still quadratic and leads to the expected power balance, where power is transferred through the system boundary. A conservative behavior in case of homogeneous BCs is demonstrated with a numerical experiment.

In the appendix of this paper, the PH formulation and its structure-preserving spatial discretization process of an inextensible string is given. Due to the algebraic constraint of no strain, the infinite-dimensional system includes a positive semi-definite operator $\mathcal{E}$.

Explicit port-Hamiltonian FEM-models for linear mechanical systems with non-uniform boundary conditions

In the above publications, we analyzed the PH velocity-stress formulation of nonlinear elastodynamics and its structure-preserving discretization. In order to treat non-uniform or mixed boundary conditions, we incorporated Dirichlet BCs via Lagrange multipliers and Neumann ones naturally into the weak form. Consequently, the subsequent Galerkin approximation yields differential algebraic equations (DAEs), i.e., an implicit PH system. Although there exists a rich theory about DAEs, from a numerical point of view, it might be more appealing to deal with ordinary differential equations (ODEs), i.e., explicit systems. Additionally, control theory offers a much wider range of tools for explicit than implicit systems. Consequently, there remains an interest to generate explicit PH state space models.

In [A3], we provided a weak formulation with mixed BCs, whose approximation leads to an explicit PH system. We considered the well-known velocity-stress formulation of linear elastodynamics and modify its weak form by replacing the Lagrange multiplier λ enforcing Dirichlet BCs and its corresponding test function by their physical interpretations with respect to the principle of virtual power. In other words, find (σ, v) such that

$$\langle w_\sigma, \mathbb{C}^{-1}\dot{\sigma}\rangle_\Omega = \langle w_\sigma, \operatorname{sym}(\operatorname{Grad}(v))\rangle_\Omega + \langle \underbrace{w_\lambda}_{N\cdot w_\sigma}, v_D - v\rangle_{\partial\Omega_D}, \tag{4.3}$$

$$\langle w_v, \rho\dot{v}\rangle_\Omega = -\langle \operatorname{sym}(\operatorname{Grad}(w_v)), \sigma\rangle_\Omega + \langle w_v, \underbrace{\lambda}_{N\cdot\sigma}\rangle_{\partial\Omega_D} + \langle w_v, \tau_N\rangle_{\partial\Omega_N}, \tag{4.4}$$

holds for all regular test functions (w_σ, w_v). This variational formulation is reminiscent of the generalized Hellinger-Reissner principle, where Dirichlet BCs are imposed weakly. Discretizing our modified weak formulation with standard mixed finite elements leads to an explicit PH state space model without Lagrange multipliers or penalty terms. This weak formulation can be easily implemented in a open finite element software.

The paper is concluded with numerical experiments using an one-dimensional rod. The results confirm conservative behavior in case of homogeneous BCs. Moreover, the eigenvalues of semi-discrete system are close to the exact ones. Nevertheless, the approach is less accurate than the strong imposition of Dirichlet BCs. Another point worth mentioning is an additional zero eigenvalue of the semi-discrete system due to weak imposition of the Dirichlet BC. Its influence and the associated problems are discussed in the next chapter.

Symplectic discrete-time control of flexible-joint robots: Experiments with two links

This article [A4] builds upon the control approach proposed in [A10], whose key concept is recalled in Section 3.3. More precisely, the symplectic discrete-time controller of [A10], initially presented for fully actuated systems, is applied to a serial robot manipulator with flexible joints. In contrast to [A10], we demonstrate the applicability of the approach to an underactuated control system. In addition, the results stem from experiments with a light-weight robot.

The entire control structure of the flexible-joint robot is divided into joint torque control shaping the motor inertia and joint position control for trajectory tracking. The outer loop position controller corresponds to a PD+ control law and runs with a lower sampling rate than the inner loop torque controller. Therefore, the time discretization process is only applied to the outer control loop and the robot manipulator plus the torque controller are regarded as our control system (3.51). Similar to [A11], we use piecewise constant inputs (zero order hold) and an equidistant sampling time. The entire control structure is realized with a Matlab/Simulink interface and a simple Newton method is applied to solve (3.52) for the implicit control law (3.53).

In several experiments, the performance of the symplectic controller is compared to the quasi-continuous one, where the sampling rate and the closed loop stiffness are varied. The discrete L^2 norms of the position error and the deviation of the input from the nominal trajectory are selected as measures of performance. The experimental results suggest superiority of the symplectic controller for low sampling rates. In addition, the symplectic controller allows an increase of the closed loop stiffness before it runs with the same performance as the quasi-continuous one. Consequently, the experiments confirm original statements given in [A10].

The article concludes with the implementation of a pure position feedback according to [A10]. Thereby, things become more challenging in case of measurement noise. Due to the numerical differentiation, high-frequency noise is amplified and could damage the robot drive system. Filtering the position values using a discrete PT1 element can already provide a remedy here. Consequently, the filtered pure position feedback leads to a similar performance as the original symplectic controller, but a proper choice of the filter time constant is required.

Optimal trajectory control of geometrically exact strings with space-time finite elements

In this article [A5], we consider a space-time variational formulation, which generates an optimal feed-forward tracking controller for geometrically exact strings. Accordingly, the control law minimizes a cost functional including the desired trajectory. More precisely, the input force acting at the one end should transfer the string from an initial configuration to a final one, whereby the opposite end of the string should follow a desired trajectory as precisely as possible.

The optimization problem is solved with an indirect approach, where a space-time Galerkin approximation with finite elements translates the problem to a set of algebraic equations. Due to the specific structure of the variational formulation, only the positional field and the corresponding adjoint variable field are approximated by continuous shape functions. Therefore, defining a finite element subspace for the (adjoint) velocity field is not required. In addition, the approximation is based on a structured rectangular mesh (with quadrilateral elements) and uses continuous bilinear Lagrange polynomials of space and time, which enables an implementation with commercial or open source finite element packages. The approximation process with these specific basis functions can be interpreted as a sequential space-time discretization. Therefore, the entire approach corresponds to a multiple-shooting method for solving the optimality conditions based on the semi-discrete problem.

The paper also contains a numerical experiment, in which we consider a planar motion of a geometrically exact string under gravity. The string performs a finite time transition between two stationary set-points, where we use a desired output trajectory with sufficiently large pre- and post actuation phases. In order to verify our results, the generated control law is applied to a initial value problem simulation. Its results confirm the applicability of our approach.

5 Discussion and future work

In this chapter, we discuss our contributions mentioned in Section 1.3. Therefore, we recapitulate our results and discuss their practical relevance. In addition, we mention further articles which are based on or related to our contributions. The discussion is split into three different topics containing modeling, feed-back, and feed-forward control of flexible mechanical systems.

- Motivated by the PH framework, in [A1], we considered the motion of a geometrically nonlinear elastic continuum by means of a velocity-stress formulation. The governing equations form a PH system in which the structure operator is modulated by the displacement field. The PH character is also highlighted in the weak formulation of the problem, in which the conservative energy transfer and the corresponding boundary ports become even clearer than in the strong form. In addition, major characteristics of the governing system can be derived by testing the weak formulation with the corresponding test function. E.g., testing the weak form with the effort or co-energy variables yields the energy balance directly. Following a Galerkin projection in space, the PH structure of the system is preserved automatically. Thus, the original characteristics can be proven on the semi-discrete level analogous to the continuous case. Another advantage of the formulation is its compatibility with standard finite element spaces for the Galerkin approximation, which facilitates the incorporation into available software. Additionally, the formulation is compatible with Pian-Sumihara-typed finite elements [128] reducing or circumventing locking effects [159]. Using appropriate time integration methods, power and momentum balance can also be preserved on the fully-discrete level. Due to the quadratic character of the Hamiltonian, the implicit midpoint rule is a valid candidate. In [33], the authors confirmed our results using a velocity-stress formulation modulated by the deformation gradient.

  Since several equations of geometrically nonlinear shells, beams, and strings have been developed, our insights gained in [A1] can be transferred to these models as well. E.g., in [A2], we discussed the velocity-stress formulation of a geometrically exact string. Following the same systematic approximation procedure as in [A1], a

semi-discrete PH state space model of a similar structure as in [35, A1] is obtained. Consequently, the implicit midpoint rule preserves the energy balance on the fully-discrete level. In [34], the authors recapitulate the numerical strategy for the simulation of geometrically nonlinear structures based on a general velocity-stress formulation modulated by the displacement field.

Due to their simplicity, our formulations might be employed across various fields including system identification, model order reduction, and control. Nevertheless, the equations of geometrically nonlinear elastodynamics are valid for large displacements and moderate strains. In order, to simulate large strains accurately a nonlinear material behavior becomes mandatory. Therefore, we enhanced our previous work [A2] with respect to material nonlinearities and proposed a PH formulation for hyperelastic strings in [A7]. Due to the nonlinear relationship between stress and strain, a Galerkin approximation of the corresponding constitutive equation is required. Accordingly, we applied a discrete gradient scheme to achieve an energy-consistent time integration. The analogy to finite-dimensional (lumped-parameter) systems is given in [A9]. In [A8], we extended on [A7] by adding viscoelasticity. The overall model results from a interconnection of two PH subsystems, the purely elastic string [A7] and generalized Maxwell elements [153]. Extending these results to general three-dimensional continua might be part of future research projects.

In [A4], we proposed a structure-preserving discretization procedure for PH models with mixed BCs to obtain explicit semi-discrete systems. Although, the numerical results seem to verify the approach there are some serious drawbacks. As already mentioned, the approach performs rather poorly compared with the strong imposition of Dirichlet BCs. Moreover, the (spurious) zero eigenvalue is a result of an unstable spatial discretization. Consequently, the corresponding eigenvector might cause an unphysical behavior. Even though, the approach lacks convergence it might produce sufficient results and is mentioned in several articles, e.g. [30, A11, 129].

- In [A10, A4], we presented and verified a discrete-time control design approach reducing the deteriorating effects caused by the sampling process on stability and performance in a digital control loop. Therefore, at low sampling rates, our approach provides a better performance than a direct implementation (in a piecewise constant manner) of the continuous control law, which corresponds to discrete-time controller design based on a first-order explicit Euler discretization. This increase

in performance results from a second-order accurate discrete-time representation of the sampling process and target dynamics stemming from an application of the implicit midpoint rule. Due to the choice of the implicit midpoint rule, the control law matching the discrete system and target dynamics, retains the original structure of the continuous control law. More precisely, continuously derived nonlinear control laws can be reused in discrete-time with only replacing the arguments by predicted stage values on the following interval. Alternatively, other second-order accurate integration schemes, like the midpoint discrete gradient, might lead to a similar performance as the implicit midpoint rule. However, these do not necessarily preserve the original structure of the continuous-time controller. E.g., gradient vectors of the original and the target energies might be replaced with the discrete gradients [A10]. Nevertheless, the implicit nature of the control law requires the numerical solution of an in general nonlinear system of algebraic equations (discrete-time target dynamics) in every time-step. Accordingly, analyzing computation times for large scale systems is mandatory to show real-time capability. In addition, the system of algebraic equations explicitly depends on the measurement of the entire state vector. Thus, our control law corresponds to a state feed-back, even if the original controller may only require a part of the state. However, the increased implementation effort might be justified by the absence of expensive high-frequency sensors.

Based on the results of [A10], several research articles have been developed in recent years. In [88], the authors extended our approach to s-stage Gauss-Legendre collocation with higher order input shaping. In [87], the authors discussed discrete-time controllers based on cubic Hermite interpolation or 3-stage Lobatto IIIA collocation. Mogler et al. [108] translated CbI to the discrete-time setting using energy-preserving collocation methods. Recently, Hermite-Obreschkoff methods were presented in the context of discrete-time passivity-based control [169].

- In [A5], we presented an optimal trajectory feed-forward controller for geometrically exact strings. The optimal control approach is motivated by the fact that it does not require the explicit analysis of semi-discrete equations of motion and the corresponding internal dynamics. Therefore, we define a Lagrange functional on a space-time domain and derive the variational identities or optimality conditions. Due to the constant mass inertia, the derivation of the variational identities is simple. In addition, they show us how to introduce BCs properly. In order to discretize the weak formulation, standard or open source finite element packages can

be used. Since we only consider structured finite element meshes, the optimality conditions might also be derived using the semi-discrete system. Our approach includes the solving of an in general nonlinear system of algebraic equation. Accordingly, the solution depends heavily on the choice of initial values. In addition, a large number of elements increases the computing time, which is incompatible with the real-time capability required for model predictive control.

In future research, our approach might be extended to three-dimensional continua. Additionally, we have not considered the challenges or advantages of unstructured space-time finite element meshes yet. Finally, it should be mentioned that we plan to apply our approach with alternative cost functions and systems of other physical disciplines.

The next step is to combine the methods of this thesis in a two degree of freedom control structure and validate them in an experimental setup, e.g., an overhead crane.

References

Own Publications

[A1] T. Thoma, P. Kotyczka, and H. Egger. On the velocity-stress formulation for geometrically nonlinear elastodynamics and its structure-preserving discretization. *Mathematical and Computer Modelling of Dynamical Systems,* 30.1 (2024), 701–720 (cf. pp. 3, 18, 27, 30, 31, 35, 41, 42, 61).

[A2] T. Thoma and P. Kotyczka. Port-Hamiltonian FE models for filaments. *IFAC-PapersOnLine,* 55.30 (2022), 353–358 (cf. pp. 3, 14, 27, 30, 35, 37, 41, 42, 82).

[A3] T. Thoma and P. Kotyczka. Explicit Port-Hamiltonian FEM-Models for Linear Mechanical Systems with Non-Uniform Boundary Conditions. *IFAC-PapersOnLine,* 55.20 (2022), 499–504 (cf. pp. 3, 30, 35, 38, 89).

[A4] T. Thoma, X. Wu, A. Dietrich, and P. Kotyczka. Symplectic Discrete-Time Control of Flexible-Joint Robots: Experiments with Two Links. *IFAC-PapersOnLine,* 54.19 (2021), 1–7 (cf. pp. 3, 33, 35, 39, 42, 96).

[A5] T. Thoma and P. Kotyczka. Optimal Trajectory Control of Geometrically Exact Strings with Space-Time Finite Elements. In: *2025 European Control Conference (ECC).* IEEE, 2025, 719–724 (cf. pp. 3, 14, 18, 34, 35, 40, 43, 104).

[A6] T. Thoma and P. Kotyczka. Structure preserving discontinuous Galerkin approximation of one-dimensional port-Hamiltonian systems. *IFAC-PapersOnLine,* 56.2 (2023), 6783–6788 (cf. p. 5).

[A7] P. L. Kinon, T. Thoma, P. Betsch, and P. Kotyczka. Port-Hamiltonian formulation and structure-preserving discretization of hyperelastic strings (2023) (cf. pp. 14, 27, 31, 42).

[A8] P. Kinon, T. Thoma, P. Betsch, and P. Kotyczka. Generalized Maxwell viscoelasticity for geometrically exact strings: Nonlinear port-Hamiltonian formulation and structure-preserving discretization. *IFAC-PapersOnLine,* 58.6 (2024), 101–106 (cf. pp. 14, 27, 31, 42).

[A9] P. L. Kinon, T. Thoma, P. Betsch, and P. Kotyczka. Discrete nonlinear elastodynamics in a port-Hamiltonian framework. *PAMM,* 23.3 (2023) (cf. pp. 31, 42).

[A10] P. Kotyczka and T. Thoma. Symplectic discrete-time energy-based control for nonlinear mechanical systems. *Automatica,* 133 (2021), 109842 (cf. pp. 32, 39, 42, 43).

[A11] P. Kotyczka and T. Thoma. From discrete modeling to explicit FE models for port-Hamiltonian systems of conservation laws. *IFAC-PapersOnLine,* 55.30 (2022), 412–417 (cf. pp. 39, 42).

Other Publications

[1] K. Abidi and J.-X. Xu. *Advanced Discrete-Time Control: Designs and Applications*. Springer Singapore, 2015 (cf. p. 5).

[2] J. Ackermann. *Sampled-Data Control Systems*. Springer Berlin Heidelberg, 1985 (cf. p. 5).

[3] M. S. Alnæs, A. Logg, K. B. Ølgaard, M. E. Rognes, and G. N. Wells. Unified form language: A domain-specific language for weak formulations of partial differential equations. *ACM Transactions on Mathematical Software,* 40.2 (2014), 1–37 (cf. p. 8).

[4] R. Altmann and J. Heiland. Simulation of multibody systems with servo constraints through optimal control. *Multibody System Dynamics,* 40.1 (2016), 75–98 (cf. pp. 7, 34).

[5] S. S. Antman. *Nonlinear Problems of Elasticity*. Springer New York, 1995 (cf. p. 12).

[6] S. Aoues, D. Matignon, and D. Alazard. Control of a flexible spacecraft using discrete IDA-PBC design. *IFAC-PapersOnLine,* 48.13 (2015), 188–193 (cf. p. 6).

[7] D. N. Arnold. Stability, Consistency, and Convergence of Numerical Discretizations. In: *Encyclopedia of Applied and Computational Mathematics*. Springer Berlin Heidelberg, 2015, 1358–1364 (cf. p. 3).

[8] D. N. Arnold and J. J. Lee. Mixed methods for elastodynamics with weak symmetry. *SIAM J. Numer. Anal.* 52 (2014), 2743–2769 (cf. p. 4).

[9] V. I. Arnold. *Mathematical Methods of Classical Mechanics*. Springer New York, 1978 (cf. p. 4).

[10] L. T. Ashchepkov, D. V. Dolgy, T. Kim, and R. P. Agarwal. *Optimal Control*. Springer International Publishing, 2021 (cf. p. 33).

[11] I. A. Baratta, J. P. Dean, J. S. Dokken, M. Habera, J. S. Hale, C. N. Richardson, M. E. Rognes, M. W. Scroggs, N. Sime, and G. N. Wells. *DOLFINx: The next generation FEniCS problem solving environment*. en. 2023 (cf. p. 8).

[12] G. Bastos, R. Seifried, and O. Brüls. Inverse dynamics of serial and parallel underactuated multibody systems using a DAE optimal control approach. *Multibody System Dynamics,* 30.3 (2013), 359–376 (cf. p. 7).

[13] G. Bastos, R. Seifried, and O. Brüls. Analysis of stable model inversion methods for constrained underactuated mechanical systems. *Mechanism and Machine Theory,* 111 (2017), 99–117 (cf. p. 7).

[14] E. Bécache, P. Joly, and C. Tsogka. A new family of mixed finite elements for the linear elastodynamic problem. *SIAM J. Numer. Anal.* 39 (2002), 2109–2132 (cf. p. 4).

[15] A. Bendimerad-Hohl, G. Haine, D. Matignon, and B. Maschke. Structure-preserving discretization of a coupled Allen-Cahn and heat equation system. *IFAC-PapersOnLine,* 55.18 (2022), 99–104 (cf. p. 5).

[16] P. Benner and J. Heiland. Time-dependent Dirichlet conditions in finite element discretizations. *ScienceOpen Research,* 0.0 (2015) (cf. pp. 17, 30).

[17] W. Blajer and K. Kołodziejczyk. A Geometric Approach to Solving Problems of Control Constraints: Theory and a DAE Framework. *Multibody System Dynamics,* 11.4 (2004), 343–364 (cf. p. 7).

[18] A. M. Bloch, M. Leok, J. E. Marsden, and D. V. Zenkov. Controlled Lagrangians and potential shaping for stabilization of discrete mechanical systems. In: *Proceedings of the 45th IEEE Conference on Decision and Control*. 2006, 3333–3338 (cf. p. 5).

[19] D. Boffi, F. Brezzi, L. F. Demkowicz, R. G. Durán, R. S. Falk, and M. Fortin. *Mixed Finite Elements, Compatibility Conditions, and Applications: Lectures given at the C.I.M.E. Summer School held in Cetraro, Italy June 26–July 1, 2006*. Ed. by D. Boffi and L. Gastaldi. Springer Berlin Heidelberg, 2008 (cf. p. 3).

[20] D. Boffi, F. Brezzi, and M. Fortin. *Mixed Finite Element Methods and Applications*. Springer Berlin Heidelberg, 2013 (cf. p. 18).

[21] B. Bona, M. Indri, and A. Tornambe. Flexible piezoelectric structures-approximate motion equations and control algorithms. *IEEE Transactions on Automatic Control,* 42.1 (1997), 94–101 (cf. p. 5).

[22] J. Bonet and R. D. Wood. *Nonlinear Continuum Mechanics for Finite Element Analysis*. Cambridge University Press, 2008 (cf. p. 12).

[23] F. Brezzi. A Survey of Mixed Finite Element Methods. In: *Finite Elements*. Springer New York, 1988, 34–49 (cf. p. 3).

[24] A. Brugnoli, D. Alazard, V. Pommier-Budinger, and D. Matignon. A Port-Hamiltonian formulation of linear thermoelasticity and its mixed finite element discretization. *J. Thermal Stresses,* 44 (2021), 643–661 (cf. pp. 4, 5).

[25] A. Brugnoli and V. Mehrmann. On the discrete equivalence of Lagrangian, Hamiltonian and mixed finite element formulations for linear wave phenomena. *IFAC-PapersOnLine,* 58.6 (2024), 95–100 (cf. p. 18).

[26] A. Brugnoli, D. Alazard, V. Pommier-Budinger, and D. Matignon. Port-Hamiltonian formulation and symplectic discretization of plate models Part I: Mindlin model for thick plates. *Appl. Math. Model.* 75 (2019), 940–960 (cf. pp. 5, 26).

[27] A. Brugnoli, D. Alazard, V. Pommier-Budinger, and D. Matignon. Port-Hamiltonian formulation and symplectic discretization of plate models Part II: Kirchhoff model for thin plates. *Appl. Math. Model.* 75 (2019), 961–981 (cf. pp. 5, 26).

[28] A. Brugnoli, D. Alazard, V. Pommier-Budinger, and D. Matignon. Port-Hamiltonian flexible multibody dynamics. *Multibody Syst. Dyn.* 51 (2021), 343–375 (cf. p. 5).

[29] A. Brugnoli, F. L. Cardoso-Ribeiro, G. Haine, and P. Kotyczka. Partitioned finite element method for structured discretization with mixed boundary conditions. *IFAC-PapersOnLine,* 53.2 (2020), 7557–7562 (cf. p. 30).

[30] A. Brugnoli, G. Haine, and D. Matignon. Explicit structure-preserving discretization of port-Hamiltonian systems with mixed boundary control. *IFAC-PapersOnLine,* 55.30 (2022), 418–423 (cf. p. 42).

[31] A. Brugnoli, G. Haine, and D. Matignon. Stokes-Dirac structures for distributed parameter port-Hamiltonian systems: An analytical viewpoint. *Communications in Analysis and Mechanics,* 15.3 (2023), 362–387 (cf. p. 26).

[32] A. Brugnoli and D. Matignon. A port-Hamiltonian formulation for the full von-Kármán plate model. In: *10th European Nonlinear Dynamics Conference (ENOC).* 2022 (cf. pp. 5, 26).

[33] A. Brugnoli, D. Matignon, and J. Morlier. Exact energy-conserving and linear discretization scheme for geometrically non-linear models. In: *Proceedings of the 16ème Colloque National en Calcul des Structures.* Giens, France, 2024 (cf. p. 41).

[34] A. Brugnoli, D. Matignon, and J. Morlier. A linearly-implicit energy-momentum preserving scheme for geometrically nonlinear mechanics based on non-canonical Hamiltonian formulations. *Nonlinear Dynamics,* (2025) (cf. p. 42).

[35] A. Brugnoli, R. Rashad, F. Califano, S. Stramigioli, and D. Matignon. Mixed finite elements for port-Hamiltonian models of von-Kármán beams. *IFAC-PapersOnLine,* 54 (2021), 186–191 (cf. pp. 5, 26, 42).

[36] O. Brüls, G. J. Bastos, and R. Seifried. A Stable Inversion Method for Feedforward Control of Constrained Flexible Multibody Systems. *Journal of Computational and Nonlinear Dynamics,* 9.1 (2013) (cf. p. 7).

[37] F. L. Cardoso-Ribeiro, G. Haine, Y. Le Gorrec, D. Matignon, and H. Ramirez. Port-Hamiltonian formulations for the modeling, simulation and control of fluids. *Computers and Fluids,* 283 (2024), 106407 (cf. pp. 5, 26).

[38] F. L. Cardoso-Ribeiro, D. Matignon, and L. Lefèvre. A structure-preserving Partitioned Finite Element Method for the 2D wave equation. *IFAC-PapersOnLine,* 51.3 (2018), 119–124 (cf. p. 5).

[39] F. L. Cardoso-Ribeiro, D. Matignon, and L. Lefèvre. A partitioned finite element method for power-preserving discretization of open systems of conservation laws. *IMA J. Math. Control Inform.* 38 (2021), 493–533 (cf. p. 5).

[40] D. Chen and B. Paden. Stable inversion of nonlinear non-minimum phase systems. *International Journal of Control,* 64.1 (1996), 81–97 (cf. p. 7).

[41] Y. Chen. Frequency response of discrete-time robot systems–Limitations of PD controllers and improvements by lag-lead compensation. In: *Proceedings. 1987 IEEE International Conference on Robotics and Automation.* Institute of Electrical and Electronics Engineers, 1987 (cf. p. 5).

[42] R. W. Clough. Original formulation of the finite element method. *Finite Elements in Analysis and Design,* 7.2 (1990), 89–101 (cf. p. 3).

[43] G. C. Cohen. *Higher-order numerical methods for transient wave equations.* Scientific Computation. Springer-Verlag, Berlin, 2002 (cf. p. 4).

[44] R. Courant. Variational methods for the solution of problems of equilibrium and vibrations. *Bulletin of the American Mathematical Society,* 49 (1943), 1–23 (cf. p. 3).

[45] P. Crouch. *Spacecraft attitude control and stabilization: Applications of geometric control theory to rigid body models.* 1984 (cf. p. 4).

[46] H. Czichos. *Mechatronik: Grundlagen und Anwendungen technischer Systeme.* Springer Fachmedien Wiesbaden, 2019 (cf. p. 2).

[47] J. C. Datz, I. Steinbrecher, C. Meier, N. Hagmeyer, L.-C. Engel, A. Popp, M. R. Pfaller, H. Schunkert, and W. A. Wall. Patient-specific coronary angioplasty simulations — A mixed-dimensional finite element modeling approach. *Computers in Biology and Medicine,* 189 (2025), 109914 (cf. p. 2).

[48] S. Drücker and R. Seifried. Application of stable inversion to flexible manipulators modeled by the absolute nodal coordinate formulation. *GAMM-Mitteilungen,* 46.1 (2023) (cf. p. 7).

[49] S. Drücker and R. Seifried. Trajectory-tracking control from a multibody system dynamics perspective. *Multibody System Dynamics,* 58.3–4 (2023), 341–363 (cf. p. 7).

[50] V. Duindam, A. Macchelli, S. Stramigioli, and H. Bruyninckx, eds. *Modeling and control of complex physical systems.* Springer-Verlag, Berlin, 2009, xxvi+423 (cf. p. 4).

[51] H. Egger, O. Habrich, and V. Shashkov. On the energy stable approximation of Hamiltonian and gradient systems. *Comput. Methods Appl. Math.* 21 (2021), 335–349 (cf. p. 5).

[52] A. Falaize and T. Hélie. Passive Guaranteed Simulation of Analog Audio Circuits: A Port-Hamiltonian Approach. *Appl. Sci.* 6 (2016), 273 (cf. p. 5).

[53] O. Farle, D. Klis, M. Jochum, O. Floch, and R. Dyczij-Edlinger. A port-Hamiltonian finite-element formulation for the Maxwell equations. In: *Proc. of the Int. Conf. on Electromagnetics in Advanced Applications (ICEAA).* IEEE, 2013 (cf. p. 5).

[54] G. Festa and J.-P. Vilotte. The Newmark scheme as velocity-stress time-staggering: An efficient PML implementation for spectral element simulations of elastodynamics. *Geophys. J. Intl.* 161 (2005), 789–812 (cf. p. 4).

[55] M. Fliess, J. Lévine, P. Martin, and P. Rouchon. Flatness and defect of nonlinear systems: Introductory theory and examples. *International Journal of Control,* 61.6 (1995), 1327–1361 (cf. p. 6).

[56] W. Flügge. *Tensor Analysis and Continuum Mechanics.* Springer Berlin Heidelberg, 1972 (cf. p. 12).

[57] L. Fox and D. F. Mayers. *Numerical Solution of Ordinary Differential Equations.* Springer Netherlands, 1987 (cf. p. 18).

[58] M. Frank, F. Holzberger, M. Horvat, J. Kirschke, M. Mayr, M. Muhr, N. Nebulishvili, A. Popp, J. Schwarting, and B. Wohlmuth. Numerical simulation of endovascular treatment options for cerebral aneurysms. *GAMM-Mitteilungen,* 47.3 (2024) (cf. p. 2).

[59] O. Gansser and B. Krol, eds. *Markt- und Absatzprognosen: Modelle - Methoden - Anwendung.* Springer Fachmedien Wiesbaden, 2015 (cf. p. 2).

[60] T. Geveci. On the application of mixed finite element methods to the wave equations. *RAIRO Modél. Math. Anal. Numér.* 22 (1988), 243–250 (cf. p. 3).

[61] G. Golo, A. van der Schaft, P. Breedveld, and B. Maschke. Hamiltonian formulation of bond graphs. In: *Nonlinear and Hybrid Systems in Automotive Control.* Ed. by R. Johansson and A. Rantzer. Springer London, 2003, 351–372 (cf. p. 4).

[62] G. Golo, V. Talasila, A. van der Schaft, and B. Maschke. Hamiltonian discretization of boundary control systems. *Automatica,* 40 (2004), 757–771 (cf. p. 5).

[63] O. Gonzalez. Time integration and discrete Hamiltonian systems. *Journal of Nonlinear Science,* 6.5 (1996), 449–467 (cf. p. 31).

[64] L. Gören-Sümer and Y. Yalcin. Gradient Based Discrete-Time Modeling and Control of Hamiltonian Systems. *IFAC Proceedings Volumes,* 41.2 (2008), 212–217 (cf. p. 6).

[65] P. L. Gould and Y. Feng. *Introduction to Linear Elasticity.* Springer International Publishing, 2018 (cf. p. 14).

[66] K. Graichen, V. Hagenmeyer, and M. Zeitz. A new approach to inversion-based feedforward control design for nonlinear systems. *Automatica,* 41.12 (2005), 2033–2041 (cf. p. 7).

[67] V. Hagenmeyer and M. Zeitz. Flachheitsbasierter Entwurf von linearen und nichtlinearen Vorsteuerungen (Flatness-based Design of Linear and Nonlinear Feedforward Controls). *at - Automatisierungstechnik,* 52.1 (2004), 3–12 (cf. p. 6).

[68] E. Hairer. *Geometric Numerical Integration: Structure-Preserving Algorithms for Ordinary Differential Equations.* Springer, 2006 (cf. pp. 18, 31).

[69] L. R. Herrmann. Elasticity equations for incompressible and nearly incompressible materials by a variational theorem. *AIAA Journal,* 3.10 (1965), 1896–1900 (cf. p. 3).

[70] M. Herrmann and P. Kotyczka. Relative-kinematic formulation of geometrically exact beam dynamics based on Lie group variational integrators. *Computer Methods in Applied Mechanics and Engineering,* 432 (2024), 117367 (cf. p. 31).

[71] H. M. Hilber, T. J. R. Hughes, and R. L. Taylor. Improved numerical dissipation for time integration algorithms in structural dynamics. *Earthquake Engineering and Structural Dynamics,* 5.3 (1977), 283–292 (cf. p. 3).

[72] K. D. Hjelmstad. *Engineering Dynamics: A Basic Introduction*. Springer Nature Switzerland, 2025 (cf. p. 11).

[73] J. Holl and K. Schlacher. Zur zeitdiskreten Implementierung nichtlinearer Regelgesetze (On the Discrete-time Implementation of Nonlinear Control Laws). *at - Automatisierungstechnik,* 54.4 (2006), 178–186 (cf. p. 5).

[74] A. Hrennikoff. Solution of Problems of Elasticity by the Framework Method. *Journal of Applied Mechanics,* 8.4 (1941), A169–A175 (cf. p. 3).

[75] J. Iqbal, M. Ullah, S. G. Khan, B. Khelifa, and S. Ćuković. Nonlinear control systems - A brief overview of historical and recent advances. *Nonlinear Engineering,* 6.4 (2017) (cf. p. 25).

[76] B. Jacob and H. J. Zwart. *Linear port-Hamiltonian systems on infinite-dimensional spaces*. Vol. 223. Operator Theory: Advances and Applications. Birkhäuser/Springer, Basel, 2012 (cf. p. 5).

[77] P. Joly. Variational methods for time-dependent wave propagation problems. In: *Topics in computational wave propagation*. Vol. 31. Lect. Notes Comput. Sci. Eng. Springer, Berlin, 2003, 201–264 (cf. p. 4).

[78] S. W. Key. A variational principle for incompressible and nearly-incompressible anisotropic elasticity. *International Journal of Solids and Structures,* 5.9 (1969), 951–964 (cf. p. 3).

[79] H. Khalil. *Nonlinear Control*. Always Learning. Pearson, 2014 (cf. p. 7).

[80] P. Khosla. Choosing sampling rates for robot control. In: *Proceedings. 1987 IEEE International Conference on Robotics and Automation*. Institute of Electrical and Electronics Engineers, 1987 (cf. p. 5).

[81] P. L. Kinon, P. Betsch, and S. R. Eugster. Energy-momentum-consistent simulation of planar geometrically exact beams in a port-Hamiltonian framework. *Multibody System Dynamics,* (2025) (cf. p. 5).

[82] P. L. Kinon, R. Morandin, and P. Schulze. *Discrete gradient methods for port-Hamiltonian differential-algebraic equations*. 2025 (cf. p. 31).

[83] T. Knüppel and F. Woittennek. Flatness based control design for a nonlinear heavy chain model. *IFAC Proceedings Volumes,* 43.14 (2010), 701–706 (cf. p. 7).

[84] P. Kotyczka. *Numerical Methods for Distributed Parameter Port-Hamiltonian Systems*. TUM.University Press, 2019 (cf. p. 5).

[85] P. Kotyczka and L. Lefèvre. Discrete-time port-Hamiltonian systems: A definition based on symplectic integration. *Systems Contr. Lettr.* 133 (2019), 104530 (cf. pp. 5, 31).

[86] P. Kotyczka and L. Lefèvre. Discrete-Time Control Design Based on Symplectic Integration: Linear Systems. In: *IFAC World Congress, Berlin, IFAC Papers-OnLine*. 2020, 7563–7568 (cf. p. 6).

[87] P. Kotyczka. Cubic Hermite Interpolation and Lobatto Collocation for Nonlinear Sampled-Data Control. *IFAC-PapersOnLine,* 56.2 (2023), 2883–2888 (cf. p. 43).

[88] P. Kotyczka, C. J. Martens, and L. Lefèvre. High Order Discrete-Time Control Based on Gauss-Legendre Collocation. *IFAC-PapersOnLine,* 54.19 (2021), 237–242 (cf. p. 43).

[89] P. Kotyczka, B. Maschke, and L. Lefèvre. Weak form of Stokes-Dirac structures and geometric discretization of port-Hamiltonian systems. *J. Comput. Phys.* 361 (2018), 442–476 (cf. p. 5).

[90] M. Kress. Lanchester Models for Irregular Warfare. *Mathematics,* 8.5 (2020), 737 (cf. p. 1).

[91] M. Kuchta. Assembly of multiscale linear PDE operators. In: *Numerical mathematics and advanced applications—ENUMATH 2019*. Vol. 139. Lect. Notes Comput. Sci. Eng. Springer, Cham, 2021, 641–650 (cf. pp. 8, 36).

[92] A. Kugi and K. Schlacher. Analyse und Synthese nichtlinearer dissipativer Systeme: Ein Überblick (Teil 1) (Analysis and Synthesis of Non-linear Dissipative Systems: An Overview (Part 1)). *at - Automatisierungstechnik,* 50.2 (2002), 63 (cf. p. 25).

[93] A. Kugi and K. Schlacher. Analyse und Synthese nichtlinearer dissipativer Systeme: Ein Überblick (Teil 2) (Analysis and Synthesis of Non-linear Dissipative Systems: An Overview (Part 2)). *at - Automatisierungstechnik,* 50.3 (2002), 103 (cf. p. 25).

[94] A. Kuhn, W. Steiner, J. Zemann, D. Dinevski, and H. Troger. A comparison of various mathematical formulations and numerical solution methods for the large amplitude oscillations of a string pendulum. *Applied Mathematics and Computation,* 67.1–3 (1995), 227–264 (cf. p. 14).

[95] D. S. Laila and A. Astolfi. DISCRETE-TIME IDA-PBC DESIGN FOR SEPARABLE HAMILTONIAN SYSTEMS. *IFAC Proceedings Volumes,* 38.1 (2005), 838–843 (cf. p. 6).

[96] Y. Le Gorrec, H. Zwart, and B. Maschke. Dirac structures and boundary control systems associated with skew-symmetric differential operators. *SIAM J. Control Optim.* 44 (2005), 1864–1892 (cf. p. 5).

[97] A. J. Lew and P. Mata A. A Brief Introduction to Variational Integrators. In: *Structure-preserving Integrators in Nonlinear Structural Dynamics and Flexible Multibody Dynamics*. Springer International Publishing, 2016, 201–291 (cf. p. 31).

[98] W. K. Liu, S. Li, and H. S. Park. Eighty Years of the Finite Element Method: Birth, Evolution, and Future. *Archives of Computational Methods in Engineering,* 29.6 (2022), 4431–4453 (cf. pp. 2, 3).

[99] A. Logg, K.-A. Mardal, and G. N. Wells, eds. *Automated solution of differential equations by the finite element method*. Vol. 84. Lecture Notes in Computational Science and Engineering. Springer, Heidelberg, 2012 (cf. pp. 8, 36).

[100] T. Luan. A Comprehensive Review of Simulation Technology: Development, Methods, Applications, Challenges and Future Trends. *International Journal of Emerging Technologies and Advanced Applications,* 1.5 (2024), 9–14 (cf. pp. 1, 2).

[101] G. Ludyk. Regelung zeitvarianter zeitdiskreter linearer Einfachsysteme/ Control of linear time-varying discrete-time single-input single-output systems. *at - Automatisierungstechnik,* 27.1–12 (1979), 167–170 (cf. p. 5).

[102] A. Macchelli, C. Melchiorri, and S. Stramigioli. Port-Based Modeling and Simulation of Mechanical Systems With Rigid and Flexible Links. *IEEE Trans. Robotics,* 25 (2009), 1016–1029 (cf. p. 5).

[103] C. G. Makridakis. On mixed finite element methods for linear elastodynamics. *Numer. Math.* 61 (1992), 235–260 (cf. p. 3).

[104] T. Malzer, H. Rams, and M. Schoberl. Energy-Based Control of Nonlinear Infinite-Dimensional Port-Hamiltonian Systems with Dissipation. In: *2018 IEEE Conference on Decision and Control (CDC)*. IEEE, 2018, 3746–3751 (cf. p. 26).

[105] K. K. Mankala and S. K. Agrawal. Dynamic Modeling and Simulation of Satellite Tethered Systems. *Journal of Vibration and Acoustics,* 127.2 (2004), 144–156 (cf. p. 14).

[106] B. Maschke and A. van der Schaft. Port-Controlled Hamiltonian Systems: Modelling Origins and Systemtheoretic Properties. *IFAC Proceedings Volumes,* 25.13 (1992), 359–365 (cf. p. 4).

[107] V. Mehrmann and B. Unger. Control of port-Hamiltonian differential-algebraic systems and applications. *Acta Numerica,* 32 (2023), 395–515 (cf. p. 24).

[108] M. Mogler, P. Kotyczka, and L. Lefèvre. Discrete-time Control by Interconnection using energy-preserving collocation methods. *IFAC-PapersOnLine,* 58.6 (2024), 172–177 (cf. p. 43).

[109] S. Monaco and D. Normand-Cyrot. Advanced tools for nonlinear sampled-data systems' analysis and control. *Eur. J. Control,* 13.2-3 (2007), 221–241 (cf. p. 6).

[110] M. Morlock, M. Burkhardt, R. Seifried, and P. Eberhard. End-effector trajectory tracking of flexible link parallel robots using servo constraints. *Multibody System Dynamics,* 56.1 (2022), 1–28 (cf. p. 6).

[111] T. Moser, J. Durmann, M. Bonauer, and B. Lohmann. MORpH: Model reduction of linear port-Hamiltonian systems in MATLAB. *at - Automatisierungstechnik,* 71.6 (2023), 476–489 (cf. p. 4).

[112] R. Müller. Time-continuous power-balanced simulation of nonlinear audio circuits: realtime processing framework and aliasing rejection. PhD thesis. Sorbonne Université, 2021 (cf. p. 5).

[113] R. M. Murray. Trajectory Generation for a Towed Cable System Using Differential Flatness. *IFAC Proceedings Volumes,* 29.1 (1996), 2792–2797 (cf. p. 7).

[114] S. Nicosia, P. Tomei, and A. Tornamè. Discrete-time modeling and control of robotic manipulators. *Journal of Intelligent and Robotic Systems,* 2.4 (1989) (cf. p. 5).

[115] J. O'Reilly. The discrete linear time invariant time-optimal control problem—An overview. *Automatica,* 17.2 (1981), 363–370 (cf. p. 5).

[116] S. Ober-Blöbaum, O. Junge, and J. E. Marsden. Discrete mechanics and optimal control: An analysis. *ESAIM: Control, Optimisation and Calculus of Variations,* 17.2 (2010), 322–352 (cf. p. 6).

[117] R. Ortega, M. Spong, F. Gomez-Estern, and G. Blankenstein. Stabilization of a class of underactuated mechanical systems via interconnection and damping assignment. *IEEE Transactions on Automatic Control,* 47.8 (2002), 1218–1233 (cf. pp. 5, 25).

[118] R. Ortega and E. García-Canseco. Interconnection and Damping Assignment Passivity-Based Control: A Survey. *European Journal of Control,* 10.5 (2004), 432–450 (cf. pp. 4, 25).

[119] R. Ortega, A. Loría, P. J. Nicklasson, and H. Sira-Ramírez. *Passivity-based Control of Euler-Lagrange Systems: Mechanical, Electrical and Electromechanical Applications.* Springer London, 1998 (cf. pp. 5, 25).

[120] R. Ortega, A. van der Schaft, F. Castanos, and A. Astolfi. Control by Interconnection and Standard Passivity-Based Control of Port-Hamiltonian Systems. *IEEE Transactions on Automatic Control,* 53.11 (2008), 2527–2542 (cf. pp. 4, 25).

[121] S. Otto and R. Seifried. Real-time trajectory control of an overhead crane using servo-constraints. *Multibody System Dynamics,* 42.1 (2017), 1–17 (cf. p. 7).

[122] S. Otto and R. Seifried. Open-Loop Control of Underactuated Mechanical Systems Using Servo-Constraints: Analysis and Some Examples. In: *Applications of Differential-Algebraic Equations: Examples and Benchmarks.* Springer International Publishing, 2018, 81–122 (cf. p. 7).

[123] M. Papageorgiou, M. Leibold, and M. Buss. *Optimierung: Statische, dynamische, stochastische Verfahren für die Anwendung.* Springer Berlin Heidelberg, 2015 (cf. p. 33).

[124] H. M. Paynter. Analysis and Design of Engineering Systems: Class Notes for M.I.T. Course 2,751. *M.I.T. Press,* (1961) (cf. p. 4).

[125] H. Peng, Q. Gao, Z. Wu, and W. Zhong. Symplectic Approaches for Solving Two-Point Boundary-Value Problems. *Journal of Guidance, Control, and Dynamics,* 35.2 (2012), 653–659 (cf. p. 6).

[126] N. Petit and P. Rouchon. Flatness of Heavy Chain Systems. *SIAM Journal on Control and Optimization,* 40.2 (2001), 475–495 (cf. p. 7).

[127] T. H. H. Pian. Derivation of element stiffness matrices by assumed stress distributions. *AIAA Journal,* 2.7 (1964), 1333–1336 (cf. p. 3).

[128] T. H.-H. Pian and K. Sumihara. Rational approach for assumed stress finite elements. *International Journal for Numerical Methods in Engineering,* 20 (1984), 1685–1695 (cf. p. 41).

[129] C. Ponce, Y. Wu, Y. L. Gorrec, and H. Ramirez. Structure-preserving discretization of multidimensional linear port-Hamiltonian systems using FEM approaches. In: *2024 IEEE 63rd Conference on Decision and Control (CDC).* IEEE, 2024, 2676–2681 (cf. p. 42).

[130] C. Rabbath and N. Léchevin. *Discrete-Time Control System Design with Applications.* Springer New York, 2014 (cf. p. 5).

[131] A. Rao. A Survey of Numerical Methods for Optimal Control. *Advances in the Astronautical Sciences,* 135 (2010) (cf. pp. 7, 33).

[132] R. Rashad, A. Brugnoli, F. Califano, E. Luesink, and S. Stramigioli. Intrinsic Nonlinear Elasticity: An Exterior Calculus Formulation. *Journal of Nonlinear Science,* 33.5 (2023) (cf. p. 5).

[133] R. Rashad, F. Califano, A. J. van der Schaft, and S. Stramigioli. Twenty years of distributed port-Hamiltonian systems: A literature review. *IMA J. Math. Contr. Infor.* 37 (2020), 1400–1422 (cf. p. 5).

[134] B. C. Reed. *Manhattan Project: The Story of the Century.* Springer International Publishing, 2020 (cf. p. 1).

[135] E. Reissner. On a Variational Theorem in Elasticity. *Journal of Mathematics and Physics,* 29.1–4 (1950), 90–95 (cf. p. 3).

[136] R. Rothfuß, J. Rudolph, and M. Zeitz. Flachheit: Ein neuer Zugang zur Steuerung und Regelung nichtlinearer Systeme. *auto,* 45.11 (1997), 517–525 (cf. p. 6).

[137] A. J. Schaft. Hamiltonian dynamics with external forces and observations. *Mathematical Systems Theory,* 15.1 (1981), 145–168 (cf. p. 4).

[138] A. J. van der Schaft and B. M. Maschke. Hamiltonian formulation of distributed-parameter systems with boundary energy flow. *J. Geom. Phys.* 42 (2002), 166–194 (cf. p. 5).

[139] A. van der Schaft. *L2 - Gain and Passivity Techniques in Nonlinear Control.* Springer London, 2000 (cf. pp. 5, 22, 25).

[140] A. van der Schaft. Port-Hamiltonian systems: an introductory survey. In: *Proceedings of the International Congress of Mathematicians Madrid, August 22–30, 2006.* EMS Press, 2007, 1339–1365 (cf. p. 4).

[141] A. van der Schaft. Port-Hamiltonian Modeling for Control. *Annual Review of Control, Robotics, and Autonomous Systems,* 3.1 (2020), 393–416 (cf. pp. 22, 24).

[142] A. van der Schaft and D. Jeltsema. Port-Hamiltonian Systems Theory: An Introductory Overview. *Foundations and Trends in Systems and Control,* 1.2 (2014), 173–378 (cf. pp. 4, 19).

[143] D. Scheer. *Computersimulationen in politischen Entscheidungsprozessen.* Springer Fachmedien Wiesbaden, 2013 (cf. p. 1).

[144] L. Scheuermann. Geschichte der Simulation / Simulation der Geschichte. Eine Einführung. de. *Digital Classics Online,* Bd. 6 (2020), 1 (2020) (cf. p. 1).

[145] M. Schoberl and A. Siuka. Analysis and comparison of port-Hamiltonian formulations for field theories - demonstrated by means of the Mindlin plate. In: *2013 European Control Conference (ECC).* IEEE, 2013, 548–553 (cf. p. 26).

[146] G. Scovazzi, T. Song, and X. Zeng. A velocity/stress mixed stabilized nodal finite element for elastodynamics: analysis and computations with strongly and weakly enforced boundary conditions. *Comput. Methods Appl. Mech. Engrg.* 325 (2017), 532–576 (cf. p. 4).

[147] M. W. Scroggs, I. A. Baratta, C. N. Richardson, and G. N. Wells. Basix: A runtime finite element basis evaluation library. *Journal of Open Source Software,* 7.73 (2022), 3982 (cf. p. 8).

[148] M. W. Scroggs, J. S. Dokken, C. N. Richardson, and G. N. Wells. Construction of Arbitrary Order Finite Element Degree-of-Freedom Maps on Polygonal and Polyhedral Cell Meshes. *ACM Transactions on Mathematical Software,* 48.2 (2022), 1–23 (cf. p. 8).

[149] A. Serhani, D. Matignon, and G. Haine. Partitioned Finite Element Method for port-Hamiltonian systems with Boundary Damping: Anisotropic Heterogeneous 2D wave equations. *IFAC-PapersOnLine,* 52.2 (2019), 96–101 (cf. p. 5).

[150] A. Serhani, D. Matignon, and G. Haine. A Partitioned Finite Element Method for the Structure-Preserving Discretization of Damped Infinite-Dimensional Port-Hamiltonian Systems with Boundary Control. In: *Geometric Science of Information.* Springer International Publishing, Serhani2019, 549–558 (cf. p. 5).

[151] A. A. Shabana. Flexible Multibody Dynamics: Review of Past and Recent Developments. *Multibody System Dynamics,* 1.2 (1997), 189–222 (cf. p. 2).

[152] H. Sharma, M. Patil, and C. Woolsey. A review of structure-preserving numerical methods for engineering applications. *Computer Methods in Applied Mechanics and Engineering,* 366 (2020), 113067 (cf. pp. 18, 31).

[153] J. Simo and T. Hughes. *Computational Inelasticity.* Interdisciplinary Applied Mathematics. Springer New York, 2006 (cf. p. 42).

[154] R. Smillie. Defense Modeling and Simulation Office: Defining the Infrastructure. In: *Proceedings of 1993 Winter Simulation Conference - (WSC '93).* IEEE, 957–961 (cf. p. 1).

[155] T. Ströhle and P. Betsch. A simultaneous space-time discretization approach to the inverse dynamics of geometrically exact strings. *International Journal for Numerical Methods in Engineering,* 123.11 (2022), 2573–2609 (cf. pp. 7, 14, 18).

[156] M. Takegaki and S. Arimoto. A New Feedback Method for Dynamic Control of Manipulators. *Journal of Dynamic Systems, Measurement, and Control,* 103.2 (1981), 119–125 (cf. p. 5).

[157] D. Taylor and S. Li. Stable inversion of continuous-time nonlinear systems by finite-difference methods. *IEEE Transactions on Automatic Control,* 47.3 (2002), 537–542 (cf. p. 7).

[158] R. Temam. Survey of the Status of Finite Element Methods for Partial Differential Equations. In: *Finite Elements.* Springer New York, 1988, 1–33 (cf. p. 3).

[159] N. Viebahn, J. Schröder, and P. Wriggers. An extension of assumed stress finite elements to a general hyperelastic framework. *Advanced Modeling and Simulation in Engineering Sciences,* 6.1 (2019) (cf. p. 41).

[160] N. M. T. Vu, L. Lefèvre, and B. Maschke. A structured control model for the thermo-magneto-hydrodynamics of plasmas in tokamaks. *Mathematical and Computer Modelling of Dynamical Systems,* 22.3 (2016), 181–206 (cf. p. 19).

[161] M. Wagner. *Lineare und nichtlineare FEM: Eine Einführung mit Anwendungen in der Umformsimulation mit LS-DYNA®.* Springer Fachmedien Wiesbaden, 2019 (cf. p. 15).

[162] M. Wang and P. Kotyczka. Trajectory control of an elastic beam based on port-Hamiltonian numerical models. *at - Automatisierungstechnik,* 69.6 (2021), 457–471 (cf. p. 6).

[163] A. Warsewa, M. Böhm, O. Sawodny, and C. Tarín. A port-Hamiltonian approach to modeling the structural dynamics of complex systems. *Appl. Math. Model.* 89 (2021), 1528–1546 (cf. pp. 5, 14, 26).

[164] E. Wehrle, I. Palomba, and R. Vidoni. Modeling, Design and Optimization of Flexible Mechanical Systems. *Applied Sciences,* 11.15 (2021), 7124 (cf. p. 2).

[165] H. Weiß. Zur Dynamik geometrisch nichtlinearer Balken. PhD thesis. Technische Universität Chemnitz, 2000 (cf. pp. 14, 37).

[166] J. C. Willems. Dissipative dynamical systems part I: General theory. *Archive for Rational Mechanics and Analysis,* 45.5 (1972), 321–351 (cf. p. 25).

[167] C. Woolsey, C. K. Reddy, A. M. Bloch, D. E. Chang, N. E. Leonard, and J. E. Marsden. Controlled Lagrangian Systems with Gyroscopic Forcing and Dissipation. *European Journal of Control,* 10.5 (2004), 478–496 (cf. p. 5).

[168] B. Zhang, Y. Yang, and M. Feng. Mixed virtual element methods for elastodynamics with weak symmetry. *J. Comput. Appl. Math.* 353 (2019), 49–71 (cf. p. 4).

[169] L. Zhang and P. Kotyczka. *Sampled-Data Control using Hermite-Obreschkoff Methods with an IDA-PBC Example.* 2025 (cf. p. 43).

[170] O. C. Zienkiewicz, R. L. Taylor, and J. Z. Zhu. *The Finite Element Method: Its Basis and Fundamentals.* Butterworth-Heinemann, 2005 (cf. p. 16).

[171] H. Zwart and V. Mehrmann. Abstract Dissipative Hamiltonian Differential-Algebraic Equations Are Everywhere. *DAE Panel,* 2 (2024) (cf. p. 26).

Appendix A

Reproduction of publications

A.1 On the velocity-stress formulation for geometrically nonlinear elastodynamics and its structure-preserving discretization

CRediT author statement:

Tobias Thoma:	Conceptualization, Acuration of Experimental Data, Methodology, Software, Visualization, Writing - Original Draft
Herbert Egger:	Conceptualization, Methodology, Visualization, Writing - Original Draft
Paul Kotyczka:	Conceptualization, Supervision, Writing - Original Draft

MATHEMATICAL AND COMPUTER MODELLING OF DYNAMICAL SYSTEMS
2024, VOL. 30, NO. 1, 701–720
https://doi.org/10.1080/13873954.2024.2397486

Taylor & Francis
Taylor & Francis Group

On the velocity-stress formulation for geometrically nonlinear elastodynamics and its structure-preserving discretization

Tobias Thoma[a], Paul Kotyczka[a] and Herbert Egger[b]

[a]TUM School of Engineering and Design, Chair of Automatic Control, Technical University of Munich, Garching, Germany; [b]Institute of Numerical Mathematics, Johannes Kepler University Linz, Linz, Austria

ABSTRACT

We consider the dynamics of an elastic continuum under large deformation but small strain. Such systems can be described by the equations of geometrically nonlinear elastodynamics in combination with the St. Venant-Kirchhoff material law. The velocity-stress formulation of the problem turns out to have a formal port-Hamiltonian structure. In contrast to the linear case, the operators of the problem are modulated by the displacement field which can be handled as a passive variable and integrated along with the velocities. A weak formulation of the problem is derived and essential boundary conditions are incorporated via Lagrange multipliers. This variational formulation explicitly encodes the transfer between kinetic and potential energy in the interior as well as across the boundary, thus leading to a global power balance and ensuring passivity of the system. The particular geometric structure of the weak formulation can be preserved under Galerkin approximation via appropriate mixed finite elements. In addition, a fully discrete power balance can be obtained by appropriate time discretization. The main properties of the system and its discretization are shown theoretically and demonstrated by numerical tests.

ARTICLE HISTORY
Received 31 January 2024
Accepted 20 August 2024

KEYWORDS
velocity-stress formulation; structure-preserving discretization; port-Hamiltonian systems

1. Introduction

Models of elastodynamics are extensively used in structural analysis and engineering design and efficient finite element methods have been developed for simulation and control. In Makridakis (1992) mixed finite elements for the *displacement-stress* and *velocity-stress* formulation of linear elastodynamics were investigated, partly based on corresponding results for the wave equation (Geveci 1988). A new family of mixed finite elements for linear elastodynamics suitable for mass lumping was presented in Bécache et al. (2002). An overview about the construction and analysis of variational numerical schemes for time-dependent wave propagation problems is given in Cohen (2002) and Joly (2003). Primal-dual and dual-primal velocity-stress formulations for linear elastodynamics are considered as examples, and stability and energy conservation are derived for semi- and fully-discrete schemes. The velocity-stress formulation is also frequently

CONTACT Tobias Thoma tobias.thoma@tum.de TUM School of Engineering and Design, Chair of Automatic Control, Technical University of Munich, Munich, Germany

used for simulations in seismology (Festa and Vilotte 2005). In Arnold and Lee (2014), dual mixed finite element methods for elastodynamics with weakly imposed symmetry for the stresses have been investigated. Another efficient stabilized nodal finite element method for elastodynamics was proposed in Scovazzi et al. (2017). Their framework is based on a space-time variational statement of the velocity-stress formulation and is compatible with weakly and strongly enforced Dirichlet boundary conditions. In Zhang et al. (2019), a dual velocity-stress formulation with weakly imposed symmetry was analysed in the context of the virtual finite element approach. A mixed finite element method based on a *port-Hamiltonian* (PH) formulation was used in Brugnoli et al. (2021) to simulate, in a power-preserving way, a coupled system of linear thermoelasticity.

The PH framework provides a general approach for modelling, analysis, and control of complex multi-physical dynamical systems (Duindam et al. 2009). Originating in a synthesis of network and Hamiltonian perspectives for *open*, i.e. controlled, finite-dimensional systems (Maschke and van der Schaft 1992), the past two decades brought important progress in the development of the theory for infinite-dimensional systems from different physical domains, including structural mechanics (see e.g. van der Schaft and Maschke 2002; Le Gorrec et al. 2005; Macchelli et al. 2009; Jacob and Zwart 2012 and the review article Rashad et al. 2020). In Rashad et al. (2023), the intrinsic geometrical structure of nonlinear elasticity is discussed in the framework of exterior calculus. In addition to the theoretical considerations concerning geometrical aspects of PH models, also the structure-preserving numerical approximation has been a major field of interest (see Golo et al. 2004; Farle et al. 2013; Kotyczka et al. 2018; Cardoso-Ribeiro et al. 2021 and, in particular Brugnoli et al. 2019a, 2019b, 2021a, 2021b; Warsewa et al. 2021, for applications in linear elastodynamics). Recent contributions to the modelling and structure-preserving discretization of nonlinear structures have been presented in Brugnoli et al. (2021), Brugnoli and Matignon (2022), Thoma and Kotyczka (2022), Kinon et al. (2023). For discretized and finite-dimensional systems, symplectic integration (Kotyczka and Lefèvre 2019), discrete gradients (Falaize and Hélie 2016), Petrov-Galerkin (Egger et al. 2021), and projection methods (Müller 2021) have been proposed for the structure-preserving time discretization.

1.1. Scope and main contributions

We consider the motion of an elastic continuum described by the equations of geometrically nonlinear elastodynamics. A velocity-stress formulation is chosen for describing the essential system dynamics which, similar to the well-studied linear setting, has a formal PH structure encoding the exchange of kinetic and potential energy as well as the balance of linear and angular momentum. Different from well-studied linearized models, the interconnection operator here is modulated by the deformation gradient, whose evolution in time has to be included in the formulation. In contrast to previous work on geometrically nonlinear beams, plates, and strings (Brugnoli et al. 2021; Brugnoli and Matignon 2022; Thoma and Kotyczka 2022), we include the displacement field in our formulation which, together with the velocity and stress field, yields a complete description of the system state at every time. The displacement can be obtained by simple integration of the velocity, thus having no direct influence on the

power balance of the system, apart from the modulation of the interconnection operator mentioned above.

The first contribution of the paper is a weak formulation of the evolution equations for velocity and stress, in which the Dirichlet boundary conditions are incorporated via Lagrange multipliers, while the Neumann conditions are treated naturally in the derivation of the weak form. Symmetry of the stress tensor is incorporated explicitly and the kinematic equation for the displacement is treated pointwise on the continuous and discrete level. We show that these variational identities are satisfied by smooth solutions of the system and they already fully encode the balance of power and momentum.

In a second step, we consider the structure-preserving discretization of the weak form of the dynamic equations derived on the continuous level. We show that the basic structure of the system is preserved automatically by Galerkin projection in space. The kinematic equation for the displacement is treated in a pointwise manner and the symmetry of the discretized stress tensor is incorporated explicitly in the approximation spaces. As a consequence, the balance equations for energy and momentum, derived on the continuous level, remain valid after discretization. We further discuss the differential-algebraic structure of the system arising after discretization, which provides insight into a mild compatibility condition between approximation spaces for the velocity and the Lagrange multiplier which is required to ensure local well-posedness of the discretized problem. The proposed discretization scheme thus addresses, at the same time, multiple challenges for numerical methods in nonlinear elastiticy, i.e.

- the treatment of mixed boundary conditions;
- the incorporation of stress-symmetry;
- the handling of geometric nonlinearities.

As demonstrated in the numerical tests, standard finite element spaces (Arnold and Lee 2014) can be used for the Galerkin approximation, facilitating the incorporation into available software.

As a final step, we also consider the systematic time-discretization by appropriate linear-implicit one-step method. We comment on the well-posedness of the fully-discrete scheme and show that the underlying balance equations for energy and momentum remain valid also after time discretization. Numerical tests are presented for illustration of these favourable properties.

1.2. Outline

The remainder of the article is organized as follows: In Section 2, we recall the basic equations of geometrically nonlinear mechanics and introduce the velocity-stress formulation of our problem. In addition, we derive its weak formulation and the underlying power balance. The structure-preserving discretization by mixed finite elements in space and the implicit midpoint rule in time is discussed in Section 3, and balance laws for energy and momentum are established on the semi- and fully-discrete level. The theoretical results are illustrated in Section 4 by numerical tests simulating the movement of a flexible robot arm. A brief discussion of our main results and some concluding remarks are given in Section 5.

2. Modeling

We start with recalling the governing equations of nonlinear continuum mechanics for a St. Venant–Kirchhoff material. After that, we present the velocity-stress formulation of the system and discuss the underlying modulated PH structure. We then derive an appropriate weak form of the governing equations and establish the inherent power balance for the system.

2.1. Nonlinear continuum mechanics

Following standard practice (Bonet and Wood 2008; Wriggers 2008), we use material coordinates. All fields therefore depend on the spatial coordinate X in reference configuration and time t, which we mostly omit in our notation. The momentum balance of the system is given by

$$\rho\ddot{u} = \mathrm{Div}(F \cdot S) + b \qquad \text{in } \Omega, \tag{1}$$

where $\Omega \subset \mathbb{R}^d$, $d = 1, 2, 3$, is the reference configuration of the body. As usual, ρ denotes the material density, $u(X, t) = x(X, t) - X$ the displacement field, and

$$F = \mathrm{Grad}(u) + I \tag{2}$$

the deformation gradient; see Figure 1 for a sketch.

Furthermore, S is the second Piola-Kirchoff stress tensor, and b the vector of volume forces caused by gravitation or other exogenous loads. In this paper, we restrict our considerations to St. Venant-Kirchhoff materials which are characterized by a linear stress-strain relation

$$S = C : E. \tag{3}$$

The fourth order stiffness tensor C is assumed symmetric and positive definite, for instance $C : E = 2\mu E + \lambda \mathrm{tr}(E)I$, and it acts on the nonlinear Green strain tensor

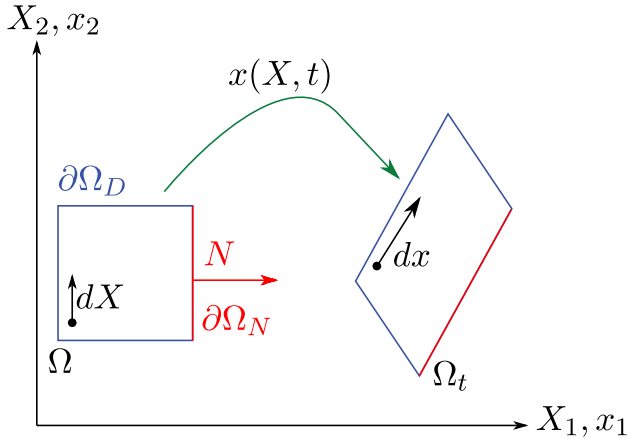

Figure 1. Mapping of an infinitesimal line element dX from the material (undeformed) configuration ($\Omega \subset \mathbb{R}^2$) to the spatial (deformed) one ($\Omega_t \subset \mathbb{R}^2$) via the deformation gradient $F = \mathrm{Grad}(x)$, $dx = F \cdot dX$.

$$E = \frac{1}{2}(F^\top \cdot F - I). \tag{4}$$

To complete the system description, we consider mixed boundary conditions

$$u = u_D \quad \text{on } \partial\Omega_D, \tag{5a}$$

$$F \cdot S \cdot N = \tau_N \quad \text{on } \partial\Omega_N. \tag{5b}$$

Here $\partial\Omega = \partial\Omega_D \cup \Omega_N$ denotes an appropriate decomposition of the boundary into Dirichlet and Neumann part, N is the outer oriented normal vector field on $\partial\Omega$, and u_D, τ_N are the given boundary data.

2.2. Velocity-stress formulation

By introducing the velocity $v = \dot{u}$ and the compliance tensor $A = C^{-1}$, the above equations can be rewritten equivalently as a first order system

$$\rho\dot{v} = \mathrm{Div}(F(u) \cdot S) + b \tag{6a}$$

$$A : \dot{S} = \mathrm{sym}(F(u)^\top \cdot \mathrm{Grad}(v)). \tag{6b}$$

Rewriting the Dirichlet boundary conditions leads to

$$v = v_D \quad \text{on } \partial\Omega_D, \tag{7a}$$

$$F(u) \cdot S \cdot N = \tau_N \quad \text{on } \partial\Omega_N, \tag{7b}$$

where $v_D = \dot{u}_D$ is the prescribed velocity at the Dirichlet boundary $\partial\Omega_D$. The *velocity-stress formulation* (6a)–(6b) does not provide a complete state representation, but has to be complemented by a kinematic equation, e.g.

$$\dot{u} = v. \tag{6c}$$

This equation allows to infer information about the displacement field u, which *modulates* the system dynamics (6a)–(6b) via the deformation gradient $F(u)$.

Remark 1. Substituting $F(u)$ by the identity matrix I leads to the velocity-stress formulation of linear elastodynamics (Makridakis 1992), which is governed by the linearized strain tensor $\varepsilon = \mathrm{sym}(\mathrm{Grad}(u))$ instead of E, and the Cauchy stress σ instead of S. Well-posedness of the corresponding initial-boundary value problem can be established by semi-group theory (Leis 1986). The natural function spaces for velocities and stresses arising in the analysis are $L^2(\Omega;\mathbb{R}^3)$ and $L^2(\Omega;\mathbb{R}^{3\times3}_{\mathrm{sym}})$ as well as certain subspaces having $\mathrm{Grad}(v) \in L^2(\Omega)^{3\times3}$ and $\mathrm{Div}(S)$ well-defined and square integrable, and accomodating the boundary conditions. Local-in-time existence and uniqueness results for the nonlinear elastiticy problem under consideration can be obtained by quasi-linear theory or parabolic regularization (Court and Kunisch 2018).

2.3. Hamiltonian and power-conjugated variables

The internal energy of the system (6a)–(6c) is given by the Hamiltonian

$$H(p,E) = \int_\Omega \frac{1}{2\rho} p \cdot p + \frac{1}{2}(C:E) : E\, dX, \tag{8}$$

consisting of the kinetic and elastic potential energy. In contrast to previous work, we do not include the body force in the definition of the Hamiltonian here, but rather treat it as an input to the system, which simplifies some of our arguments later on. We choose the momentum density $p = \rho v$ and the Green strain tensor E as the *state variables*, in compliance with a unified energy storage model, underlying the PH modeling paradigm or its graphical representation by generalized bond graphs. The corresponding *co-state variables* given by the variational derivatives

$$\delta_p H(p,E) = \frac{p}{\rho} = v, \qquad \delta_E H(p,E) = C:E = S \tag{9}$$

of the Hamiltonian here correspond to the velocity and stress, respectively.

Remark 2. The differential equations (6a)–(6b) may be written compactly as

$$\begin{bmatrix} \dot{p} \\ \dot{E} \end{bmatrix} = \begin{bmatrix} 0 & \mathrm{Div}(F(u)\cdot\times) \\ \mathrm{sym}(F(u)^{\mathrm{T}}\cdot\mathrm{Grad}(\times)) & 0 \end{bmatrix} \begin{bmatrix} v \\ S \end{bmatrix} + \begin{bmatrix} I \\ 0 \end{bmatrix} b, \tag{10}$$

according to the formulation as a distributed parameter PH system; see e.g (van der Schaft and Maschke 2002; Mehrmann and Unger 2023). In this language, $x = (p,E)$ and $e = (v,S)$ are called the *state* (or energy) and co-state (or co-energy or *effort*) variables. The time derivatives of the states $f = (-\dot{p}, -\dot{E})$, the *flows*, here with the commonly used sign convention, are power-conjugated to the efforts, such that $\dot{H} + \langle e,f\rangle_\Omega = 0$, with $\langle\cdot,\cdot\rangle_\Omega$ the appropriate duality product. The PH formulation is completed by the definition of *output* variables, which are power-conjugated to the imposed *inputs*, and which naturally emerge in the power balance equation, after possible integration by parts. In the considered case, we have the *distributed port* (b,v) and the *boundary ports* $(v_D, F(u)\cdot S\cdot N)$, (τ_N, v) on $\partial\Omega_D$ and $\partial\Omega_N$, respectively. The differential operator on the right hand side, which here is *modulated* by the displacement u, is *formally skew-adjoint* and describes the in-domain exchange between kinetic and elastic energy, and the coupling with the boundary ports. Related PH representations for beams, plates, and strings can be found in Brugnoli et al. (2021), Brugnoli and Matignon (2022), Thoma and Kotyczka (2022).

2.4. Variational identities

As a next step, we derive an appropriate weak form of the Equations (6a)–(6b) which encodes the underlying energy exchange mechanism and reveals the role of input and output variables. The kinematic constraint (6c), which is required to track the current modulation state, is treated separately. For ease of notation, we introduce

$$\langle a, b\rangle_M = \int_M a \odot b \, dX$$

for the integration of products of scalar, vector, and tensor valued functions over some manifold M. We further use a Lagrange multiplier approach to enforce the Dirichlet boundary conditions (7a), which leads to the following assertions.

Lemma 2.1. *Let* (v, S, u) *be a sufficiently regular solution of* (6a)–(6b) *and* (7a)–(7b), *and further define the reaction force* $\lambda := F(u) \cdot S \cdot N \in L^2(\partial\Omega_D; \mathbb{R})$ *on* $\partial\Omega_D$. *Then* $S = S^{\mathrm{T}}$ *and the variational identities*

$$\langle \rho\dot{v}, \delta v\rangle_\Omega = -\langle S, F(u)^{\mathrm{T}} \cdot \mathrm{Grad}(\delta v)\rangle_\Omega + \langle b, \delta v\rangle_\Omega \tag{11a}$$

$$+ \langle \lambda, \delta v\rangle_{\partial\Omega_D} + \langle \tau_N, \delta v\rangle_{\partial\Omega_N}$$

$$\langle A : \dot{S}, \delta S\rangle_\Omega = \langle F(u)^{\mathrm{T}} \cdot \mathrm{Grad}(v), \delta S\rangle_\Omega \tag{11b}$$

$$\langle v, \delta\lambda\rangle_{\partial\Omega_D} = \langle v_D, \delta\lambda\rangle_{\partial\Omega_D} \tag{11c}$$

hold for all regular test functions $(\delta v, \delta S, \delta\lambda)$ *with* $\delta S = \delta S^{\mathrm{T}}$, *and all* $t \geq 0$ *of interest.*

Proof. By testing Equation (6a) and integration by parts, one can see that

$$\langle \rho\dot{v}, \delta v\rangle_\Omega = \langle \mathrm{Div}(F(u) \cdot S), \delta v\rangle_\Omega + \langle b, \delta v\rangle_\Omega$$

$$= -\langle S, F(u)^{\mathrm{T}} \cdot \mathrm{Grad}(\delta v)\rangle_\Omega + \langle b, \delta v\rangle_\Omega + \langle F(u) \cdot S \cdot N, \delta v\rangle_{\partial\Omega}.$$

By substituting τ_N and λ for $F(u) \cdot S \cdot N$ on $\partial\Omega_N$ and $\partial\Omega_D$, respectively, we already arrive at (11a). Equation (11b) follows immediately by testing (6b) and exploiting the symmetry of δS, which gives rise to

$$\langle \mathrm{sym}(F(u)^{\mathrm{T}} \cdot \mathrm{Grad}(v)), \delta S\rangle_\Omega = \langle F(u)^{\mathrm{T}} \cdot \mathrm{Grad}(v), \delta S\rangle_\Omega.$$

The identity (11c) is simply the weak form of the boundary condition (7a). □

Remark 3. Note that $\mathrm{Grad}(v)$ and $\mathrm{Grad}(\delta v)$ are the only terms in (11a)–(11c) involving differential operators, while no derivatives for the stress components appear. On the other hand, symmetry of the stress components has to be required explicitly. Furthermore, the kinematic equation (6c) was not used in the derivation. Hence the variational identities (11a)–(11c) are not sufficient for studying the well-posedness of the problem under consideration, but they allow to establish some important properties of solutions and serve as starting point for our discretization strategy.

Using Lemma 2.1, we can establish some important properties of solutions, which we will try to preserve later on during the discretization process.

2.5. Power balance

The proof of the following result shows that the power balance of the system is already fully encoded in the weak formulation of the problem and further also sheds light on the role of input and output port variables.

Proposition 2.2. *Let* (v, S, u, λ) *be sufficiently regular solution of* (6a)–(6c) *and the boundary conditions* (7a)–(7b) *and define* $\lambda := F(u) \cdot S \cdot N$ *on* $\partial\Omega_D$. *Then*

$$\frac{d}{dt} H(\rho v, A : S) = \langle b, v \rangle_\Omega + \langle \lambda, v_D \rangle_{\partial\Omega_D} + \langle \tau_N, v \rangle_{\partial\Omega_N}. \tag{12}$$

Proof. We will only employ the weak form (11a)–(11c) of the dynamic equations and $S = S^{\mathrm{T}}$ in the following arguments. By formally taking the time derivative of the Hamiltonian defined in (8), we obtain

$$\frac{d}{dt} H(\rho v, A : S) = \langle \rho \dot{v}, v \rangle_\Omega + \langle A : \dot{S}, S \rangle_\Omega.$$

By using (11a) with $\delta v = v$ and (11b) with $\delta S = S$, we then further see that

$$\frac{d}{dt} H(\rho v, A : S) = -\langle S, F(u)^{\mathrm{T}} \cdot \mathrm{Grad}(v) \rangle_\Omega + \langle b, v \rangle_\Omega + \langle \lambda, v \rangle_{\partial\Omega_D}$$

$$+ \langle \tau_N, v \rangle_{\partial\Omega_N} + \langle S, F(u)^{\mathrm{T}} \cdot \mathrm{Grad}(v) \rangle_\Omega.$$

The first and last term on the right hand side cancel each other, and (11c) allows to replace the third term on the right hand side. This already leads to the claim. □

2.6. Balance of momentum

We next show that the weak form (11a)–(11c) of the dynamic equations also already encodes the balance of linear and angular momentum.

Proposition 2.3. *Let* (v, S, u) *be a regular solution of* (6a)–(6c) *and* (7a)–(7b), *and define* $\lambda := F(u) \cdot S \cdot N$ *on* $\partial\Omega_D$. *Further, let* $\zeta = \alpha + \beta \times x$ *with* $\alpha, \beta \in \mathbb{R}^3$ *and* $x = x(X, t) = X + u(X, t)$ *the position in body coordinates. Then*

$$\frac{d}{dt} \langle \rho v, \zeta \rangle_\Omega = \langle b, \zeta \rangle_\Omega + \langle \tau_N, \zeta \rangle_{\partial\Omega_N} + \langle \lambda, \zeta \rangle_{\partial\Omega_D}. \tag{13}$$

Proof. We again utilize the weak form of the dynamic equations. By testing (11a) with $\delta v = \alpha$ constant, we obtain (13) for $\zeta = \alpha$. For $\zeta = \beta \times x$, we utilize that

$$\frac{d}{dt} \langle \rho v, \beta \times x \rangle_\Omega = \langle \rho \dot{v}, \beta \times x \rangle_\Omega + \langle \rho v, \beta \times \dot{x} \rangle_\Omega = (i) + (ii).$$

We use $x = x(X, t) = X + u(X, t)$ and $\dot{u} = v$ to see that $(ii) = \langle \rho v, \beta \times v \rangle_\Omega = 0$. For the first term, we observe that $\beta \times x = A_\beta \cdot x$ with anti-symmetric matrix A_β. Hence

$$\mathrm{Grad}(\zeta) = \mathrm{Grad}(A_\beta \cdot x) = A_\beta \cdot \mathrm{Grad}(x) = A_\beta \cdot F(u),$$

where we used $x = u + X$ as before and the definition (2) of $F(u)$ for the last step. Since A_β is anti-symmetric, we see that $F(u)^{\mathrm{T}} \cdot \mathrm{Grad}(\beta \times x)$ is also anti-symmetric. Therefore, $\langle S, F(u)^{\mathrm{T}} \cdot A_\beta \cdot F(u) \rangle_\Omega = 0$ follows due to $S = S^{\mathrm{T}}$. By testing (11a) with $\delta v = \beta \times x$, we thus obtain (13) also for the choice $\zeta = \beta \times x$. □

3. Structure-preserving discretization

We now demonstrate that the variational identities (11a)–(11c) are also well-suited for the design of a structure-preserving discretization strategy. Like on the continuous level, a kinematic equation will be added explicitly, but it is not important for deriving discrete versions of the power and momentum balance equations.

3.1. Spatial discretization

For the discretization in space, we use a Galerkin approximation of the variational identities (11a)–(11c). To this end, let us denote by

$$\mathcal{V}_h \subset H^1(\Omega;\mathbb{R}), \quad \mathcal{S}_h \subset L^2(\Omega;\mathbb{R}^{d\times d}_{\mathrm{sym}}), \quad \text{and} \quad \Lambda_h \subset L^2(\partial\Omega_D;\mathbb{R})$$

appropriate finite dimensional subspaces. In view of Remark 3, this is the natural setting for treating the variational identities (11a)–(11c). As indicated in Section 4.2, standard finite element spaces can be used for the approximation. We will search for an approximation $(v_h, S_h, \lambda_h) : [0,T] \to V_h \times S_h \times \Lambda_h$ for the solution of our problem satisfying the discretized identities

$$\langle \rho \dot{v}_h, \delta v_h \rangle_\Omega = -\langle S_h, F(u_h)^{\mathrm{T}} \cdot \mathrm{Grad}(\delta v_h) \rangle_\Omega + \langle b, \delta v_h \rangle_\Omega \tag{14a}$$

$$+ \langle \lambda_h, \delta v_h \rangle_{\partial\Omega_D} + \langle \tau_N, \delta v_h \rangle_{\partial\Omega_N}$$

$$\langle A : \dot{S}_h, \delta S_h \rangle_\Omega = \langle F(u_h)^{\mathrm{T}} \cdot \mathrm{Grad}(v_h), \delta S_h \rangle_\Omega \tag{14b}$$

$$\langle v_h, \delta\lambda_h \rangle_{\partial\Omega_D} = \langle v_D, \delta\lambda_h \rangle_{\partial\Omega_D} \tag{14c}$$

for all $\delta v_h \in \mathcal{V}_h, \delta S_h \in \mathcal{S}_h$, and $\delta\lambda_h \in \Lambda_h$, and for all $t \geq 0$ of relevance. The discrete displacement field $u_h : [0,T] \to V_h$ will be constructed such that

$$\dot{u}_h = v_h \tag{14d}$$

which amounts to the discretized kinematic relation. As a first step, let us discuss the existence and uniqueness of discrete solutions by switching to the algebraic level.

3.2. Differential-algebraic form

By choosing some basis for the approximation spaces V_h, S_h, Λ_h, the variational identities (14a)–(14c) can be turned into a system of differential-algebraic equations

$$\begin{bmatrix} M_v & 0 & 0 \\ 0 & M_S & 0 \\ 0 & 0 & 0 \end{bmatrix} \begin{bmatrix} \dot{v} \\ \dot{S} \\ \dot{\lambda} \end{bmatrix} = \begin{bmatrix} 0 & -D(u) & B \\ D(u)^\top & 0 & 0 \\ -B^\top & 0 & 0 \end{bmatrix} \begin{bmatrix} v \\ S \\ \lambda \end{bmatrix} + \begin{bmatrix} G_b & G_\tau & 0 \\ 0 & 0 & 0 \\ 0 & 0 & G_v \end{bmatrix} \begin{bmatrix} b \\ \tau_N \\ v_D \end{bmatrix}, \tag{15}$$

where v, S, λ, and so on, are the vector representations of the corresponding discretized functions; see Bonet and Wood (2008), Wriggers (2008) for details. Let us note that systems of similar structure were also obtained in Brugnoli et al. (2021), Thoma and Kotyczka (2022) for beams and strings. Using the same basis for the expansion of v_h and u_h, the kinematic equation takes the form

$$\dot{u} = v. \tag{16}$$

Since no time derivative of the Lagrange multiplier λ appears and the last equation on the right hand side of (15) is independent of λ, the above system amounts to a differential-algebraic equation of index $\nu \geq 2$; see e.g. (Kunkel and Mehrmann 2006). The variables v, S, and u are of differential nature, while λ is the algebraic variable.

Lemma 3.1. *Assume that* $B^\top \cdot B$ *is regular. Then the above system is a regular differential-algebraic equation with index* $\nu = 2$.

Proof. After reordering, the system can be seen to be of Hessenberg form

$$M\dot{y} = f(y, z), \quad 0 = g(y) \tag{17}$$

with regular matrix M in front of the time derivatives, and variables $y = (v, S, u)$ and $z = \lambda$. By differentiating the second equation, one obtains the *hidden constraint*

$$0 = g_y(y) \cdot \dot{y} = g_y(y) \cdot M^{-1} \cdot f(y, z) =: h(y, z). \tag{18}$$

This equation allows to uniquely determine z as a function of y, if

$$\partial_z h(y, z) = B^\top M^{-1} B \quad \text{is regular.} \tag{19}$$

Since M is regular, this condition is equivalent to $B^\top \cdot B$ being regular. Hence a differential equation for $\dot{z}$ can be obtained by differentiating the hidden constraint and, as a consequence, the index of the system is $\nu = 2$; we refer to (Kunkel and Mehrmann 2006) for details.

Remark 4. The regularity condition for $B^\top \cdot B$ is equivalent to assuming that B is injective, which is required to uniquely determine the Lagrange multiplier λ. On the level of the Galerkin approximation, this means that

$$\langle \lambda_h, \delta v_h \rangle_{\partial\Omega_D} = 0 \qquad \delta v_h \qquad \text{implies that} \qquad \lambda_h = 0. \tag{20}$$

This amounts to a compatibility condition for the approximation spaces V_h, Λ_h, which can be satisfied, e.g. by choosing $\Lambda_h = V_h|_{\partial\Omega_D}$; see Section 4 below. Uniqueness of a solution for appropriate initial values is then guaranteed by regularity of the system (17). In order to guarantee existence of a solution $(y, z) = (v, S, \lambda, u)$, the initial values have to satisfy the compatibility conditions

$$g(y(0)) = 0 \qquad \text{and} \qquad h(y(0), z(0)) = 0. \tag{21}$$

These conditions can be translated directly to conditions for $\mathrm{v}(0)$, $\mathrm{S}(0)$, $\lambda(0)$, $\mathrm{u}(0)$ or the corresponding discrete functions.

3.3. Balance of energy and momentum

We now use the variational identities defining the discrete solution to derive balance equations for energy and momentum. Since the structure of the equations was preserved under Galerkin approximation, we can use the very same arguments as employed on the continuous level. We therefore only sketch the main arguments of the proofs.

Proposition 3.2. *Let* $(v_h, S_h, \lambda_h, u_h)$ *denote a solution of* (14a)–(14d). *Then*

$$\frac{d}{dt} H(\rho v_h, A : S_h) = \langle b, v_h \rangle_\Omega + \langle \lambda_h, v_D \rangle_{\partial\Omega_D} + \langle \tau_N, v_h \rangle_{\partial\Omega_N}. \tag{22}$$

The identity follows by testing (14a)–(14c) with $\delta v_h = v_h$, $\delta S_h = S_h$ and $\delta\lambda_h = \lambda_h$. For details on the intermediate steps, we refer to the proof of Proposition 2.2. Like before, we also obtain a balance equation for linear and angular momentum.

Proposition 3.3. *Let* $(v_h, S_h, \lambda_h, u_h)$ *denote a solution of* (14a)–(14d). *Further assume that* V_h *contains all* $\zeta_h = \alpha + \beta \times (X + w_h)$ *for* $\alpha, \beta \in \mathbb{R}^3$ *and* $w_h \in V_h$. *Then*

$$\frac{d}{dt} \langle \rho v_h, \zeta_h \rangle_\Omega = \langle b, \zeta_h \rangle_\Omega + \langle \tau_N, \zeta_h \rangle_{\partial\Omega_N} + \langle \lambda_h, \zeta_h \rangle_{\partial\Omega_D}. \tag{23}$$

The proof of this statement follows by testing (14a) with $\delta v_h = \zeta_h$ and using the same arguments as employed in the proof of Proposition 2.3.

3.4. Time discretization

We now demonstrate that the particular geometric structure and the corresponding power balance are also preserved by appropriate time discretization. Let $\tau > 0$ be a fixed step size and $t^n = n\tau$, $n \geq 0$ be the discrete time steps. We define

$$d_\tau a^{n+1/2} = \frac{1}{\tau}\left(a^{n+1} - a^n\right) \quad \text{and} \quad a^{n+1/2} = \frac{1}{2}\left(a^{n+1} + a^n\right)$$

to denote the difference and average of a sequence of numbers defined over the time grid. Applying the midpoint rule to (14a)–(14c) leads to

$$\langle \rho d_\tau v_h^{n+1/2}, \delta v_h \rangle_\Omega = -\langle S_h^{n+1/2}, F(\tilde{u}_h^{n+1/2})^{\mathrm{T}} \cdot \mathrm{Grad}(\delta v_h) \rangle_\Omega \tag{24a}$$

$$+ \langle b^{n+1/2}, \delta v_h \rangle_\Omega + \langle \lambda_h^{n+1/2}, \delta v_h \rangle_{\partial\Omega_D} + \langle \tau_N^{n+1/2}, \delta v_h \rangle_{\partial\Omega_N}$$

$$\langle A : d_\tau S_h^{n+1/2}, \delta S_h \rangle_\Omega = \langle F(\tilde{u}_h^{n+1/2})^\top \cdot \mathrm{Grad}(v_h^{n+1/2}), \delta S_h \rangle_\Omega \tag{24b}$$

$$\langle v_h^{n+1/2}, \delta\lambda_h \rangle_{\partial\Omega_D} = \langle v_D^{n+1/2}, \delta\lambda_h \rangle_{\partial\Omega_D} \tag{24c}$$

for all $\delta v_h \in \mathcal{V}_h$, $\delta S_h \in \mathcal{S}_h$, and $\delta\lambda_h \in \Lambda_h$, and for all time steps $n \geq 0$ of relevance. The discrete displacement field is approximated on a staggered grid and updated by

$$d_\tau \tilde{u}_h^n = v_h^n \tag{24d}$$

We use $\tilde{u}^{n+1/2}$ to denote the values at intermediate time steps and define the corresponding difference quotient $d_\tau \tilde{u}_h^n = \frac{1}{\tau}(\tilde{u}^{n+1/2} - \tilde{u}^{n-1/2})$ accordingly.

Remark 5. One can update $\tilde{u}_h^{n+1/2} = \tilde{u}_h^{n-1/2} + \tau v_h^n$ before solving (24a)–(24c) for the remaining variables v_h^{n+1}, S_h^{n+1}, and λ_h^{n+1}. As a consequence, only a single linear system has to be solved in every time iteration. Moreover, under the compatibility conditions for the approximation spaces discussed in Section 3.2, the well-posedness of the fully-discrete scheme can be guaranteed. Instead of defining $\tilde{u}^{n+1/2}$ at intermediate time steps $t^{n+1/2}$, one could alternatively also use the update formula

$$d_\tau u_h^{n+1/2} = v_h^{n+1/2}$$

to obtain approximations u_h^n at time steps t^n, and replace $\tilde{u}_h^{n+1/2}$ with $\bar{u}_h^{n+1/2} = 1/2(u_h^{n+1} + u_h^n)$. This leads to a fully implicit scheme, for which a nonlinear system has to be solved in every time step. This choice leads to an improved balance of angular momentum, which might justify the additional computational effort to some extent; see Remark 6.

Important properties of solutions are again already encoded in the discrete variational identities. This allows to show the following results.

Proposition 3.4 *Let* $(v_h^n, S_h^n, \lambda_h^n, \tilde{u}_h^{n+1/2})$, $n \geq 0$ *be a solution of* (24a)–(24d). *Then*

$$d_\tau H(\rho v_h^{n+1/2}, A : S_h^{n+1/2}) \tag{25}$$

$$= \langle b^{n+1/2}, v_h^{n+1/2} \rangle_\Omega + \langle \lambda_h^{n+1/2}, v_D^{n+1/2} \rangle_{\partial\Omega_D} + \langle \tau_N^{n+1/2}, v_h^{n+1/2} \rangle_{\partial\Omega_N}.$$

Proof. It is not difficult to check that $\frac{1}{2\tau}(a^2 - b^2) = \left(\frac{a-b}{\tau}\right) \cdot \left(\frac{a+b}{2}\right)$. This yields

$$d_\tau H(\rho v_h^{n+1/2}, A : S_h^{n+1/2}) = \langle \rho d_\tau v_h^{n+1/2}, v_h^{n+1/2} \rangle_\Omega + \langle A : d_\tau S_h^{n+1/2}, S_h^{n+1/2} \rangle_\Omega.$$

The power-balance then follows immediately from the variational identities (24a)–(24c) by using $\delta v_h = v_h^{n+1/2}$, $\delta S_h = S_h^{n+1/2}$, and $\delta\lambda_h = \lambda_h^{n+1/2}$ as the test functions. □

Using similar arguments as on the continuous and semi-discrete level, we can again also establish a balance equation for linear and angular momentum.

Proposition 3.5. *Let* $(v_h^n, S_h^n, \lambda_h^n, \tilde{u}_h^{n-1/2})$, $n \geq 0$ *be a solution of* (24a)–(24d) *and define* $u_h^n = \tilde{u}_h^{n-1/2} + \frac{\tau}{2} v_h^n$ *and* $\zeta_h^n = \alpha + \beta \times (X + u_h^n)$ *for all* $n \geq 1$. *Further assume that* V_h *contains all* $\alpha + \beta \times (X + w_h)$ *with* $\alpha, \beta \in \mathbb{R}^3$ *and* $w_h \in V_h$. *Then*

$$d_\tau \langle \rho v_h, \zeta_h \rangle_\Omega^{n+1/2} = \langle b^{n+1/2}, \tilde{\zeta}_h^{n+1/2} \rangle_\Omega + \langle \tau_N^{n+1/2}, \tilde{\zeta}_h^{n+1/2} \rangle_{\partial\Omega_N} + \langle \lambda_h^{n+1/2}, \tilde{\zeta}_h^{n+1/2} \rangle_{\partial\Omega_D}.$$

Proof. For $\beta = 0$ we have $\zeta_h^n = \alpha$ for all $n \geq 0$, and the result for this choice then follows by testing (24a) with $\delta v_h = \alpha$. Note that $A_\beta = 0$ in that case. For $\zeta_h^n = \beta \times x_h^n$ with $x_h^n := (X + u_h^n)$ we proceed as follows. As a first step, we note that

$$d_\tau \langle \rho v_h, \beta \times x_h \rangle_\Omega^{n+1/2} = \langle \rho d_\tau v_h^{n+1/2}, \beta \times \bar{x}_h^{n+1/2} \rangle_\Omega + \langle \rho v_h^{n+1/2}, \beta \times d_\tau x_h^{n+1/2} \rangle_\Omega$$

$$= \langle \rho d_\tau v_h^{n+1/2}, \beta \times \tilde{x}_h^{n+1/2} \rangle_\Omega + \langle \rho d_\tau v_h^{n+1/2}, \beta \times \tfrac{\tau^2}{4} d_\tau v_h^{n+1/2} \rangle_\Omega$$

$$+ \langle \rho v_h^{n+1/2}, \beta \times d_\tau x_h^{n+1/2} \rangle_\Omega.$$

From the definition of u_h^n and using (24d), we further deduce that $d_\tau x_n^{n+1/2} = v^{n+1/2}$. Hence the second and third term in the above inequality vanish. By testing Equation (24a) with $\delta v_h = \beta \times (X + \tilde{u}_h^{n+1/2})$, we then obtain the result for the second case $\zeta_h^n = \beta \times (X + u_h^n)$.□

Remark 6. According to the Proposition 3.5, we obtain the expected balance for the linear momentum also on the fully discrete level. The angular momentum balance might be improved, if $\bar{u}_h^{n+1/2}$ is used instead of $\tilde{u}_h^{n+1/2}$. This could be achieved, e.g. by the fully implicit update formula for u_h^n mentioned in Remark 5. The proof of this angular momentum balance is similar to Proposition 3.5, except that we test (24a) with $\delta v_h = \beta \times (X + \bar{u}_h^{n+1/2})$.

4. Numerical tests

In order to illustrate the theoretical results derived in the previous sections, we now present some numerical results for a typical model problem. In addition, we discuss some details of the implementation that were not required for the analysis before.

4.1. Model problem

We consider a compliant mechanism as part of a soft robotic arm. A rubber-type body is attached to a pivot, whose rotation angle can be controlled. We consider a planar motion under gravity. The angle of the rigid pivot is prescribed as

$$\phi(t) = \begin{cases} 0, & t \leq 0, \\ \frac{\pi}{4}\left(10(\frac{t}{T_c})^3 - 15(\frac{t}{T_c})^4 + 6(\frac{t}{T_c})^5\right), & 0 < t \leq T_c, \\ \frac{\pi}{4}, & t > T_c. \end{cases} \tag{26}$$

The corresponding velocity is imposed as Dirichlet boundary condition (7a) to the contact areas $\partial\Omega_D$, depicted in red in Figure 2. The initial conditions at time $t = 0$ are given by

$$v(0) = 0, \quad S(0) = S_0, \quad u(0) = u_0, \quad \lambda(0) = \lambda_0, \tag{27}$$

and the initial data S_0, u_0, λ_0 are obtained by solving the corresponding static elasticity problem. One can verify that these data satisfy the compatibility conditions (21). The system is modelled in plane strain and its further parameters are listed in Table 1.

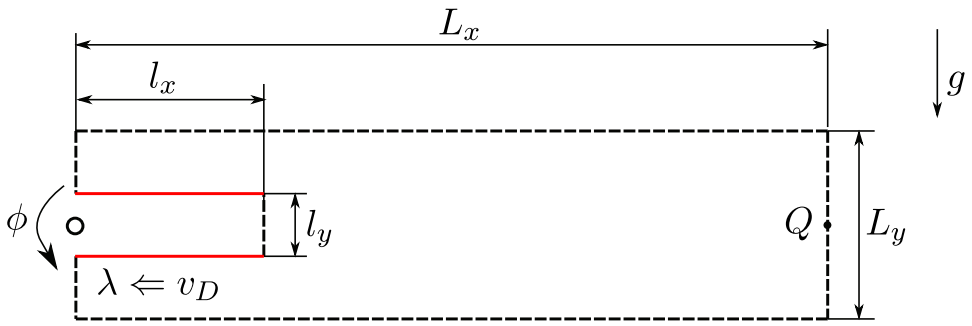

Figure 2. Schematic sketch of the geometry. Red lines mark the Dirichlet boundary $\partial\Omega_D$ for which the displacement velocity v_D is prescribed. The Lagrange multiplier corresponds to the reaction forces.

Table 1. Parameters of the numerical experiment.

L_x	L_y	l_x	l_y	ρ	E	ν	g	T_c
60 cm	15 cm	15 cm	5 cm	960 kg/m^3	$6 \cdot 10^6$ N/m^2	0.49	9.81 m/s^2	0.5 s

4.2. Details on the discretization

A mixed finite element method is used for the spatial discretization. The domain is partitioned into a uniform triangular mesh $\mathcal{T}_h$ and the Galerkin approximation spaces are defined as

$$V_h = [P_1(\mathcal{T}_h) \cap H^1(\Omega)]^2, \qquad S_h = P_0(\mathcal{T}_h; \mathbb{R}^{2\times 2}_{\text{sym}}), \qquad \Lambda_h = V_h|_{\partial\Omega_D}.$$

The mesh size for our tests is chosen as $h \approx 9$ mm. The time step is set to $\tau = 0.25$ ms and the simulations are run until final time $T = 1$ s. All computations were realized in the finite element framework FEniCS (Logg et al. 2012; Kuchta 2021), in which the above finite element spaces (continuous Lagrange polynomials[1] and discontinuous piecewise polynomials[2]) are readily available. The symmetry of the stress tensor can be realized explicitly.

4.3. Computational results

The motion of the robot arm can be approximately described as that of a rigid body. In Figure 3, we show two snapshots of the motion of the rigid and the elastic body.

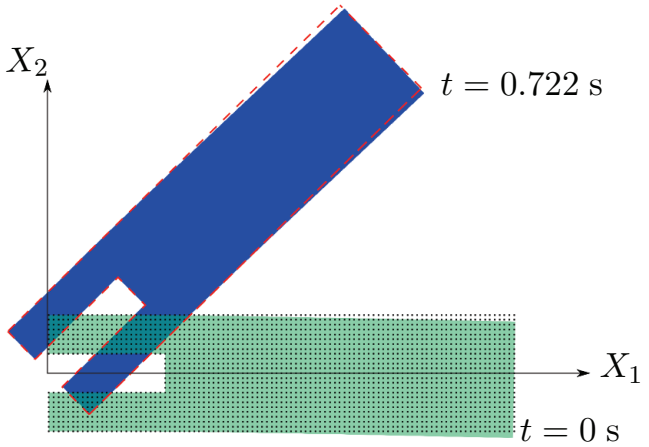

Figure 3. Snapshots at $t = 0$ s (green) and $t = 0.722$ s (blue), dots represent the reference configuration Ω, and the red dashed lines demonstrate the rigid body configuration. Images generated with ParaView (Ayachit 2015).

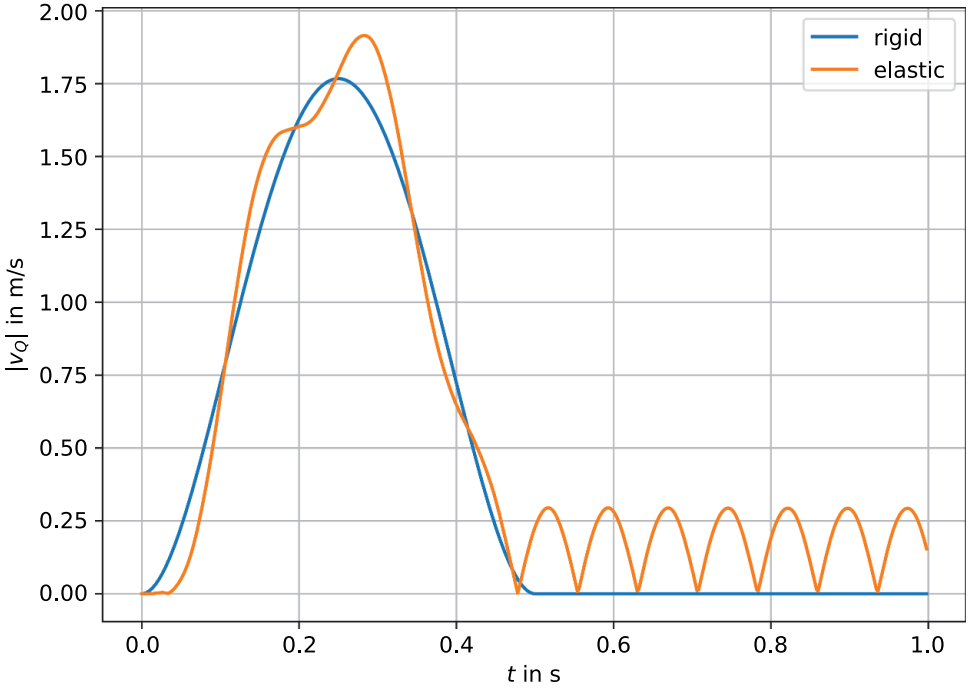

Figure 4. Absolut velocities $|v|$ at the point $Q = (L_x, 0)$ for a rigid body motion (blue) compared to the true elastic motion (orange). Elastic vibrations pertain after the motion of the pivot has been stopped.

As expected, the absolute deviations in the displacement are rather small, which to some extent justifies the use of a rigid body model as a surrogate in simulations. In Figure 4, we illustrate in more detail the differences in velocity between the simplified rigid body and the elastic model considered in this paper. Note that the time variation of the angle $\phi(t)$ leads to elastic deformations causing vibrations of the body. Due to lack of a damping mechanism, the vibrations do not fade away when stopping the motion of the pivot at time $t \geq 0.5$s. In the flexible case, a more sophisticated trajectory planning based on the elastic model is needed for the reduction of such structure-induced oscillations, complemented by feedback control, if necessary; see e.g. Wang and Kotyczka (2021).

4.4. Energy balance

As a next step, we would like to illustrate the exact preservation of the total energy due to the discrete balance equation derived in the previous section. To do so, we introduce the total energy of the system

$$H_{tot}(v, S, u) := H(v, S) + H_{gra}(u), \tag{28}$$

consisting of the internal energy $H(v, X) = \frac{1}{2}\langle \rho v, v\rangle_\Omega + \frac{1}{2}\langle A : S, S\rangle_\Omega$ and the potential energy $H_{gra}(u) = -\langle b, u\rangle_\Omega$ due to the graviational forces. The approximation of the total energy in the fully discrete setting is then given by

$$H^n_{h,tot} = H(v^n_h, S^n_h) + H_{gra}(u^n_h) \tag{29}$$

with $u^n_h = \bar{u}^{n-1/2}_h + \frac{\tau}{2} v^n_h = \bar{u}^{n+1/2}_h - \frac{\tau}{2} v^n_h$. With this approximation, the discrete power balance stated in Proposition 3.4 can be rephrased as

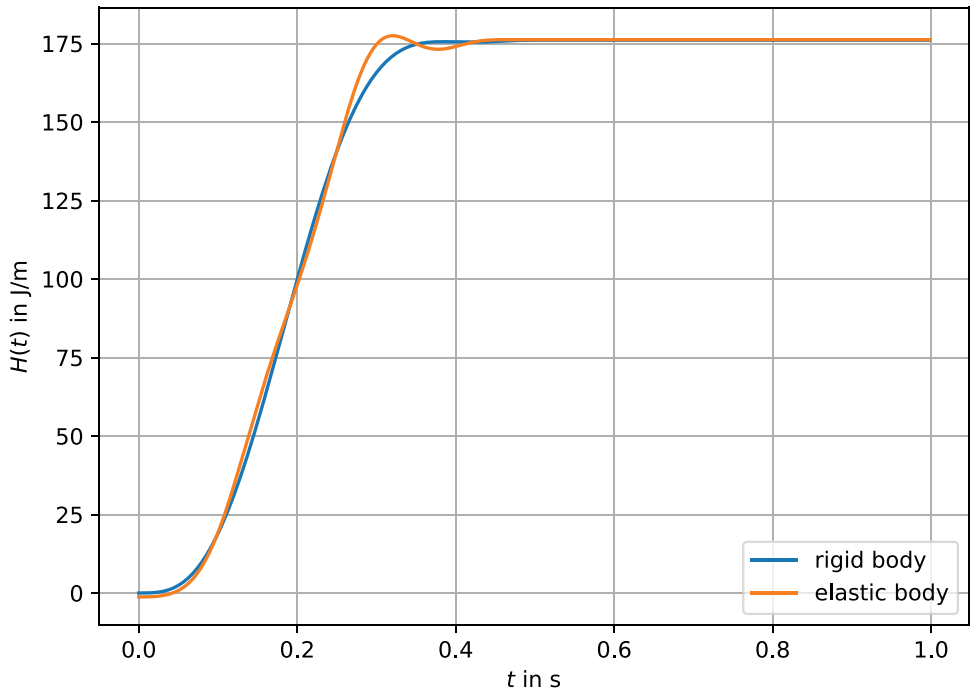

Figure 5. Approximation of the total energy H_{tot} (per meter) obtained for the rigid body model and the structure-preserving fully discrete approximation of the elasticity system proposed in this paper.

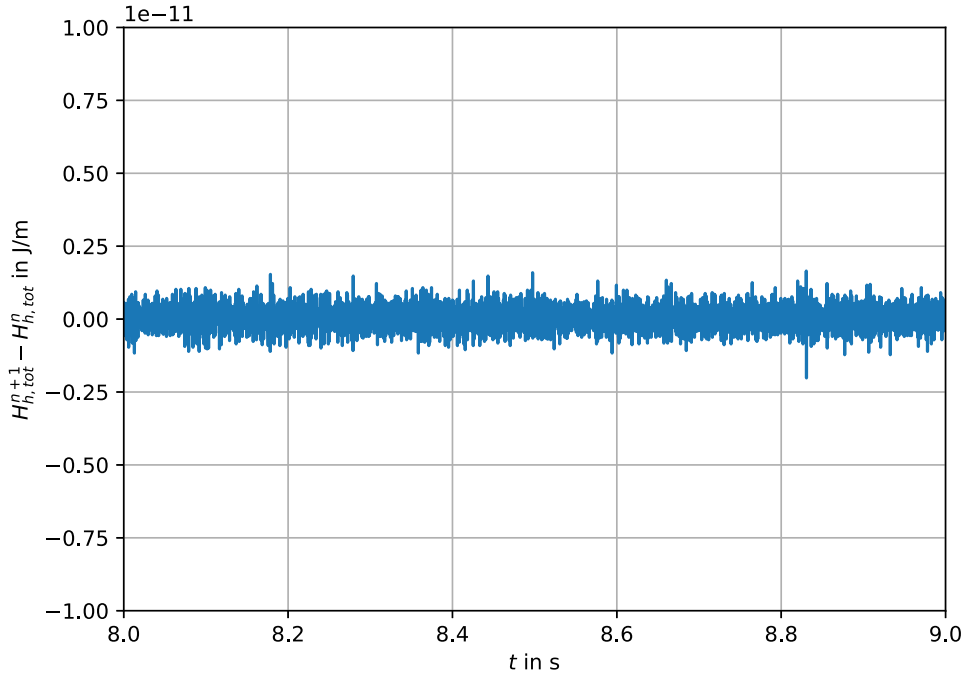

Figure 6. Discrete increments demonstrating energy conversation, i.e. down to the level of solver tolerance.

$$d_\tau H_{h,tot}^{n+1/2} = \langle \lambda_h^{n+1/2}, v_D^{n+1/2} \rangle_{\partial\Omega_D} + \langle \tau_N^{n+1/2}, v_h^{n+1/2} \rangle_{\partial\Omega_N}. \tag{30}$$

In our test example, we have $v_D = 0$ and $\tau_N = 0$ for all $t \geq 0.5$ s. Hence the total energy of the discrete system should be conserved after this time instant. In Figure 5, we display the corresponding results.

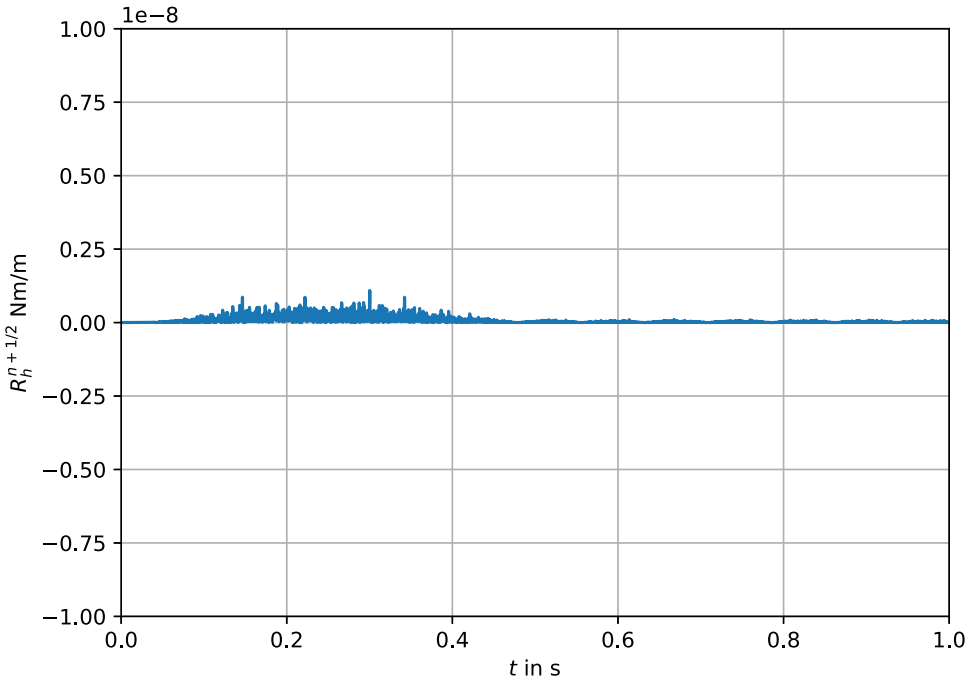

Figure 7. Discrete increments demonstrating momentum balance, i.e. down to the level of solver tolerance.

In the initial phase of the simulation, the motion is prescribed on part of the boundary through inhomogeneous Dirichlet boundary conditions, and the corresponding reaction forces λ lead to an increase in energy. For $t \geq 0.5\,\mathrm{s}$, only the gravitational body forces act and hence the total energy of the system stays constant for the rest of the simulation. In fact, the variations in the total energy observed in our computations stay in the order of round-off errors. As a consequence, the energy remains constant even when simulating over very long time intervals, see Figure 6. These results are in perfect agreement with our theoretical investigations.

4.5. Balance of momentum

Let us finally also illustrate the validity of the discrete momentum balance. To do so, we consider the residual in the equation for the angular momentum, i.e.

$$R_h^{n+1/2} := d_\tau \langle \rho v_h, \zeta_h \rangle_\Omega^{n+1/2} - \langle b^{n+1/2}, \tilde{\zeta}_h^{n+1/2} \rangle_\Omega$$

$$- \langle \tau_N^{n+1/2}, \tilde{\zeta}_h^{n+1/2} \rangle_{\partial\Omega_N} - \langle \lambda_h^{n+1/2}, \tilde{\zeta}_h^{n+1/2} \rangle_{\partial\Omega_D}$$

with $\zeta_h = \beta \times (X + u_h)$. According to Proposition 3.5, we expect that $R_h^{n+1/2} = 0$ for all time-steps.

The results depicted in Figure 7 thus clearly demonstrate the validity of the discrete balance equation for the angular momentum up to round-off errors.

5. Discussion

The motion of a geometrically nonlinear elastic continuum was considered by means of a velocity-stress formulation. The governing equations have the form of a PH system in which the skew-symmetric energy transfer operator is modulated by the displacement field. Based on a weak formulation of the problem, in which the Dirichlet boundary conditions are incorporated by Lagrange multipliers, we derived a power balance and discussed the structure-preserving discretization by mixed finite element methods in space and an implicit midpoint rule in time. A different time integration of the kinematic relation for the displacement field led to a linear implicit time-stepping scheme. The power balance of the system could be proven to be preserved on the semi-discrete and fully-discrete level. The main theoretical results were illustrated by numerical tests for an application inspired by a soft robotics manoeuvre.

In summary, we obtained a structure-preserving discretization for geometrically nonlinear elastodynamics, which can be realized at the same computational effort as in the linear case. A key step to achieve this was to utilize the PH structure of the velocity-stress formulation, while treating the displacement field as an additional passive kinematic variable. The restriction to St. Venant–Kirchhoff materials used in this paper is suitable for application with large deformation but small strains. The extension to more complex nonlinear energies including multiphysical effects and damping mechanisms is topic of future research.

Notes

1. VectorFunctionSpace(mesh, 'CG', degree = 1, dim = 2).
2. TensorElement('DG', mesh.ufl _ cell(), degree = 0, shape=(2, 2), symmetry=True).

Disclosure statement

No potential conflict of interest was reported by the author(s).

References

Arnold DN, Lee JJ. 2014. Mixed methods for elastodynamics with weak symmetry. SIAM J Numer Anal. 52(6):2743–2769. doi: 10.1137/13095032X.

Ayachit U. 2015. The paraview guide: updated for paraview version 4.3. Kitware.

Bécache E, Joly P, Tsogka C. 2002. A new family of mixed finite elements for the linear elastodynamic problem. SIAM J Numer Anal. 39(6):2109–2132. doi: 10.1137/S0036142999359189.

Bonet J, Wood RD. 2008. Nonlinear continuum mechanics for finite element analysis. 2nd ed. Cambridge: Cambridge University Press.

Brugnoli A, Alazard D, Pommier-Budinger V, Matignon D. 2019a. Port-Hamiltonian formulation and symplectic discretization of plate models part I: Mindlin model for thick plates. Appl Math Model. 75:940–960. doi: 10.1016/j.apm.2019.04.035.

Brugnoli A, Alazard D, Pommier-Budinger V, Matignon D. 2019b. Port-Hamiltonian formulation and symplectic discretization of plate models part II: Kirchhoff model for thin plates. Appl Math Model. 75:961–981. doi: 10.1016/j.apm.2019.04.036.

Brugnoli A, Alazard D, Pommier-Budinger V, Matignon D. 2021a. Port-Hamiltonian flexible multibody dynamics. Multibody Syst Dyn. 51(3):343–375. doi: 10.1007/s11044-020-09758-6.
Brugnoli A, Alazard D, Pommier-Budinger V, Matignon D. 2021b. A port-Hamiltonian formulation of linear thermoelasticity and its mixed finite element discretization. J Therm Stresses. 44 (6):643–661. doi: 10.1080/01495739.2021.1917322.
Brugnoli A, Matignon D. 2022. A port-Hamiltonian formulation for the full von-Kármán plate model. 10th European Nonlinear Dynamics Conference (ENOC); Jul 2022; Lyon, France.
Brugnoli A, Rashad R, Califano F, Stramigioli S, Matignon D. 2021. Mixed finite elements for port-Hamiltonian models of von Kármán beams. IFAC-Papersonline. 54(19):186–191. doi: 10.1016/j.ifacol.2021.11.076.
Cardoso-Ribeiro FL, Matignon D, Lefèvre L. 2021. A partitioned finite element method for power-preserving discretization of open systems of conservation laws. IMA J Math Control Inf. 38(2):493–533. doi: 10.1093/imamci/dnaa038.
Cohen GC. 2002. Higher-order numerical methods for transient wave equations. Berlin: Scientific Computation, Springer-Verlag.
Court S, Kunisch K. 2018. Almost global existence of weak solutions for the nonlinear elastodynamics system for a class of strain energies. Adv Differ Equations. 23(1/2):135–160. doi: 10.57262/ade/1508983364.
Duindam V, Macchelli A, Stramigioli S, and H. Bruyninckx, eds. 2009. Modeling and control of complex physical systems. Berlin: Springer-Verlag.
Egger H, Habrich O, Shashkov V. 2021. On the energy stable approximation of Hamiltonian and gradient systems. Comput Methods Appl Math. 21(2):335–349. doi: 10.1515/cmam-2020-0025.
Falaize A, Hélie T. 2016. Passive guaranteed simulation of analog audio circuits: a port-Hamiltonian approach. Appl Sci. 6(10):273. doi: 10.3390/app6100273.
Farle O, Klis D, Jochum M, Floch O, Dyczij-Edlinger R. 2013. A port-Hamiltonian finite-element formulation for the Maxwell equations. Proceedings of the International Conference on Electromagnetics in Advanced Applications (ICEAA); Turin. IEEE.
Festa G, Vilotte JP. 2005. The newmark scheme as velocity-stress time-staggering: an efficient PML implementation for spectral element simulations of elastodynamics. Geophys J Intl. 161 (3):789–812. doi: 10.1111/j.1365-246X.2005.02601.x.
Geveci T. 1988. On the application of mixed finite element methods to the wave equations. RAIRO Modél Math Anal Numér. 22(2):243–250. doi: 10.1051/m2an/1988220202431.
Golo G, Talasila V, van der Schaft A, Maschke B. 2004. Hamiltonian discretization of boundary control systems. Automatica. 40(5):757–771. doi: 10.1016/j.automatica.2003.12.017.
Jacob B, Zwart HJ. 2012. Linear port-Hamiltonian systems on infinite-dimensional spaces. Operator Theory: Adv And Appl. 223. Birkhäuser/Springer, Basel.
Joly P. 2003. Variational methods for time-dependent wave propagation problems, in topics in computational wave propagation. Lect Notes Comput Sci Eng. 31:201–264. Springer, Berlin.
Kinon PL, Thoma T, Betsch P, Kotyczka P. 2023. Port-Hamiltonian formulation and structure-preserving discretization of hyperelastic strings. ECCOMAS Thematic Conference on Multibody Dynamics, Lisboa.
Kotyczka P, Lefèvre L. 2019. Discrete-time port-Hamiltonian systems: a definition based on symplectic integration. Syst Contr Lettr. 133:104530. doi: 10.1016/j.sysconle.2019.104530.
Kotyczka P, Maschke B, Lefèvre L. 2018. Weak form of Stokes–Dirac structures and geometric discretization of port-Hamiltonian systems. J Comput Phys. 361:442–476. doi: 10.1016/j.jcp.2018.02.006.
Kuchta M. 2021. Assembly of multiscale linear PDE operators, in numerical mathematics and advanced applications—enumath 2019. Lect Notes Comput Sci Eng. 139:641–650. Springer, Cham.
Kunkel P, Mehrmann V. 2006. Differential-algebraic equations. Zürich: EMS Textbooks in Mathematics, European Mathematical Society (EMS).
Le Gorrec Y, Zwart H, Maschke B. 2005. Dirac structures and boundary control systems associated with skew-symmetric differential operators. SIAM J Control Optim. 44(5):1864–1892. doi: 10.1137/040611677.

Leis R. 1986. Initial-boundary value problems in mathematical physics. B. G. Teubner, Stuttgart: John Wiley & Sons, Ltd.
Logg A, Mardal KA, Wells GN. 2012. Automated solution of differential equations by the finite element method. Lect Notes In Comput Sci Eng Springer, Heidelberg. 84.
Macchelli A, Melchiorri C, Stramigioli S. 2009. Port-based modeling and simulation of mechanical systems with rigid and flexible links. IEEE Trans Robot. 25(5):1016–1029. doi: 10.1109/TRO.2009.2026504.
Makridakis CG. 1992. On mixed finite element methods for linear elastodynamics. Numer Math. 61(1):235–260. doi: 10.1007/BF01385506.
Maschke BM, van der Schaft AJ. 1992. Port-controlled Hamiltonian systems: modelling origins and systemtheoretic properties. IFAC Proc. 25(13):359–365. doi: 10.1016/S1474-6670(17)52308-3.
Mehrmann V, Unger B. 2023. Control of port-Hamiltonian differential-algebraic systems and applications. Acta Numer. 32:395–515. doi: 10.1017/S0962492922000083.
Müller R. 2021. Time-continuous power-balanced simulation of nonlinear audio circuits: realtime processing framework and aliasing rejection [Ph.D. diss.]. Sorbonne Université.
Rashad R, Brugnoli A, Califano F, Luesink E, Stramigioli S. 2023. Intrinsic nonlinear elasticity: an exterior calculus formulation. J Nonlinear Sci. 33(5). doi: 10.1007/s00332-023-09945-7.
Rashad R, Califano F, van der Schaft AJ, Stramigioli S. 2020. Twenty years of distributed port-Hamiltonian systems: a literature review. IMA J Math Contr Infor. 37(4):1400–1422. doi: 10.1093/imamci/dnaa018.
Scovazzi G, Song T, Zeng X. 2017. A velocity/stress mixed stabilized nodal finite element for elastodynamics: analysis and computations with strongly and weakly enforced boundary conditions. Comput Methods Appl Mech Engrg. 325:532–576. doi: 10.1016/j.cma.2017.07.018.
Thoma T, Kotyczka P. 2022. Port-Hamiltonian FE models for filaments. IFAC-Papersonline. 55(30):353–358. doi: 10.1016/j.ifacol.2022.11.078.
van der Schaft AJ, Maschke BM. 2002. Hamiltonian formulation of distributed-parameter systems with boundary energy flow. J Geom Phys. 42(1–2):166–194. doi: 10.1016/S0393-0440(01)00083-3.
Wang M, Kotyczka P. 2021. Trajectory control of an elastic beam based on port-Hamiltonian numerical models. at - Automatisierungstechnik. 69(6):457–471. doi: 10.1515/auto-2020-0159.
Warsewa A, Böhm M, Sawodny O, Tarn C. 2021. A port-Hamiltonian approach to modeling the structural dynamics of complex systems. Appl Math Model. 89:1528–1546. doi: 10.1016/j.apm.2020.07.038.
Wriggers P. 2008. Nonlinear finite element methods. Berlin: Springer-Verlag.
Zhang B, Yang Y, Feng M. 2019. Mixed virtual element methods for elastodynamics with weak symmetry. J Comput Appl Math. 353:49–71. doi: 10.1016/j.cam.2018.12.020.

A.2 Port-Hamiltonian FE models for filaments

CRediT author statement:

Tobias Thoma:	Conceptualization, Acuration of Experimental Data, Methodology, Software, Visualization, Writing - Original Draft
Paul Kotyczka:	Conceptualization, Supervision, Writing - Original Draft

Available online at www.sciencedirect.com

ScienceDirect

IFAC PapersOnline CONFERENCE PAPER ARCHIVE

IFAC PapersOnLine 55-30 (2022) 353–358

Port-Hamiltonian FE models for filaments

Tobias Thoma *, **Paul Kotyczka** *

* *Technical University of Munich, TUM School of Engineering and Design, Chair of Automatic Control, Garching, Germany (e-mail: tobias.thoma@tum.de, kotyczka@tum.de).*

Abstract: In this article, we present the port-Hamiltonian representation, the structure preserving discretization and the resulting finite-dimensional state space model of one-dimensional filaments based on a mixed finite element formulation. Due to the fact that the equations of motion of a filamentous body are based on the theory of geometrically nonlinear mechanical systems, the port-Hamiltonian formulation is expressed by means of its co-energy (effort) variables. The resulting port-Hamiltonian state space model features a quadratic Hamiltonian and the nonlinearity is reflected in the state dependence of its interconnection matrix. Numerical experiments generated with FEniCS illustrate the properties of the resulting finite element models.

Keywords: port-Hamiltonian systems, mixed finite elements, geometrically nonlinear mechanical systems, structure preserving discretization, filamentous bodies

1. INTRODUCTION

Port-Hamiltonian (PH) systems provide a framework for modeling, analysis and control of complex dynamical systems (Duindam et al., 2009) where the complexity might result from multi-physical couplings, non-trivial domains and nonlinearity. Since modeling many engineering problems requires handling partial differential equations (PDEs), the PH community has been heavily involved in the theory of infinite-dimensional PH systems (Jacob and Zwart, 2012; Kotyczka, 2019) in recent years (Rashad et al., 2020). Thus, some PDEs of different pyhsical domains have already been transformed into a PH structure. Also, the benefits of PH modeling for linear mechanical systems have already been outlined in several articles, e.g. Macchelli and Melchiorri (2004); Warsewa et al. (2021).

In addition to the PH modeling of linear mechanical systems, the PH community dealt with modeling and discretization of nonlinear mechanical systems. Examples are the interconnection of linear elastodynamics with (nonlinear) rigid body motion (Brugnoli et al., 2020a), the direct discretization of nonlinear PDEs of continuum mechanics (Brugnoli et al., 2021) or the formulation of explicit PH FEM models of geometrically nonlinear mechanical systems based on the Hellinger-Reissner principle (Thoma and Kotyczka, 2022). The considered PDEs follow mostly from the theory of geometrically nonlinear continuum mechanics [1] (Bonet and Wood, 2008). By means of further assumptions on the geometrically nonlinear continuum mechanics, special system classes, such as beams and shells, can be derived (Brugnoli and Matignon, 2022).

One special infinite-dimensional nonlinear mechanical system class frequently represented in engineering is the one of the so-called filamentous bodies (Weiß, 2000; Dresig and Fidlin, 2014), e.g., ropes, cables, belts. Its field of application includes harbor cranes, cable robots, bionic robotic hands, underwater cables, satellite systems and much more. As can be seen from the examples, filamentous bodies are usually only a sub-module of large systems and are accordingly interconnected with their environment. This environmental coupling makes filamentous bodies an ideal choice for PH modeling. To the best of our knowledge, the modeling of filamentous bodies has not yet received any attention from the PH community.

In this contribution, the PH formulation of a one-dimensional elastic filament model is represented. With momentum density and strain as states, the Hamiltonian is quadratic, i.e., the constitutive equations are linear. The nonlinearity appears in a nonlinear interconnection operator that depends on the (derivative of the) position vector. The corresponding PH state differential equations undergo a spatial discretization based on the mixed finite element method, which preserves the (energetic) structure of a PH system (Cardoso-Ribeiro et al., 2020). Since the filament modeling, like the von-Kármán beam modeling, is based on the theory of geometrically nonlinear continuum mechanics, the resulting finite-dimensional system bears a strong resemblance to the one in Brugnoli et al. (2021).

This article is organized as follows. In Section 2, we recall the equations of motion of an elastic filament and show its PH representation. The mixed finite element discretization procedure is demonstrated in Section 3. Section 4 focuses on numerical simulations and their discussion. Section 5 gives a short conclusion.

2. MODELING

In this section, we recall the most important concepts of filamentous bodies and show the PH formulation of an elastic filament.

[1] Due to the strong geometry change of a body, the basic mechanical equations have to be represented by nonlinear functions. However, the material behavior (constitutive equation) can be described with a linear relationship between stress and strain.

10.1016/j.ifacol.2022.11.078

2.1 Lagrange realization

As already mentioned, the modeling of filamentous bodies follows from several assumptions concerning nonlinear continuum mechanics, which allows to take into account large displacements of a body. These assumptions will be briefly presented in the following, and the reader is referred to Kuhn et al. (1995); Weiß (2000); Mankala and Agrawal (2004) for more information.

The first assumption concerns the geometry of filamentous bodies. Since the cross-sectional dimensions are significantly smaller compared to the longitudinal dimension of a filament, the considered body is modeled as a one-dimensional continuum. To achieve this, the Bernoulli hypothesis is used. I.e., cross sections remain perpendicular to the normal axis and plane. This ensures that no warping can occur in the cross-section of a body. In addition, only small distortions, a purely elastic behavior and a negligible heat transfer by friction are assumed, which leads to a linear material law. Thus, the bodies considered in this article can be classified as geometrically nonlinear mechanical systems. Moreover, constant cross sections are assumed in the following. So far, mainly the assumptions for the derivation of the nonlinear Timoshenko beam have been presented. Neglecting some shear distortion components, the nonlinear Euler-Bernoulli beam is obtained. Finally, assuming a rotational symmetric cross-section and neglecting bending and torsional stiffness, the equations of motion of an elastic filamentous body shown below are obtained.

Remark 1. Using the model of a one-dimensional continuum, effects caused by the internal structure of a body cannot be described, e.g. internal friction of a multi-layer spiral rope (Weiß, 2000). Nevertheless, a one-dimensional model should be used whenever possible. Otherwise, the computational costs of a FE simulation for multi-dimensional systems increase considerably due to the high number of required elements [2].

In order to enable integration over a constant spatial domain in the finite element method, the balance equation of a body is expressed with respect to a reference (material) configuration. In the following we consider the one-dimensional reference configuration $\Omega = [0, L] \subset \mathbb{R}^3$ of length L. The material coordinate or arc length coordinate

$$s = X_1 \in \mathbb{R} \tag{1}$$

describes the position of each particle in the reference configuration. By means of the position vector $r(s,t) \in \mathbb{R}^3$, the current (spatial) configuration $\Omega_t \subset \mathbb{R}^3$ or the current position of each particle can be determined at any time $t \in \mathbb{R}$. Accordingly, the time evolution of r describes the movement of the particles. The concept is illustrated in Figure 1.

The momentum balance equation of an elastic filament (Weiß, 2000) in material coordinates is given by

$$\rho A \ddot{r} = \frac{\partial}{\partial s}\left(\sigma \frac{\frac{\partial r}{\partial s}}{\sqrt{\frac{\partial r}{\partial s}^T \frac{\partial r}{\partial s}}}\right) + f \tag{2}$$

with the density $\rho \in \mathbb{R}$, the cross-sectional area $A \in \mathbb{R}$, the tangent vector $\frac{\partial r}{\partial s} \in \mathbb{R}^3$ and the normal force $\sigma \in \mathbb{R}$, which is connected to the strain

[2] A small number of elements would lead to excessive stiffening.

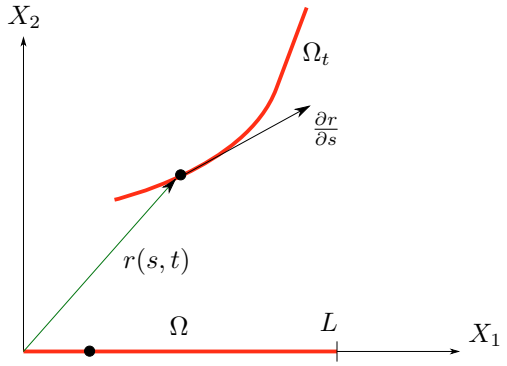

Fig. 1. Undeformed and deformed body configurations on $\mathbb{R}^2$.

$$\epsilon = \sqrt{\frac{\partial r}{\partial s}^T \frac{\partial r}{\partial s}} - 1 \in \mathbb{R} \tag{3}$$

by a linear relationship

$$\sigma = EA\epsilon. \tag{4}$$

The vector $f \in \mathbb{R}^3$ denotes the forces per unit length.

Remark 2. To obtain the equations of motion of an inelastic filament, one requires

$$\frac{\partial r}{\partial s}^T \frac{\partial r}{\partial s} = 1, \tag{5}$$

with which there is no strain. This requirement combined with the balance equation

$$\rho A \ddot{r} = \frac{\partial}{\partial s}\left(\xi \frac{\partial r}{\partial s}\right) + f \tag{6}$$

leads to a differential algebraic system, where the Lagrange multiplier $\xi \in \mathbb{R}$ represents the reaction (normal) force ensuring the inelasticity. The balance equation (6) can also be derived from an Euler-Bernoulli beam without longitudinal elongation. The PH realization and subsequent discretization of an inelastic filament is presented in Appendix A.

Remark 3. For simplicity, we assume that no forces per unit length are present, accordingly $f = 0$. This is not a major restriction, since in the case of a PH representation, these forces can be completed by adding an external port or augmenting the Hamiltonian, if f results from a potential, see Section 4.

2.2 Port-Hamiltonian representation

We represent the PH realization of elastic filaments.

State differential equations. Due to the assumptions of geometrical nonlinearity the total energy

$$H = \frac{1}{2}\int_\Omega p^T \frac{1}{\rho A} p + \epsilon EA\epsilon \, d\Omega \tag{7}$$

can be expressed in terms of linear momenta $p = \rho A \dot{r} \in \mathbb{R}^3$ per unit length and the strain $\epsilon \in \mathbb{R}$. The variational derivatives, which, for the Hamiltonian without spatial derivatives, are simply the partial derivatives of the Hamiltonian density,

$$\frac{\delta H(p,\epsilon)}{\delta p} = \frac{p}{\rho A} \tag{8}$$

$$\frac{\delta H(p,\epsilon)}{\delta \epsilon} = EA\epsilon, \tag{9}$$

defined as the co-energy variables (efforts) the velocities $v = \frac{p}{\rho A} \in \mathbb{R}^3$ and the normal force $\sigma = EA\epsilon \in \mathbb{R}$.

Theorem 4. The state differential equations for elastic filaments in PH form are given by

$$\underbrace{\begin{bmatrix}\dot{p}\\ \dot{\epsilon}\\ \dot{r}\end{bmatrix}}_{\dot{x}} = \underbrace{\begin{bmatrix} 0 & \frac{\partial}{\partial s}\left(\frac{\frac{\partial r}{\partial s}}{\sqrt{\frac{\partial r}{\partial s}^T\frac{\partial r}{\partial s}}}\times\right) & -I \\ \left(\frac{\frac{\partial r}{\partial s}^T}{\sqrt{\frac{\partial r}{\partial s}^T\frac{\partial r}{\partial s}}}\right)\frac{\partial \times}{\partial s} & 0 & 0 \\ I & 0 & 0 \end{bmatrix}}_{\mathcal{J}(r)} \underbrace{\begin{bmatrix} v \\ \sigma \\ \frac{\delta H}{\delta r}\end{bmatrix}}_{e} \tag{10}$$

with the formally skew-adjoint operator [3] $\mathcal{J}(r)$.

Proof. To obtain the first state equation of the PH form (10), the left hand side of (2) is rewritten in terms of the linear momenta p. Taking the time derivative of (3) leads to the second state equation. In order to close the system, an extra equation for r has to be included, which leads to the augmented system (10).

Since we assumed in (7) that $H(p,\epsilon)$ does not explicitly depend on r, it follows $b = \frac{\delta H}{\delta r} = 0$. In general, $b \in \mathbb{R}^3$ can be interpreted as an potential internal volume force, with which gravity can be taken into account. Due to the choice of state variables, the PH representation (11) can be rewritten in terms of acceleration and normal force rate,

$$\begin{bmatrix}\rho A\dot{v}\\ (EA)^{-1}\dot{\sigma}\\ \dot{r}\end{bmatrix} = \mathcal{J}(r)\begin{bmatrix} v \\ \sigma \\ 0\end{bmatrix}. \tag{11}$$

Energy balance and boundary ports. The energy balance for the filament

$$\begin{aligned}\dot{H} &= \int_\Omega \frac{\delta H}{\delta p}^T \dot{p} + \frac{\delta H}{\delta \epsilon}\dot{\epsilon} + \frac{\delta H}{\delta r}^T \dot{r}\, d\Omega \\ &= \int_\Omega e^T \mathcal{J}(r) e\, d\Omega\end{aligned} \tag{12}$$

gives after integration by parts

$$\begin{aligned}\dot{H} &= \int_\Omega v^T \frac{\partial}{\partial s}\left(\frac{\frac{\partial r}{\partial s}}{\sqrt{\frac{\partial r}{\partial s}^T\frac{\partial r}{\partial s}}}\sigma\right) + \sigma\frac{\frac{\partial r}{\partial s}^T}{\sqrt{\frac{\partial r}{\partial s}^T\frac{\partial r}{\partial s}}}\frac{\partial v}{\partial s}\, d\Omega \\ &= \left[\sigma\frac{\frac{\partial r}{\partial s}^T}{\sqrt{\frac{\partial r}{\partial s}^T\frac{\partial r}{\partial s}}} v\right]_0^L\end{aligned} \tag{13}$$

from which formal skew-adjointness of $\mathcal{J}(r)$ can be deduced. Besides the strong form (11), solving the initial boundary value problem of the PH system requires initial and boundary conditions. The boundary $\partial\Omega = \{0, L\} = \Sigma_D \cup \Sigma_N$ can in general be split into two subsets on which the Neumann and Dirichlet boundary conditions are applied. The Neumann condition, e.g., at $s = L$,

$$\sigma\frac{\frac{\partial r}{\partial s}}{\sqrt{\frac{\partial r}{\partial s}^T\frac{\partial r}{\partial s}}} = \bar{\tau} = u_N \qquad \text{on} \quad \Sigma_N \tag{14}$$

with the traction vector $\bar{\tau} \in \mathbb{R}^3$ results form the infinitesimal force equilibrium at the ends of the filament. The Dirichlet condition, e.g., at $s = 0$,

$$v = \bar{\nu} = u_D \qquad \text{on} \quad \Sigma_D \tag{15}$$

imposes the desired velocity $\bar{\nu} \in \mathbb{R}^3$ on the Dirichlet boundary. Thus, we obtain the characteristic energy balance

$$\dot{H} = u_D y_D + u_N y_N \tag{16}$$

of a PH system, with the y_D and y_N as power conjugated outputs.

3. MIXED FE FORMULATION

We now derive the finite dimensional PH representation of an elastic filament based on the mixed finite element method (Zienkiewicz et al., 2005). For the sake of simplicity, we assume that there are no Dirichlet boundary conditions in the following, accordingly $\partial\Omega = \Sigma_N$. This is not a major restriction, since Dirichlet conditions can be inserted by means of Lagrange multipliers as shown in Brugnoli et al. (2020b).

3.1 Weak form

To derive a finite element discretization, a weak (or variational) form of (11) is required. The weak form of (11) is given by

$$\int_\Omega \delta v^T \rho A\dot{v} - \delta v^T \frac{\partial}{\partial s}\left(\frac{\frac{\partial r}{\partial s}}{\sqrt{\frac{\partial r}{\partial s}^T\frac{\partial r}{\partial s}}}\sigma\right)\, d\Omega = 0 \tag{17a}$$

$$\int_\Omega \delta\sigma (EA)^{-1}\dot{\sigma} - \delta\sigma\left(\frac{\frac{\partial r}{\partial s}^T}{\sqrt{\frac{\partial r}{\partial s}^T\frac{\partial r}{\partial s}}}\right)\frac{\partial v}{\partial s}\, d\Omega = 0 \tag{17b}$$

$$\int_\Omega \delta b^T \dot{r} - \delta b^T v\, d\Omega = 0 \tag{17c}$$

containing the test functions δv, $\delta\sigma$ and δb. Due to the choice of test functions (power pairing) the weak form can be interpreted in terms of virtual power. In case of (17a) the principle of virtual velocities fulfills the force equilibrium and the principle of virtual forces in (17b) and (17c) the kinematics.

Remark 5. In case of non-uniform boundary conditions, the modified weak form should not be set up as shown in Thoma and Kotyczka (2021). Due to scalar dimension of the virtual normal force $\delta\sigma \in \mathbb{R}$, the three-dimensional residual $v - \bar{\nu} \in \mathbb{R}^3$ can not be included in (17b) for the weak imposition of (15).

3.2 Discretization

Theorem 6. By applying a mixed Galerkin discretization of (11) based on the weak formulation (17) and using trial and test functions from the same bases

[3] $\mathcal{J}(r)$ includes the identity matrix $I \in \mathbb{R}^{3\times 3}$.

$$v(s,t) = \phi(s)^T \hat{v}(t), \qquad \delta v(s) = \phi(s)^T \delta\hat{v},$$
$$\sigma(s,t) = \psi(s)^T \hat{\sigma}(t), \qquad \delta\sigma(s) = \psi(s)^T \delta\hat{\sigma},$$
$$r(s,t) = \phi(s)^T \hat{r}(t), \qquad \delta b(s) = \phi(s)^T \delta\hat{b},$$

the PH state space model

$$\underbrace{\begin{bmatrix} M_v & 0 & 0 \\ 0 & M_\sigma & 0 \\ 0 & 0 & M_v \end{bmatrix}}_{M=M^T>0} \begin{bmatrix} \dot{\hat{v}} \\ \dot{\hat{\sigma}} \\ \dot{\hat{r}} \end{bmatrix} = \underbrace{\begin{bmatrix} 0 & -K(\hat{r}) & -M_v{}^T \\ K^T(\hat{r}) & 0 & 0 \\ M_v & 0 & 0 \end{bmatrix}}_{J(\hat{r})=-J(\hat{r})^T} \begin{bmatrix} \hat{v} \\ \hat{\sigma} \\ 0 \end{bmatrix} + \underbrace{\begin{bmatrix} G_\tau \\ 0 \\ 0 \end{bmatrix}}_{G} \bar{\tau} \tag{18}$$

$$y = \underbrace{\begin{bmatrix} G_\tau^T & 0 & 0 \end{bmatrix}}_{G^T} \begin{bmatrix} \hat{v} \\ \hat{\sigma} \\ 0 \end{bmatrix} \tag{19}$$

with the approximate quadratic Hamiltonian

$$\hat{H} = \frac{1}{2}\hat{v}^T M_v \hat{v} + \frac{1}{2}\hat{\sigma}^T M_\sigma \hat{\sigma} \tag{20}$$

is obtained.

Proof. Before the actual discretization is performed, (17a) is integrated by parts, which leads to

$$\int_\Omega \delta v^T \rho A \dot{v} - \frac{\partial \delta v}{\partial s}^T \left(\frac{\frac{\partial r}{\partial s}}{\sqrt{\frac{\partial r}{\partial s}^T \frac{\partial r}{\partial s}}} \sigma \right) d\Omega - \left[\delta v^T \bar{\tau} \right]_{\Sigma_N} = 0. \tag{21}$$

Inserting the approximations depending on the basis functions allows us to take all variables except $\hat{r}$ out of the integrals. Since $\delta\hat{v}$, $\delta\hat{\sigma}$ and $\delta\hat{b}$ are arbitrary, we get the state space model (18) containing the matrices

$$M_v = \int_\Omega \phi \rho A \phi^T \, d\Omega \tag{22}$$
$$M_\sigma = \int_\Omega \psi (EA)^{-1} \psi^T \, d\Omega \tag{23}$$
$$K(\hat{r}) = \int_\Omega \frac{\partial \phi}{\partial s} \left(\frac{\frac{\partial (\phi^T \hat{r})}{\partial s}}{\sqrt{\frac{\partial (\phi^T \hat{r})}{\partial s}^T \frac{\partial (\phi^T \hat{r})}{\partial s}}} \psi^T \right) d\Omega \tag{24}$$
$$G_\tau = [\phi]_{\Sigma_N}. \tag{25}$$

The discrete Hamiltonian (20) is obtained by substituting the approximated co-energy variables into $H(v,\sigma)$. Its time derivative

$$\dot{\hat{H}} = \hat{v}^T G_\tau \bar{\tau} \tag{26}$$

gives the power conjugated output (19), which concludes the proof.

4. NUMERICAL RESULTS

In this section, we demonstrate a simple FEniCS (Logg et al., 2012) simulation of a planar (i.e., we consider $\mathbb{R}^2$ instead of $\mathbb{R}^3$ as the embedding space) filament pendulum written in its PH formulation. The pendulum of length L is firmly clamped on its left side ($s = 0$) and is loaded with the force $\bar{\tau}$ on its right side ($s = L$). This results in the boundary conditions

$$v(s=0,t) = \bar{\nu} \tag{27}$$
$$\left[\sigma \frac{\frac{\partial r}{\partial s}^T}{\sqrt{\frac{\partial r}{\partial s}^T \frac{\partial r}{\partial s}}} \right]_{s=L} = \bar{\tau}. \tag{28}$$

In addition to the force $\bar{\tau}$, the system is subject to gravity, what leads to the augmented Hamiltonian

$$H = \frac{1}{2}\int_\Omega p^T \frac{1}{\rho A} p + \epsilon E A \epsilon \, d\Omega + V \tag{29}$$

with the gravitational potential

$$V = \int_\Omega r^T b \, d\Omega = \int_\Omega r^T \begin{bmatrix} 0 \\ \rho A g \end{bmatrix} d\Omega. \tag{30}$$

We consider the initial conditions

$$v(s,t=0) = [0 \text{ m/s } 0 \text{ m/s}]^T \tag{31}$$
$$\sigma(s,t=0) = 0 \text{ N} \tag{32}$$
$$r(s,t=0) = \begin{bmatrix} \frac{\sqrt{2}}{2}s & -\frac{\sqrt{2}}{2}s \end{bmatrix}^T. \tag{33}$$

The physical parameters are listed in Table 1.

Table 1. Parameters for the filament pendulum simulation

Symbol	Value
L	3 m
ρA	0.0025 kg/m
EA	49.06 N
g	9.81 N
$\bar{\nu}$	$\begin{bmatrix} 0 \text{ m/s} & 0 \text{ m/s} \end{bmatrix}^T$
$\bar{\tau}$	$\begin{cases} \begin{bmatrix} 0 \text{ N} & 0.01 \text{ N} \end{bmatrix}^T & \forall t \in (0 \text{ s}, 0.2 \text{ s}] \\ \begin{bmatrix} 0 \text{ N} & 0 \text{ N} \end{bmatrix}^T & t = 0 \text{ s} \ \& \ \forall t > 0.2 \text{ s} \end{cases}$

The filament is discretized with 100 equidistant line elements, first order Lagrange polynomials for ϕ (velocities, position), zero order discontinuous basis functions for ψ (normal force).

Due to the Lagrange multiplier $\lambda \in \mathbb{R}^2$ (Brugnoli et al., 2020b) satisfying the Dirichlet boundary condition (15) the spatial discretization procedure results in a differential algebraic system,

$$\underbrace{\begin{bmatrix} M_v & 0 & 0 & 0 \\ 0 & M_\sigma & 0 & 0 \\ 0 & 0 & M_v & 0 \\ 0 & 0 & 0 & 0 \end{bmatrix}}_{M=M^T\geq 0} \begin{bmatrix} \dot{\hat{v}} \\ \dot{\hat{\sigma}} \\ \dot{\hat{r}} \\ \dot{\lambda} \end{bmatrix} = \underbrace{\begin{bmatrix} 0 & -K(\hat{r}) & -M_v{}^T & G_\lambda \\ K^T(\hat{r}) & 0 & 0 & 0 \\ M_v & 0 & 0 & 0 \\ -G_\lambda^T & 0 & 0 & 0 \end{bmatrix}}_{J=-J^T} \begin{bmatrix} \hat{v} \\ \hat{\sigma} \\ \hat{b} \\ \lambda \end{bmatrix} + \underbrace{\begin{bmatrix} G_\tau & 0 \\ 0 & 0 \\ 0 & 0 \\ 0 & I \end{bmatrix}}_{G} \begin{bmatrix} \bar{\tau} \\ \bar{\nu} \end{bmatrix} \tag{34}$$

$$y = \underbrace{\begin{bmatrix} G_\tau^T & 0 & 0 & 0 \\ 0 & 0 & 0 & I \end{bmatrix}}_{G^T} \begin{bmatrix} \hat{v} \\ \hat{\sigma} \\ \hat{b} \\ \lambda \end{bmatrix} \tag{35}$$

with $G_\lambda = [\phi]_{\Sigma_D}$. This finite-dimensional system is simulated for $T = 1$ s using the implicit midpoint rule and sampling time $\Delta t = 1$ ms. Its nonlinear equations are solved

by Newton iterations. The matrix $K(\hat{r})$ is evaluated at each time step using numerical integration.

Figure 2 shows the Hamiltonian which keeps its constant level for $t \geq 0.2$ s due to the fact that no more power is transmitted at the boundaries. Figure 3 demonstrates snapshots of the pendulum at different time steps.

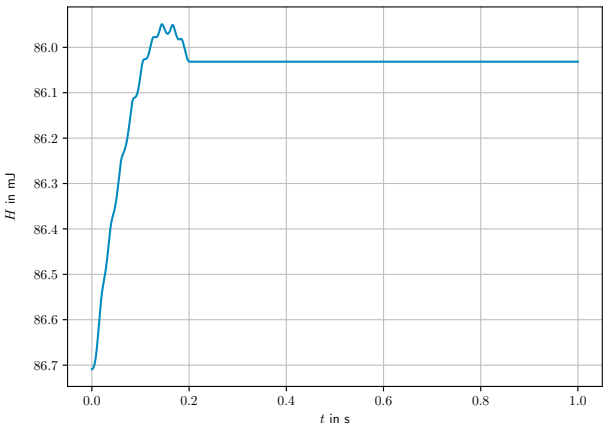

Fig. 2. Total energy H of the filament. Since the Dirichlet boundary condition is $\bar{\nu} = 0$, only $\bar{\tau}$ controls the flow of energy to the system.

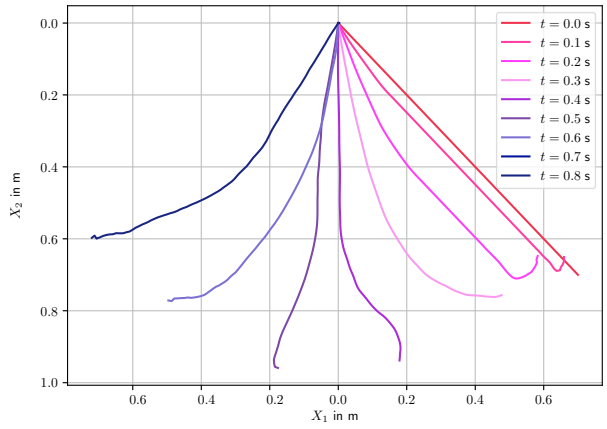

Fig. 3. Filament configuration at different time steps.

5. CONCLUSION

We presented a mixed finite element discretization procedure for one-dimensional filaments in order to achieve a PH state space model. The considered system class follows from the theory of geometrically nonlinear mechanical systems. Due to the chosen structure of the weak form and an appropriate discretization, a PH state space model with a quadratic Hamiltonian and nonlinear energy matrix could be generated.

REFERENCES

Bonet, J. and Wood, R.D. (2008). *Nonlinear Continuum Mechanics for Finite Element Analysis*. Cambridge University Press. doi:10.1017/cbo9780511755446.

Brugnoli, A., Alazard, D., Pommier-Budinger, V., and Matignon, D. (2020a). Port-Hamiltonian flexible multibody dynamics. *Multibody System Dynamics*, 51(3), 343–375. doi:10.1007/s11044-020-09758-6.

Brugnoli, A., Cardoso-Ribeiro, F.L., Haine, G., and Kotyczka, P. (2020b). Partitioned finite element method for structured discretization with mixed boundary conditions. *IFAC-PapersOnLine*, 53(2), 7557–7562. doi:10.1016/j.ifacol.2020.12.1351.

Brugnoli, A. and Matignon, D. (2022). A port-Hamiltonian formulation for the full von-Kármán plate model. In *10th European Nonlinear Dynamics Conference (ENOC)*.

Brugnoli, A., Rashad, R., Califano, F., Stramigioli, S., and Matignon, D. (2021). Mixed finite elements for port-Hamiltonian models of von-Kármán beams. *IFAC-PapersOnLine*, 54(19), 186–191. doi:10.1016/j.ifacol.2021.11.076.

Cardoso-Ribeiro, F.L., Matignon, D., and Lefèvre, L. (2020). A partitioned finite element method for power-preserving discretization of open systems of conservation laws. *IMA Journal of Mathematical Control and Information*, 38(2), 493–533. doi:10.1093/imamci/dnaa038.

Dresig, H. and Fidlin, A. (2014). *Schwingungen mechanischer Antriebssysteme*. Springer Berlin Heidelberg. doi:10.1007/978-3-642-24117-8.

Duindam, V., Macchelli, A., Stramigioli, S., and Bruyninckx, H. (2009). *Modeling and Control of Complex Physical Systems*. Springer Berlin Heidelberg. doi:10.1007/978-3-642-03196-0.

Jacob, B. and Zwart, H. (2012). *Linear Port-Hamiltonian Systems on Infinite-dimensional Spaces*, volume 223. Springer. doi:10.1007/978-3-0348-0399-1.

Kotyczka, P. (2019). *Numerical Methods for Distributed Parameter Port-Hamiltonian Systems*. TUM.University Press. doi:10.14459/2019md1510230.

Kuhn, A., Steiner, W., Zemann, J., Dinevski, D., and Troger, H. (1995). A comparison of various mathematical formulations and numerical solution methods for the large amplitude oscillations of a string pendulum. *Applied Mathematics and Computation*, 67(1-3), 227–264. doi:10.1016/0096-3003(94)00060-h.

Logg, A., Mardal, K.A., and Wells, G.N. (2012). *Automated Solution of Differential Equations by the Finite Element Method*. Springer. doi:10.1007/978-3-642-23099-8.

Macchelli, A. and Melchiorri, C. (2004). Modeling and control of the Timoshenko beam. The distributed port-Hamiltonian approach. *SIAM Journal on Control and Optimization*, 43(2), 743–767. doi:10.1137/s0363012903429530.

Mankala, K.K. and Agrawal, S.K. (2004). Dynamic modeling and simulation of satellite tethered systems. *Journal of Vibration and Acoustics*, 127(2), 144–156. doi:10.1115/1.1891811.

Rashad, R., Califano, F., van der Schaft, A.J., and Stramigioli, S. (2020). Twenty years of distributed port-Hamiltonian systems: A literature review. *IMA Journal of Mathematical Control and Information*, 37(4), 1400–1422. doi:10.1093/imamci/dnaa018.

Thoma, T. and Kotyczka, P. (2021). Explicit port-Hamiltonian FEM-models for linear mechanical systems with non-uniform boundary conditions. In *(submitted*

to) 10th Vienna International Conference on Mathematical Modelling.
Thoma, T. and Kotyczka, P. (2022). Explicit port-Hamiltonian FEM models for geometrically nonlinear mechanical systems. In *(submitted to) Mathematical and Computer Modelling of Dynamical Systems.* doi: 10.48550/ARXIV.2202.02097.
Warsewa, A., Böhm, M., Sawodny, O., and Tarín, C. (2021). A port-Hamiltonian approach to modeling the structural dynamics of complex systems. *Applied Mathematical Modelling*, 89, 1528–1546. doi: 10.1016/j.apm.2020.07.038.
Weiß, H. (2000). *Zur Dynamik geometrisch nichtlinearer Balken.* Ph.D. thesis, Technische Universität Chemnitz.
Zienkiewicz, O.C., Taylor, R.L., and Zhu, J.Z. (2005). *The Finite Element Method: Its Basis and Fundamentals.* Butterworth-Heinemann. doi:10.1016/C2009-0-24909-9.

Appendix A. INELASTIC FILAMENTS

In this section, we demonstrate the PH FE model of inelastic filaments. Its derivation is quite similar to that of the elastic filaments discussed in the main part of this article.

A.1 Port-Hamiltonian representation

Due to the constraint (5) the total energy

$$H = \frac{1}{2}\int_\Omega p^T \frac{1}{\rho A} p \, d\Omega \tag{A.1}$$

only contains the angular momenta p as state variable leading to the effort (8).

Theorem 7. The differential-algebraic state equations in PH form are given by

$$\begin{bmatrix}\dot p\\ 0\\ \dot r\end{bmatrix} = \underbrace{\begin{bmatrix} 0 & \frac{\partial}{\partial s}\left(\frac{\partial r}{\partial s}\times\right) & -I\\ \frac{\partial r}{\partial s}^T\frac{\partial \times}{\partial s} & 0 & 0\\ I & 0 & 0\end{bmatrix}}_{\mathcal{J}(r)} \begin{bmatrix} v\\ \xi\\ \frac{\delta H}{\delta r}\end{bmatrix} \tag{A.2}$$

with the formally skew-adjoint operator $\mathcal{J}(r)$.

Proof. The proof is similar to the one of Theorem 4 except that the second state (algebraic) equation results from the time derivative of (5).

Repeating the same conclusions as in Section 2, e.g., $\frac{\delta H}{\delta r} = 0$, the PH state differential equations can be written as

$$\begin{bmatrix}\rho A\dot v\\ 0\\ \dot r\end{bmatrix} = \mathcal{J}(r)\begin{bmatrix} v\\ \xi\\ 0\end{bmatrix}. \tag{A.3}$$

Considering the time derivative of (A.1) leads to the power balance

$$\dot H = \int_\Omega \frac{\delta H}{\delta p}^T \dot p \, d\Omega = \left[\xi \frac{\partial r}{\partial s}^T v\right]_0^L. \tag{A.4}$$

Therefore the total energy of the system is controlled by the Neumann

$$\frac{\partial r}{\partial s}\xi = \bar\tau \qquad \text{on} \quad \Sigma_N \tag{A.5}$$

and Dirichlet boundary condition

$$v = \bar\nu \qquad \text{on} \quad \Sigma_D \tag{A.6}$$

transferring power over the boundary $\partial\Omega = \{0, L\}$.

A.2 Mixed FE formulation

Theorem 8. The implicit PH state space model with pure Neumann boundary conditions

$$\underbrace{\begin{bmatrix} M_v & 0 & 0\\ 0 & 0 & 0\\ 0 & 0 & M_v\end{bmatrix}}_{M=M^T\geq 0}\begin{bmatrix}\dot{\hat v}\\ \dot{\hat\xi}\\ \dot{\hat r}\end{bmatrix} = \underbrace{\begin{bmatrix} 0 & -K(\hat r) & -M_v{}^T\\ K^T(\hat r) & 0 & 0\\ M_v & 0 & 0\end{bmatrix}}_{J(\hat r)=-J(\hat r)^T}\begin{bmatrix}\hat v\\ \hat\xi\\ 0\end{bmatrix} + \underbrace{\begin{bmatrix} G_\tau\\ 0\\ 0\end{bmatrix}}_{G}\bar\tau \tag{A.7}$$

$$y = \underbrace{\begin{bmatrix} G_\tau^T & 0 & 0\end{bmatrix}}_{G^T}\begin{bmatrix}\hat v\\ \hat\xi\\ 0\end{bmatrix} \tag{A.8}$$

with the approximate quadratic Hamiltonian

$$\hat H = \frac{1}{2}\hat v^T M_v \hat v \tag{A.9}$$

is obtained by applying a mixed finite elment discretization of (A.2) where trial and test functions from the same bases

$$\begin{aligned} v(s,t) &= \phi(s)^T\hat v(t), & \delta v(s) &= \phi(s)^T\delta\hat v,\\ \xi(s,t) &= \psi(s)^T\hat\sigma(t), & \delta\xi(s) &= \psi(s)^T\delta\hat\xi,\\ r(s,t) &= \phi(s)^T\hat r(t), & \delta b(s) &= \phi(s)^T\delta\hat b,\end{aligned}$$

are used.

Proof. The proof is similar to the one of Theorem 6, except that it includes the weak form

$$\int_\Omega \delta v^T\rho A\dot v - \delta v^T\frac{\partial}{\partial s}\left(\frac{\partial r}{\partial s}\xi\right) d\Omega = 0 \tag{A.10a}$$

$$\int_\Omega \delta\xi\frac{\partial r}{\partial s}^T\frac{\partial v}{\partial s}\, d\Omega = 0 \tag{A.10b}$$

$$\int_\Omega \delta b^T\dot r - \delta b^T v \, d\Omega = 0 \tag{A.10c}$$

as starting point. Correspondingly, the state space model contains the slightly modified matrices

$$M_v = \int_\Omega \phi\rho A\phi^T \, d\Omega \tag{A.11}$$

$$K(\hat r) = \int_\Omega \frac{\partial\phi}{\partial s}\frac{\partial(\phi^T\hat r)}{\partial s}\psi^T \, d\Omega \tag{A.12}$$

$$G_\tau = [\phi]_{\Sigma_N}. \tag{A.13}$$

Remark 9. Inserting Dirichlet boundary conditions works exactly as in Section 4.

A.3 Explicit port-Hamiltonian FEM-models for linear mechanical systems with non-uniform boundary conditions

CRediT author statement:

Tobias Thoma:	Conceptualization, Acuration of Experimental Data, Methodology, Software, Visualization, Writing - Original Draft
Paul Kotyczka:	Conceptualization, Supervision, Writing - Original Draft

Available online at www.sciencedirect.com

ScienceDirect

IFAC PapersOnline CONFERENCE PAPER ARCHIVE

IFAC PapersOnLine 55-20 (2022) 499–504

Explicit Port-Hamiltonian FEM-Models for Linear Mechanical Systems with Non-Uniform Boundary Conditions

Tobias Thoma *, **Paul Kotyczka** *

* *Technical University of Munich, TUM School of Engineering and Design, Chair of Automatic Control, Garching, Germany (e-mail: tobias.thoma@tum.de)*

Abstract: In this contribution, we present how to obtain explicit state space models in port-Hamiltonian form when a mixed finite element method is applied to a linear mechanical system with non-uniform boundary conditions. The key is to express the variational problem based on the principle of virtual power, with both the Dirichlet (velocity) and Neumann (stress) boundary conditions imposed in a weak sense. As a consequence, the formal skew-adjointness of the system operator becomes directly visible after integration by parts, and, after compatible FE discretization, the boundary degrees of freedom of both causalities appear as explicit inputs in the resulting state space model. The rationale behind our formulation is illustrated using a lumped parameter example, and numerical experiments on a one-dimensional rod show the properties of the approach in practice.

Keywords: port-Hamiltonian systems, elastodynamics, non-uniform boundary conditions, structure-preserving discretization, mixed finite elements, weak form, principle of virtual power

1. INTRODUCTION

Port-Hamiltonian (PH) systems provide a framework for modeling, analysis and control of complex dynamical systems where the complexity can result from multi-physical domains and their couplings. Since several engineering problems are described by partial differential equations the theory of infinite-dimensional PH systems (van der Schaft and Maschke, 2002; Villegas, 2007; Jacob and Zwart, 2012) has become increasingly important in recent years. The progress in modeling different physical domains by means of the PH framework is documented in the review article Rashad et al. (2020). Also the possibilities and advantages of the PH formulation for structural mechanics have been presented in several articles see e.g. the recent works Brugnoli et al. (2020a) and Warsewa et al. (2021).

For the numerical approximation of distributed parameter PH systems, which is required for simulation and (late lumping) control design, various approaches have been developed in the past 20 years that aim at the preservation of the PH structure, see e.g. the overview in Kotyczka (2019). One of the most successful techniques is the partitioned finite element method (PFEM) (Farle et al., 2013; Cardoso-Ribeiro et al., 2020). If applied to a system of conservation/balance laws or the variational formulation of an elastic mechanical system, one half of the equations written in a weak form are integrated by parts. The choice of the partially integrated equation determines which boundary condition is satisfied in a weak sense and which type of input variables appears in the resulting finite dimensional control system. With non-uniform boundary conditions (of both Neumann and Dirichlet type) the approaches presented until now do not immediately lead to an explicit state space model. The first method presented in Brugnoli et al. (2020b) employs Lagrange multipliers and leads to a differential-algebraic finite-dimensional PH system. The second one is based on the virtual decomposition of the domain to interconnect models with different causalities. A mixed finite element approach, which leads to the desired explicit state space models with non-uniform causality is introduced in Kotyczka et al. (2018). There, however, the choice of original finite element spaces requires (tunable) power-preserving mappings to define the discrete states.

In this article, we show how to obtain explicit FE models with both inputs and a skew-symmetric interconnection matrix as a visible expression of energy routing in PH systems. We write the equations of elastodynamics in a variational form, with weakly imposed boundary conditions, reminiscent of the *Hellinger-Reissner* variational principle [1] (Lu et al., 2019), and revealing the principle of virtual power. An advantage of the resulting explicit state space representations is the direct applicability of well-established order reduction techniques for ODE control models.

This article starts with the elastodynamics partial differential equations (PDEs) in Section 2. In Section 3, we demonstrate the weak formulation based on the principle of virtual power and the discretization process. In Section 4, the formulation is illustrated with a one-dimensional rod under Dirichlet-Neumann boundary conditions and its finite-dimensional (approximate) counterpart, a mass-

[1] The Hellinger-Reisner principle is a mixed variational principle using a two-field functional, where displacements and stresses are varied separately.

Peer review under responsibility of International Federation of Automatic Control.
10.1016/j.ifacol.2022.09.144

spring chain. Section 5 shows numerical results, and Section 6 gives some short conclusions.

2. PRELIMINARIES

This section recalls the first-order (port-)Hamiltonian representation of the linear elastodynamics PDE

$$\rho\ddot{u} - D^T E D u = 0 \tag{1}$$

on a three dimensional domain $\Omega \subset \mathbb{R}^3$ in vector notation (Zienkiewicz et al., 2005; Brugnoli et al., 2020a). The total energy is

$$H(u,\dot{u}) = \frac{1}{2}\int_\Omega \left(\dot{u}^T\dot{u}\rho + (Du)^T E D u\right)\, d\Omega \tag{2}$$

with the displacements

$$u = [u_1 \;\; u_2 \;\; u_3]^T \in \mathbb{R}^3 \tag{3}$$

from an undeformed configuration and the velocities $\dot{u} \in \mathbb{R}^3$, the constant mass density $\rho \in \mathbb{R}$, the spatial differentiation operator

$$D = \begin{bmatrix} \frac{\partial}{\partial x_1} & 0 & 0 \\ 0 & \frac{\partial}{\partial x_2} & 0 \\ 0 & 0 & \frac{\partial}{\partial x_3} \\ \frac{\partial}{\partial x_2} & \frac{\partial}{\partial x_1} & 0 \\ 0 & \frac{\partial}{\partial x_3} & \frac{\partial}{\partial x_2} \\ \frac{\partial}{\partial x_3} & 0 & \frac{\partial}{\partial x_1} \end{bmatrix} \tag{4}$$

and the matrix of Hooke's law elastic coefficients

$$E = \begin{bmatrix} \lambda+2G & \lambda & \lambda & 0 & 0 & 0 \\ \lambda & \lambda+2G & \lambda & 0 & 0 & 0 \\ \lambda & \lambda & \lambda+2G & 0 & 0 & 0 \\ 0 & 0 & 0 & G & 0 & 0 \\ 0 & 0 & 0 & 0 & G & 0 \\ 0 & 0 & 0 & 0 & 0 & G \end{bmatrix} \in \mathbb{R}^{6\times 6}, \tag{5}$$

where $\lambda \in \mathbb{R}$ and $G \in \mathbb{R}$ are known as Lamé coefficients. Since the strains and stresses are symmetric tensors, they can be represented as a strain vector

$$\epsilon = [\epsilon_{11} \;\; \epsilon_{22} \;\; \epsilon_{33} \;\; \gamma_{12} \;\; \gamma_{23} \;\; \gamma_{13}]^T \in \mathbb{R}^6 \tag{6}$$

and a stress vector

$$\sigma = [\sigma_{11} \;\; \sigma_{22} \;\; \sigma_{33} \;\; \sigma_{12} \;\; \sigma_{23} \;\; \sigma_{13}]^T \in \mathbb{R}^6. \tag{7}$$

Notation. All field quantities depend on the spatial coordinate $x \in \mathbb{R}^3$ and the time $t \in \mathbb{R}$, which we omit for brevity.

Port-Hamiltonian model. Defining the vectors of linear momenta $p \in \mathbb{R}^3$ and strains $\epsilon \in \mathbb{R}^6$,

$$p = \rho v \tag{8}$$

$$\epsilon = Du \tag{9}$$

as energy variables (or states), the Hamiltonian (2) can be rewritten as $H(p,\epsilon)$. We obtain the fields of co-energy quantities (efforts, co-states) velocity $v \in \mathbb{R}^3$ and stress $\sigma \in \mathbb{R}^6$ from $H(p,\epsilon)$ applying the variational derivative,

$$v = \dot{u} = \left(\frac{\delta H(p,\epsilon)}{\delta p}\right)^T \tag{10}$$

$$\sigma = E\epsilon = \left(\frac{\delta H(p,\epsilon)}{\delta \epsilon}\right)^T. \tag{11}$$

Now Eq. (1) can be written in a first order co-energy representation

$$\rho\dot{v} = D^T\sigma \tag{12a}$$

$$E^{-1}\dot{\sigma} = Dv, \tag{12b}$$

or summarized,

$$\begin{bmatrix} \rho I & 0 \\ 0 & E^{-1} \end{bmatrix} \begin{bmatrix} \dot{v} \\ \dot{\sigma} \end{bmatrix} = \begin{bmatrix} 0 & D^T \\ D & 0 \end{bmatrix} \begin{bmatrix} v \\ \sigma \end{bmatrix}, \tag{13}$$

with a s.p.d. matrix on the left, and a formally skew-adjoint differential operator matrix on the right.

Boundary conditions. Since this article focuses on non-uniform boundary conditions the boundary $\partial\Omega = \Sigma_D \cup \Sigma_N$ is split into two subsets on which the Neumann and Dirichlet boundary condition are applied. The Neumann condition [2]

$$N^T\sigma = \bar{\tau} \quad \text{on } \Sigma_N \tag{14}$$

with the applied surface traction $\bar{\tau} \in \mathbb{R}^3$ and the matrix

$$N^T = \begin{bmatrix} n_1 & 0 & 0 & n_2 & 0 & n_3 \\ 0 & n_2 & 0 & n_1 & n_3 & 0 \\ 0 & 0 & n_3 & 0 & n_2 & n_1 \end{bmatrix} \in \mathbb{R}^{3\times 6} \tag{15}$$

containing the outward normal vector direction components of the surface results form the infinitesimal equilibrium at the surface. The Dirichlet condition

$$v = \bar{\nu} \quad \text{on } \Sigma_D \tag{16}$$

imposes the desired velocity $\bar{\nu} \in \mathbb{R}^3$ on the surface. Differentiating $H(v,\sigma)$ in time, and exploiting the definition of effort variables gives the power balance / conservation law for energy

$$\begin{aligned} \dot{H} &= \int_{\partial\Omega} v^T N^T\sigma \, d\partial\Omega \\ &= \int_{\Sigma_N} v^T\bar{\tau}\, d\Sigma_N + \int_{\Sigma_D} \bar{\nu}^T N^T\sigma \, d\Sigma_D. \end{aligned} \tag{17}$$

The surface traction and the velocity field on $\partial\Omega$ are the boundary port variables, their pairing gives the power supplied to the domain Ω. Their causality is opposite on the Neumann and the Dirichlet boundary.

3. MAIN RESULTS

In this section we derive the finite dimensional PH system of the elastodynamics equations based on the partitioned finite element method (Cardoso-Ribeiro et al., 2020). By a careful formulation of the problem in weak form we ensure that the structural power balance is immediately visible in the form of the resulting matrices.

3.1 Weak form

We start with (12) written in the weak form

$$\begin{aligned} \delta P_v = &\int_\Omega \left(\delta v^T\rho\dot{v} - \delta v^T D^T\sigma\right)\, d\Omega \\ &+ \int_{\Sigma_N} \delta v^T(N^T\sigma - \bar{\tau})\, d\Sigma_N = 0 \end{aligned} \tag{18a}$$

$$\begin{aligned} \delta P_\sigma = &\int_\Omega \left(\delta\sigma^T E^{-1}\dot{\sigma} - \delta\sigma^T D v\right)\, d\Omega \\ &+ \int_{\Sigma_D} \delta\sigma^T N(v - \bar{\nu})\, d\Sigma_D = 0 \end{aligned} \tag{18b}$$

with the test functions δv and $\delta\sigma$, and including the boundary conditions (14), (16). Equation (18a) represents

[2] With the bar we indicate imposed/known quantities.

the residual of the momentum balance equation on Ω and the Neumann boundary, (18b) represents the residual of the kinematic equation on Ω and the Dirichlet boundary. The test functions δv and $\delta\sigma$ give a nice interpretation in terms of virtual power, when paired (involving integration) with velocities and stresses.

Remark 1. The structure of (18) is reminiscent of the *Hellinger-Reissner* principle, where Dirichlet boundary conditions can also be imposed weakly (Lu et al., 2019).

3.2 Discretization

Theorem 2. The mixed Galerkin discretization of (13) with Neumann and Dirichlet boundary conditions (14) and (16) based on the weak formulation (18) and using trial and test functions from the same bases,

$$v(x,t) = \phi(x)^T \hat{v}(t), \qquad \delta v(x) = \phi(x)^T \delta\hat{v}, \tag{19}$$

$$\sigma(x,t) = \psi(x)^T \hat{\sigma}(t), \qquad \delta\sigma(x) = \psi(x)^T \delta\hat{\sigma}, \tag{20}$$

$$\bar{\tau}(x,t) = \xi(x)^T \hat{\tau}(t), \qquad \bar{\nu}(x,t) = \zeta(x)^T \hat{\nu}(t), \tag{21}$$

leads to the explicit PH state space model in co-energy form [3]

$$\underbrace{\begin{bmatrix} M_v & 0 \\ 0 & M_\sigma \end{bmatrix}}_{M} \underbrace{\begin{bmatrix} \dot{\hat{v}} \\ \dot{\hat{\sigma}} \end{bmatrix}}_{\dot{\hat{e}}} = \underbrace{\begin{bmatrix} 0 & -K \\ K^T & 0 \end{bmatrix}}_{J} \underbrace{\begin{bmatrix} \hat{v} \\ \hat{\sigma} \end{bmatrix}}_{\hat{e}} + \underbrace{\begin{bmatrix} G_v & 0 \\ 0 & G_\sigma \end{bmatrix}}_{G} \underbrace{\begin{bmatrix} \hat{\tau} \\ \hat{\nu} \end{bmatrix}}_{\hat{u}} \tag{22}$$

$$\hat{y} = \underbrace{\begin{bmatrix} G_v^T & 0 \\ 0 & G_\sigma^T \end{bmatrix}}_{G^T} \underbrace{\begin{bmatrix} \hat{v} \\ \hat{\sigma} \end{bmatrix}}_{\hat{e}}, \tag{23}$$

where $\hat{e} = \nabla\hat{H}$ with the approximate Hamiltonian

$$\hat{H} = \frac{1}{2}\hat{e}^T M \hat{e}. \tag{24}$$

The sub-matrices are given by

$$M_v = \int_\Omega \phi\rho\phi^T \, d\Omega \tag{25}$$

$$M_\sigma = \int_\Omega \psi E^{-1}\psi^T \, d\Omega \tag{26}$$

$$K = \int_\Omega (D\phi^T)^T\psi^T \, d\Omega - \int_{\Sigma_D} \phi N^T\psi^T \, d\Sigma_D \tag{27}$$

$$G_v = \int_{\Sigma_N} \phi\xi^T \, d\Sigma_N \tag{28}$$

$$G_\sigma = \int_{\Sigma_D} \psi N\zeta^T \, d\Sigma_D. \tag{29}$$

Proof. After integration by parts of (18a), the weak form can be written as

$$\delta P_v = \int_\Omega \left(\delta v^T\rho\dot{v} + (D\delta v)^T\sigma\right) \, d\Omega - \int_{\partial\Omega} \delta v^T N^T\sigma \, d\partial\Omega + \int_{\Sigma_N} \delta v^T(N^T\sigma - \bar{\tau}) \, d\Sigma_N = 0, \tag{30a}$$

$$\delta P_\sigma = \int_\Omega \left(\delta\sigma^T E^{-1}\dot{\sigma} - \delta\sigma^T Dv\right) \, d\Omega + \int_{\Sigma_D} \delta\sigma^T N(v - \bar{\nu}) \, d\Sigma_D = 0. \tag{30b}$$

[3] Here, $\hat{u}$ denotes the input vector, and not the displacement degrees of freedom. The representation is explicit, because M is invertible.

Splitting the second integral in (30a) into the parts on Σ_N and Σ_D, we get

$$\delta P_v = \underbrace{\int_\Omega \delta v^T\rho\dot{v} \, d\Omega + \int_\Omega (D\delta v)^T\sigma \, d\Omega}_{-\delta P_{\text{int}}} \underbrace{- \int_{\Sigma_D} \delta v^T N^T\sigma \, d\Sigma_D - \int_{\Sigma_N} \delta v^T\bar{\tau} \, d\Sigma_N}_{-\delta P_{\text{ext}}} = 0, \tag{31a}$$

$$\delta P_\sigma = \int_\Omega \delta\sigma^T E^{-1}\dot{\sigma} \, d\Omega - \int_\Omega \delta\sigma^T Dv \, d\Omega + \int_{\Sigma_D} \delta\sigma^T Nv \, d\Sigma_D - \int_{\Sigma_D} \delta\sigma^T N\bar{\nu} \, d\Sigma_D = 0. \tag{31b}$$

The second and third terms already suggest the appearance of a (formally) skew-adjoint operator, which will turn to a skew-symmetric interconnection matrix in the discretized model.

(31a) represents the well-known balance between the negative internal virtual δP_{int} and external power δP_{ext}. δP_{int} includes the virtual power due to inertia and virtual stress power. δP_{ext} describes the virtual power due to external forces. (31b) follows by the principle of virtual forces and fulfills the kinematic equation and the Dirichlet condition. Because the vector $\bar{\nu}$ due to the Dirichlet boundary conditions is applied in a weak sense, the space of virtual velocities δv will not be restricted due to the constraints resulting from the Dirichlet boundary conditions. Therefore, the term $\int_{\Sigma_D} \delta v^T N^T\sigma \, d\Sigma_D \neq 0$ representing reaction forces – being compatible with the Dirichlet constraints – does not vanish compared to the case of strong Dirichlet conditions, where $\int_{\Sigma_D} \delta v^T N^T\sigma \, d\Sigma_D = 0$ due to the principle of d'Alembert. A difference to the application of PFEM reported until now is the boundary integral in the definition (27) of K. If Lagrange multipliers are used (Brugnoli et al., 2020b), a corresponding terms appears in front of them. Section 4 will illustrate this idea using a simple example.

Inserting the test and trial functions according to (19), (31) turns to

$$\delta P_v = \int_\Omega \left(\delta\hat{v}^T\phi\rho\phi^T\dot{\hat{v}} + \delta\hat{v}^T(D\phi^T)^T\psi^T\hat{\sigma}\right) \, d\Omega - \int_{\Sigma_D} \delta\hat{v}^T\phi N^T\psi^T\hat{\sigma} \, d\Sigma_D - \int_{\Sigma_N} \delta\hat{v}^T\phi\xi^T\hat{\tau} \, d\Sigma_N = 0, \tag{32a}$$

$$\delta P_\sigma = \int_\Omega \left(\delta\hat{\sigma}^T\psi E^{-1}\psi^T\dot{\hat{\sigma}} - \delta\hat{\sigma}^T\psi(D\phi^T)\hat{v}\right) \, d\Omega + \int_{\Sigma_D} \delta\hat{\sigma}^T\psi N\phi^T\hat{v} \, d\Sigma_D - \int_{\Sigma_D} \delta\hat{\sigma}^T\psi N\zeta^T\hat{\nu} \, d\Sigma_D = 0. \tag{32b}$$

Since all quantities not depending on the spatial coordinates x can be taken out of the integral, and the equations must hold for all $\delta\hat{v}$ and $\delta\hat{\sigma}$, we obtain the resulting set of ODEs (22) with matrices (25)–(29).

Inserting the approximation of the co-energy variables in $H(u, \dot{u})$ according to (2) with $EDu = \sigma$ and $\dot{u} = v$, yields

$$\hat{H} = \frac{1}{2} \int_\Omega \left(\hat{v}^T \phi \rho \phi^T \hat{v} + \hat{\sigma}^T \psi E^{-1} \psi^T \hat{\sigma} \right) \, d\Omega, \tag{33}$$

or, written in compact form, (24).

From the time derivative of the discretized energy,

$$\dot{\hat{H}} = \hat{v}^T G_v \hat{\tau} + \hat{\sigma}^T G_\sigma \hat{\nu}, \tag{34}$$

we obtain the natural definition of the discrete power-conjugated outputs (23), what concludes the proof. □

Remark 3. Integration by parts of (18b) is also an option to get a discrete PH system. However, since ψ usually represents discontinuous basis functions between elements, this option is uncommon in elastodynamics.

Remark 4. A mixed formulation (18) can lead to higher accuracy compared to single field principles (Zienkiewicz et al., 2005).

4. A ONE-DIMENSIONAL EXAMPLE

To illustrate that the approach of weak imposition of both types of boundary conditions has an intuitive interpretation also in finite dimension, we consider a one dimensional rod and the depicted mass-damper chain (with $N = 2$ springs for simplicity) as its finite-dimensional counterpart.

4.1 One-dimensional rod

First we consider a rod of length L

$$\rho \dot{v} = \frac{\partial \sigma}{\partial x} \tag{35a}$$

$$\frac{1}{EA} \dot{\sigma} = \frac{\partial v}{\partial x} \tag{35b}$$

with the energy variables momentum density $p = \rho v$ and strain $\varepsilon = \sigma/(EA)$ and the co-energy variables velocity v and normal force σ. The boundary conditions are

$$v(x = 0, t) = \bar{\nu} \tag{36a}$$

$$\sigma(x = L, t) = \bar{\tau}. \tag{36b}$$

Imposing them in weak form as described in Section 3.1 gives us for all variations $\delta v(x)$ and $\delta\sigma(x)$

$$\delta P_v = \int_0^L \delta v \rho \dot{v} + \frac{\partial \delta v}{\partial x} \sigma \, dx + \delta v(0)\sigma(0) - \delta v(L)\bar{\tau} = 0, \tag{37}$$

$$\delta P_\sigma = \int_0^L \delta\sigma \frac{\dot{\sigma}}{EA} - \delta\sigma \frac{\partial v}{\partial x} \, dx + \delta\sigma(0) \cdot (\bar{\nu} - v(0)) = 0, \tag{38}$$

which has a nice connection to the following finite-dimensional system.

4.2 Spring-mass chain

For simplicity we consider $N = 2$ springs and $N+1$ (mass) points at their terminals, see Fig. 1. The argumentation holds for arbitrary N.

Dirichlet and Neumann BCs. If we impose a Dirichlet BC at a terminal point (here the left one, index 0), its mass is not considered in the lumped kinetic energy. The reason is that the velocity of the (mass) point is not derived from its kinetic energy, but directly imposed as a BC. For Neumann BC (here the right terminal), the input force specifies the value of the external force $F_{N+1} = F_3$, which contributes to the acceleration of the corresponding mass.

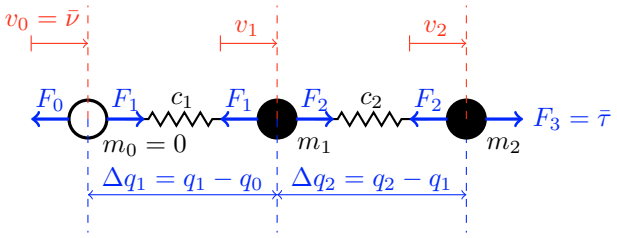

Fig. 1. Spring-mass chain with $N = 2$

States and co-states. With this convention we first set up the canonical states, the energies and the co-states for masses and springs as storage elements for kinetic and potential energy. With p_1, p_2 the momenta of the masses, and $\Delta q_1 = q_1 - q_0$, $\Delta q_2 = q_2 - q_1$ the elongations of the springs from their undeformed state, the total energy is

$$H(p, \Delta q) = \sum_{i=1}^{2} \frac{1}{2m_i} p_i^2 + \sum_{i=1}^{2} \frac{1}{2} c_i \Delta q_i^2, \tag{39}$$

with m_i and c_i, $i = 1, 2$, masses and stiffnesses. The velocities v_1, v_2 and the restoring spring forces F_1, F_2, as shown in Fig. 1, are co-state or effort variables that are derived from the Hamiltonian:

$$v_i = \frac{\partial H}{\partial p_i}, \quad F_i = \frac{\partial H}{\partial \Delta q_i}, \qquad i = 1, 2. \tag{40}$$

Virtual power based on velocity variations. We express two formulations of the principle of virtual power. The first is the virtual power balance based on virtual velocities δv_0, δv_1, δv_2 (we allow for $\delta v_0 \neq 0$, as v_0 is imposed only *weakly*):

$$\delta P_v = -\delta P^m + \delta P_{ic}^v = 0, \tag{41}$$

where

$$\begin{aligned} \delta P^m &= \dot{p}_1 \delta v_1 + \dot{p}_2 \delta v_2 \\ &= -f_1^m \delta e_1^m - f_1^m \delta e_2^m \end{aligned} \tag{42}$$

expresses the variation of power supplied to the kinetic energy storage elements (masses), and $f_i^m = -\dot{p}_i$, $i = 1, 2$ are the canonical flows using a generator sign convention. On the contrary,

$$\delta P_{ic}^v = (F_1 - F_0)\delta v_0 + (F_2 - F_1)\delta v_1 + (F_3 - F_2)\delta v_2 \tag{43}$$

is the variation of the power injected to the remaining system and its environment at the locations of the masses. Specifying the right boundary force in a weak sense,

$$(\bar{\tau} - F_3)\delta v_2 = 0 \qquad \forall \, \delta v_2, \tag{44}$$

and adding this expression to (41), we obtain after sorting terms,

$$\begin{aligned} \delta P_v = &(F_0 - F_1)\delta v_0 \\ &+ (\dot{p}_1 + F_1 - F_2)\delta v_1 + (\dot{p}_2 + F_2 - \bar{\tau})\delta v_2 = 0. \end{aligned} \tag{45}$$

Requiring the expression to vanish for all velocity variations, we recover the ODEs for the momenta of the masses and the expression for the reaction force at the left boundary. Note on the other hand that we can re-sort the terms on the right as

$$\delta P_v = \sum_{i=1}^{2} (\delta v_i \dot{p}_i + \Delta\delta v_i F_i) + \delta v_0 F_0 - \delta v_2 \bar{\tau} = 0 \quad (46)$$

with $\Delta\delta v_i = \delta v_i - \delta v_{i-1}$, which is the discrete version of (37).

Virtual power based on force variations. We now consider the variations δF_1, δF_2 of the restoring forces (which originate in variations $\delta\Delta q_1$, $\delta\Delta q_2$) and the resulting virtual power balance

$$\delta P_F = -\delta P^c + \delta P_{ic}^F = 0. \quad (47)$$

The term

$$\begin{aligned} \delta P^c &= \Delta\dot{q}_1 \delta F_1 + \Delta\dot{q}_2 \delta F_2 \\ &= -f_1^c \delta e_1^c - f_2^c \delta e_2^c \end{aligned} \quad (48)$$

represents the power variation supplied to the springs, while

$$\delta P_{ic}^F = -v_0 \delta F_1 + v_1(\delta F_1 - \delta F_2) + v_2 \delta F_2 \quad (49)$$

is the power variation flowing to the rest of the system at the nodes. Adding the velocity boundary condition in weak form

$$(v_0 - \bar{\nu})\delta F_1 = 0 \qquad \forall\, \delta F_1, \quad (50)$$

to (47), we obtain (after a change of sign)

$$\delta P_F = \sum_{i=1}^{2} \delta F_i \Delta\dot{q}_i - \delta F_i(v_i - v_{i-1}) + \delta F_i(\bar{\nu} - v_0) = 0, \quad (51)$$

which is the discrete version of (38). Again, we re-sort the terms and obtain

$$\delta P_F = (\Delta\dot{q}_1 - v_1 + \bar{\nu})\delta F_1 + (\Delta\dot{q}_2 + v_1 - v_2)\delta F_2 = 0, \quad (52)$$

from which, for arbitrary variations δF_1, δF_2 the ODEs for the elongations Δq_1, Δq_2 follow. With $\dot{q}_0 = v_0 = \bar{\nu}$ and the initial values of q_0, q_1 and q_2, the motion of the system is completely determined.

5. NUMERICAL RESULTS

The performance of our approach is now demonstrated with a simple FEniCS simulation (Logg et al., 2012). Therefore, the one dimensional rod of Section 4.1 with the initial conditions

$$v(x, t = 0) = 0 \text{ m/s} \quad (53)$$

$$\sigma(x, t = 0) = 0 \text{ N} \quad (54)$$

is our benchmark system. The rod is first discretized with 100 and then with 200 elements, second order Lagrange polynomials for ϕ and first order discontinuous basis functions for ψ leading in case of 100 elements to $\hat{v} \in \mathbb{R}^{201}$ and $\hat{\sigma} \in \mathbb{R}^{200}$. This common choice results from a classic finite element approach for mechanical systems, where the displacements are usually discretized with Lagrange polynomials of order δ leading to discontinuous stresses of order $\delta - 1$ (see. (9) and (11)). The benchmark system is simulated for $T = 10$ ms using the implicit midpoint rule and sampling time $\Delta T = 1 \cdot 10^{-3}$ ms. Further simulation parameters are listed in Table 1.

Fig. 2 shows the Hamiltonian of the rod, which remains as expected constant for $t > 0.5$ ms up to machine precision. The energy introduced into the system results from the Neumann boundary condition. The energy residual (in the approximation spaces)

$$\Delta H = H - \int_0^t \bar{\nu} \cdot \sigma(x = 0, t)\, dt - \int_0^t v(x = L, t) \cdot \bar{\tau}\, dt \quad (55)$$

Table 1. Simulation parameters

Symbol	Value
L	1 m
ρ	0.7850 kg/m
E	$200 \cdot 10^3$ N/mm^2
A	100 mm^2
$\bar{\nu}$	0 m/s
$\bar{\tau}$	$\forall t \in (0 \text{ ms}, 0.5 \text{ ms}]$ $\tau = 1000$ N else $\tau = 0$ N

is shown in Fig. 3. Figures 4 and 5 illustrate compliance with the boundary conditions in a weak sense. For the sake of completeness, Fig. 6 shows the velocities at $x = L$.

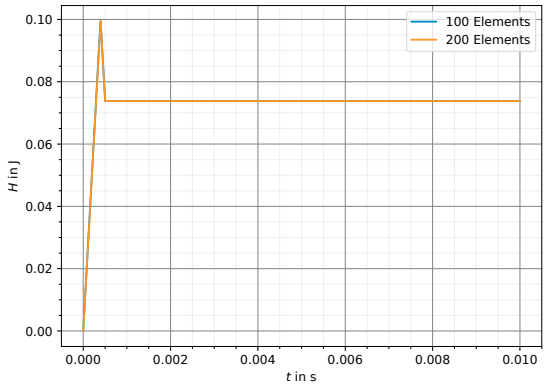

Fig. 2. Hamiltonian H of the rod

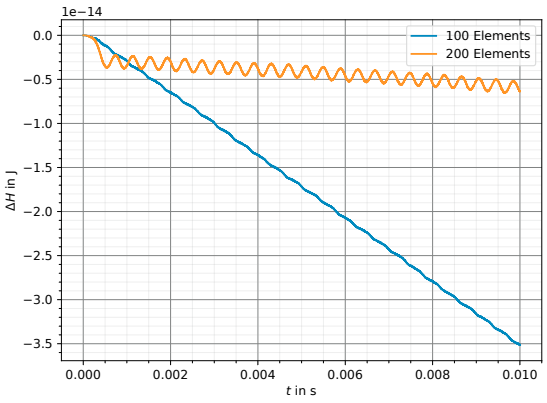

Fig. 3. Energy residual ΔH. Since (55) is calculated using the trapezoidal rule, ΔH is zero to machine precision.

Another point worth mentioning is the resulting eigenvalues of the discrete system compared to the exact ones. The first six scaled eigenvalues $\lambda = \frac{\rho}{EA}\omega^2$, where ω represents the eigenfrequencies of the conjugate complex eigenvalue pairs, are clarified in Table 2. The discretized system (22) has an additional eigenvalue in 0 due to the odd dimension of the skew-symmetric interconnection matrix J. This eigenvalue/-vector establishes an invariant out of a combination of some node velocities $\hat{v}$.

6. CONCLUSIONS

We presented a systematic approach for structure-preserving discretization of infinite dimensional mechanical

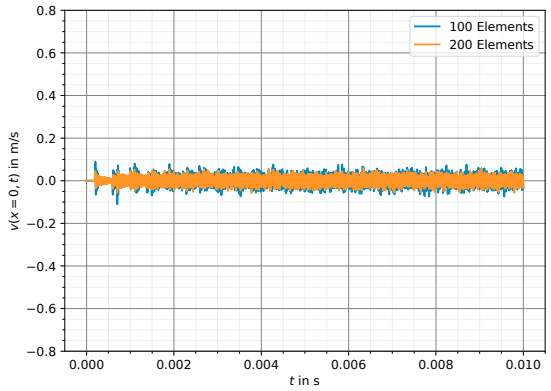

Fig. 4. Dirichlet boundary condition. $v(x = 0, t)$ meets $\bar{\nu} = 0$ in a weak sense.

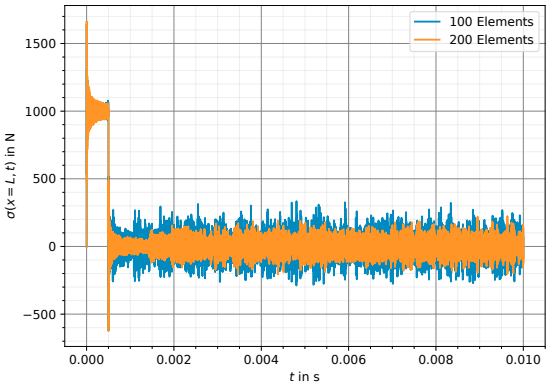

Fig. 5. Neumann boundary condition. $\sigma(x = L, t)$ meets $\bar{\tau}$ according to Table 1 in a weak sense.

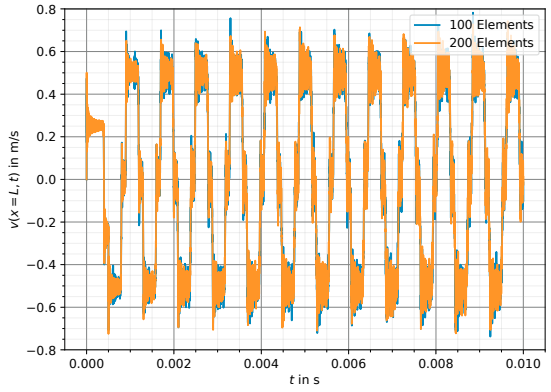

Fig. 6. Velocity $v(x = L, t)$

systems with non-uniform boundary conditions. Our approach is motivated by the principle of virtual power and can be easily extended to other systems like systems of conservation/balance laws. The explicit nature of the resulting finite-dimensional models is a valuable property for their further control-oriented treatment, e.g., structure-preserving order reduction.

Table 2. Scaled eigenvalues $\lambda = \frac{\rho}{EA}\omega^2$

Number	computed (100 elements)	exact
1	0	-
2	2.4674	2.4674
3	22.2067	22.2066
4	61.6854	61.6850
5	120.9042	120.9027
6	199.8637	199.8595

REFERENCES

Brugnoli, A., Alazard, D., Pommier-Budinger, V., and Matignon, D. (2020a). Port-Hamiltonian flexible multibody dynamics. *Multibody System Dynamics*.

Brugnoli, A., Cardoso-Ribeiro, F.L., Haine, G., and Kotyczka, P. (2020b). Partitioned finite element method for structured discretization with mixed boundary conditions. *IFAC-PapersOnLine*.

Cardoso-Ribeiro, F.L., Matignon, D., and Lefèvre, L. (2020). A partitioned finite element method for power-preserving discretization of open systems of conservation laws. *IMA Journal of Mathematical Control and Information*.

Farle, O., Klis, D., Jochum, M., Floch, O., and Dyczij-Edlinger, R. (2013). A port-Hamiltonian finite-element formulation for the Maxwell equations. In *International Conference on Electromagnetics in Advanced Applications*, 324–327.

Jacob, B. and Zwart, H. (2012). *Linear Port-Hamiltonian Systems on Infinite-dimensional Spaces*, volume 223. Springer.

Kotyczka, P. (2019). *Numerical Methods for Distributed Parameter Port-Hamiltonian Systems*. TUM.University Press.

Kotyczka, P., Maschke, B., and Lefèvre, L. (2018). Weak form of Stokes-Dirac structures and geometric discretization of port-Hamiltonian systems. *Journal of Computational Physics*, 361, 442–476.

Logg, A., Mardal, K.A., and Wells, G.N. (2012). *Automated Solution of Differential Equations by the Finite Element Method*. Springer.

Lu, K., Augarde, C., Coombs, W., and Hu, Z. (2019). Weak impositions of Dirichlet boundary conditions in solid mechanics: A critique of current approaches and extension to partially prescribed boundaries. *Computer Methods in Applied Mechanics and Engineering*.

Rashad, R., Califano, F., van der Schaft, A.J., and Stramigioli, S. (2020). Twenty years of distributed port-Hamiltonian systems: A literature review. *IMA Journal of Mathematical Control and Information*.

van der Schaft, A.J. and Maschke, B.M. (2002). Hamiltonian formulation of distributed-parameter systems with boundary energy flow. *Journal of Geometry and Physics*, 42, 166–194.

Villegas, J.A. (2007). *A port-Hamiltonian approach to distributed parameter systems*. Ph.D. thesis, University of Twente.

Warsewa, A., Böhm, M., Sawodny, O., and Tarín, C. (2021). A port-Hamiltonian approach to modeling the structural dynamics of complex systems. *Applied Mathematical Modelling*.

Zienkiewicz, O.C., Taylor, R.L., and Zhu, J.Z. (2005). *The Finite Element Method: Its Basis and Fundamentals*. Butterworth-Heinemann.

A.4 Symplectic discrete-time control of flexible-joint robots: Experiments with two links

CRediT author statement:

Tobias Thoma:	Conceptualization, Acuration of Experimental Data, Methodology, Software, Visualization, Writing - Original Draft
Xuwei Wu:	Acuration of Experimental Data, Software, Writing - Review & Editing
Alexander Dietrich:	Conceptualization, Supervision, Writing - Review & Editing
Paul Kotyczka:	Conceptualization, Methodology, Supervision, Writing - Original Draft

Available online at www.sciencedirect.com

ScienceDirect

IFAC PapersOnline CONFERENCE PAPER ARCHIVE

IFAC PapersOnLine 54-19 (2021) 1–7

Symplectic Discrete-Time Control of Flexible-Joint Robots: Experiments with Two Links ⋆

Tobias Thoma *, **Xuwei Wu** **, **Alexander Dietrich** **, **Paul Kotyczka** *

* *Technical University of Munich, Department of Mechanical Engineering, Chair of Automatic Control, Garching, Germany (e-mail: tobias.thoma@tum.de, kotyczka@tum.de)*

** *German Aerospace Center (DLR), Institute of Robotics and Mechatronics, Oberpfaffenhofen, Germany (e-mail: xuwei.wu@dlr.de, alexander.dietrich@dlr.de)*

Abstract: We present the application and experimental validation of discrete-time control implementation based on symplectic integration – in short referred to as symplectic discrete-time control – to a serial robot manipulator with flexible-joints. Applying the implicit midpoint rule as a simple and popular symplectic integration scheme to both the model of the sampled system and the desired target dynamics, yields a discrete-time control law with the same structure as in continuous time. The arguments are, however, predicted stage values on the subsequent sampling interval resulting from a half implicit Euler step for the target system. The approach can be easily extended to a purely position-based feedback law. The experimental validation on a lightweight robot (KUKA LWR IV+) confirms the expected improvements at low sampling rates, with an increase in the assignable closed-loop stiffness of up to 29 %.

Keywords: Sampled-data systems, discrete-time control, symplectic integration, nonlinear mechanical systems, flexible-joint robots, serial elastic actuators, KUKA LWR.

1. INTRODUCTION

Thanks to the growing field of service robotics and smart factories, modern robot systems have become significant tools in industry and society. While mechanically stiff robots operate in cages (Oberer-Treitz et al., 2013), modern lightweight manipulators include flexible components and often interact with their environment. Especially the physical contact between human and robot sharing the same working space is predestined for flexible robots (Nakamura et al., 2003). Human-robot collaboration (Chandrasekaran and Conrad, 2015) is a promising research field offering a wide range of new opportunities, but it also poses significant challenges to control design.

In order to handle the increasing complexity in robotic tasks, suitable controllers are essential. Since rigid-body controllers (de Wit et al., 1996) applied to flexible-joint robots often perform unsatisfactorily, various control laws have been developed over the past few decades (Spong, 1990; Brogliato et al., 1995; Ozgoli and Taghirad, 2008). Control theory of flexible-joint robots considers multiple approaches, e. g., feedback linearization (Spong, 1987), backstepping (Nicosia and Tomei, 1992; Loría and Avila-Becerril, 2014), passivity-based (Lozano and Brogliato, 1992; Ortega et al., 1995; Ott et al., 2008), fuzzy (Tang et al., 2001), and adaptive control (Hassanzadeh et al., 2008), which are typically digitized with a programmable logic controller.

Most of the literature addressing control theory of flexible-joint robots does not cover the sampling process (Ackermann, 1985). Deterioration effects of quasi-continuous control laws in digital control loops with low sampling rates are well-known (Chen, 1987). In Khosla (1987) the significance of high sampling rates to achieve large effective stiffnesses is stated. Dedicated discrete-time controllers provide the means to improve the handling and performance of digital control loops.

Nonlinear control design under explicit consideration of the sampling process is described in Monaco and Normand-Cyrot (2007) based on series expansions. Bloch et al. (2006) present a discrete-time *Controlled Lagrangian* approach based on a midpoint approximation of the Lagrangian. More recently, a midpoint discrete gradient has been applied to IDA-PBC of linear mechanical systems in Aoues et al. (2015). Moreschini et al. (2019) propose damping injection based on discrete gradients and a differential-difference representation of sampled port-Hamiltonian dynamics. The present work follows the philosophy of our previous works (Kotyczka and Lefèvre, 2019, 2020; Kotyczka and Thoma, 2021) that symplectic [1] integration schemes, as a particular class of structure-preserving methods, which conserve a modified Hamiltonian (Hairer et al.,

⋆ This paper was not presented at any IFAC meeting.

[1] Symplectic refers to area preservation in the phase space of (unforced) Hamiltonian systems.

10.1016/j.ifacol.2021.11.046

2006), qualify naturally to translate the notions of (port-)Hamiltonian control systems and also nonlinear energy-based control to discrete time. A main feature of the control implementation based on the implicit midpoint rule, a second order symplectic method, is that continuously derived nonlinear control laws can be reused in discrete time, with only replacing the arguments by predicted stage values on the following interval (Kotyczka and Thoma, 2021). This property directly translates to higher-order multi-stage schemes in conjunction with appropriate hold elements (Kotyczka et al., 2021).

In this contribution we show the applicability of the approach based on the implicit midpoint rule, initially presented for fully actuated systems, to the example of a commercial series elastic robot. Experimental studies prove a considerable increase in assignable stiffness of up to 29 % at low sampling rates with the "symplectic" controller compared to the direct, "quasi-continuous" implementations of a control law designed in continuous time.

In Section 2, we recall the most relevant properties of modeling and control of flexible-joint robots, followed by the introduction of symplectic discrete-time control of serial elastic manipulators in Section 3. Section 4 addresses the experimental setup and the performance of the symplectic controller compared to its quasi-continuous counterpart in practice. Section 5 gives a brief conclusion.

2. PRELIMINARIES

We recall the dynamic model of flexible-joint robots, effects of torque feedback, a trajectory tracking control technique for flexible-joint robots, and we discuss the control structure of the experimental system used in Section 4.

2.1 Standard model of flexible-joint robots

Under Spong's assumptions [2] (Spong, 1987) which are justified for robots with high gear ratios, the equations of motion of a flexible-joint robot can be described by the simplified model

$$M(q)\ddot{q} + C(q,\dot{q})\dot{q} + \nabla V(q) = \tau + DK^{-1}\dot{\tau} + \tau_{\text{ext}} \quad (1a)$$

$$B\ddot{\theta} + \tau + DK^{-1}\dot{\tau} = \tau_m \quad (1b)$$

$$\tau = K(\theta - q). \quad (1c)$$

The vector $q \in \mathbb{R}^n$ represents the n link-side joint positions and $\theta \in \mathbb{R}^n$ the corresponding motor positions. The link-side inertia matrix $M(q) \in \mathbb{R}^{n\times n}$ is symmetric and positive definite, $C(q,\dot{q}) \in \mathbb{R}^{n\times n}$ is the Coriolis and centrifugal matrix such that $\dot{M} - 2C$ is skew-symmetric and $V(q)$ denotes the gravity potential. The internal torque $\tau \in \mathbb{R}^n$ transmitted through the intrinsically elastic joint can be calculated by the relationship (1c) containing the diagonal and positive definite stiffness matrix $K \in \mathbb{R}^{n\times n}$. The diagonal and positive definite damping matrix $D \in \mathbb{R}^{n\times n}$ scales the relative velocities. The diagonal and positive definite matrix $B \in \mathbb{R}^{n\times n}$ contains the rotor inertias. $\tau_m \in \mathbb{R}^n$ contains the motor torques or control inputs, respectively. The link side dynamics (1a) is coupled with the motor dynamics (1b) via the internal torque that involves a spring and a damper.

[2] The kinetic energy of the rotor depends mainly on its own rotation and will not be affected significantly by the link-side movements.

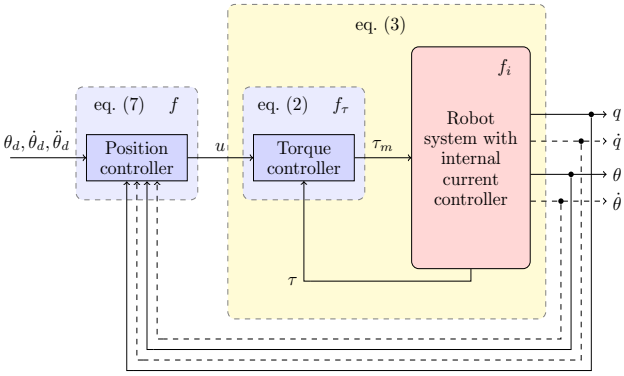

Fig. 1. Control structure. The yellow box represents (3) containing the inner-loop torque controller, current controller and the robot system.

Assumption 1. We do not consider any kind of external forces $\tau_{\text{ext}} \in \mathbb{R}^n$. Therefore, $\tau_{\text{ext}} = 0$.

Remark 2. Further friction effects are neglected. In practice an explicit friction compensation action is commonly used (Albu-Schäffer et al., 2007).

2.2 Joint control of robots with flexible-joints

The following control approach is divided into (a) joint torque control in order to shape the motor inertia and (b) joint position control.

Joint torque control In flexible-joint robots such as the used KUKA LWR IV+, the motor inertias are often reduced to a desired diagonal matrix B_d by active control, in order to increase control performance and to improve back-drivability (Ott et al., 2008). The corresponding feedback law involves the measured joint torque and can be realized through

$$\tau_m = BB_d^{-1}u + (I - BB_d^{-1})(\tau + DK^{-1}\dot{\tau}) \; . \quad (2)$$

It modifies (1) to the new system dynamics

$$M(q)\ddot{q} + C(q,\dot{q})\dot{q} + \nabla V(q) = \tau + DK^{-1}\dot{\tau} \quad (3a)$$

$$B_d\ddot{\theta} + \tau + DK^{-1}\dot{\tau} = u \quad (3b)$$

with the new input $u \in \mathbb{R}^n$. From now on, we assume that (3), illustrated in Fig. 1, is the initial model of the discrete-time control approach to be developed in the following [3] .

Notation 3. The dynamic model (3) can also be written in state space form

$$\dot{q} = \xi \quad (4a)$$

$$\dot{\theta} = \nu \quad (4b)$$

$$\dot{\xi} = f(q,\theta,\xi,\nu) \quad (4c)$$

$$\dot{\nu} = g(q,\theta,\xi,\nu) + B_d^{-1}u \quad (4d)$$

where

$$f = M^{-1}(-C\dot{q} - \nabla V + \tau + DK^{-1}\dot{\tau}), \quad (5)$$

$$g = B_d^{-1}(-\tau - DK^{-1}\dot{\tau}). \quad (6)$$

Remark 4. Usually, τ_m denotes the desired motor torque handed to a current controller with significantly higher sampling rate. As a consequence, the dynamics of the electrical subsystem can be neglected (Ott et al., 2008).

[3] We assume that the joint torque controller works with a much higher sampling rate than the following position controller, see Fig. 1.

Joint trajectory control The PD+ control law (Paden and Panja, 1988)

$$u = (M(\theta) + B_d)\ddot{\theta}_d + C(\theta,\dot{\theta})\dot{\theta}_d + \nabla V(\theta) - K_P(\theta - \theta_d) - K_D(\dot{\theta} - \dot{\theta}_d) \quad (7)$$

represents a common motor position based trajectory tracking approach. The control law contains a PD control component, where both $K_P \in \mathbb{R}^{n\times n}$ and $K_D \in \mathbb{R}^{n\times n}$ are symmetric and positive definite. The vector $\theta_d \in \mathbb{R}^n$ represents the desired joint positions in motor coordinates.

Notation 5. A general closed-loop target system can be expressed as the state space model

$$\dot{q} = \xi \quad (8a)$$
$$\dot{\theta} = \nu \quad (8b)$$
$$\dot{\xi} = f(q,\theta,\xi,\nu) \quad (8c)$$
$$\dot{\nu} = g_d(q,\theta,\xi,\nu,t), \quad (8d)$$

where the explicit time dependence of g_d stems from the application of (7) with $\theta_d = \theta_d(t)$ for trajectory tracking. The continuous-time feedback control law that transforms (4) to (8) (also (7) can be cast in this form) is

$$u = B_d g_d(q,\theta,\xi,\nu,t) - B_d g(q,\theta,\xi,\nu). \quad (9)$$

2.3 Control structure of the KUKA LWR IV+

We summarize the control structure of the KUKA LWR IV+, see also Fig. 1. The current controller runs at a sampling rate of $f_i = 40$ kHz, whereas the torque controller operates at $f_\tau = 3$ kHz. In order to feed the outer-loop position controller with the joint and motor velocities (dashed lines in Fig. 1), these are determined numerically every millisecond using a finite difference method (applied to the first order lowpass filtered position signals). The position controller operates at $f = \frac{1}{h} \leq 1$ kHz.

From now on we focus on the position controller (outermost loop in Fig. 1) working with the lowest sampling rate. Its sampling time h is varied in the subsequent experimental studies to display the deterioration effects coming from low sampling and the improvement due to the second order accurate symplectic control implementation.

3. SYMPLECTIC DISCRETE-TIME CONTROL

The approach presented in Kotyczka and Thoma (2021) exploits the discrete-time approximations of sampled plant and controlled system using the implicit midpoint rule. While "symplectic" refers to the property of the discrete-time flow of a (canonical) Hamiltonian target system, the second order accurate method also applies to more general, including damped, target systems. In the following we show the applicability of the symplectic control approach to flexible-joint robots as representatives of underactuated systems. Moreover, we augment the original pure position feedback by first order filtering, indispensable in practice.

3.1 Approximation of the sampling process

The symplectic control approach requires the numerical approximation of the sampling process. The considered digital control loop is represented in Fig. 2. Sampled variables are indicated with subscript k (value at sampling time t_k), in contrast to the continuous-time versions that depend on t. Further below, we realize a pure position feedback and shift the numerical determination of the velocities into the position controller.

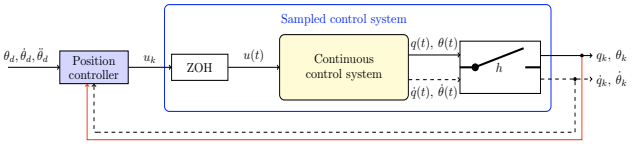

Fig. 2. Sampled control system. The blue box represents the discrete-time system containing (3), a zero order hold element and a sampler. The dashed lines indicate that the velocities are not directly measured.

Assumption 6. We consider piecewise constant inputs (zero order hold) $u(t) = u_k$, $t \in [t_k, t_{k+1})$ and equidistant sampling $t_k = kh$, $k = 0,1,2,\ldots$, with h such that Shannon's sampling theorem is satisfied.

The second order discrete-time approximation of the solution of (4) under piecewise constant input $u(t)$ using the implicit midpoint rule is then given by

$$q_{k+1} = q_k + h\xi_{k+\frac{1}{2}} \quad (10a)$$
$$\theta_{k+1} = \theta_k + h\nu_{k+\frac{1}{2}} \quad (10b)$$
$$\xi_{k+1} = \xi_k + hf(q_{k+\frac{1}{2}}, \theta_{k+\frac{1}{2}}, \xi_{k+\frac{1}{2}}, \nu_{k+\frac{1}{2}}) \quad (10c)$$
$$\nu_{k+1} = \nu_k + hg(q_{k+\frac{1}{2}}, \theta_{k+\frac{1}{2}}, \xi_{k+\frac{1}{2}}, \nu_{k+\frac{1}{2}}) + hB_d^{-1}u_k \quad (10d)$$

with the stage values

$$q_{k+\frac{1}{2}} = \frac{q_k + q_{k+1}}{2}, \qquad \theta_{k+\frac{1}{2}} = \frac{\theta_k + \theta_{k+1}}{2}, \quad (11a)$$
$$\xi_{k+\frac{1}{2}} = \frac{\xi_k + \xi_{k+1}}{2}, \qquad \nu_{k+\frac{1}{2}} = \frac{\nu_k + \nu_{k+1}}{2}. \quad (11b)$$

3.2 Discrete-time target system

To determine a second-order accurate discrete-time implementation of the control law (9), the control model (10) is compared with a second-order accurate discrete-time representation of the target dynamics (8), again obtained from applying the implicit midpoint rule,

$$q_{k+1} = q_k + h\xi_{k+\frac{1}{2}} \quad (12a)$$
$$\theta_{k+1} = \theta_k + h\nu_{k+\frac{1}{2}} \quad (12b)$$
$$\xi_{k+1} = \xi_k + hf(q_{k+\frac{1}{2}}, \theta_{k+\frac{1}{2}}, \xi_{k+\frac{1}{2}}, \nu_{k+\frac{1}{2}}) \quad (12c)$$
$$\nu_{k+1} = \nu_k + hg_d(q_{k+\frac{1}{2}}, \theta_{k+\frac{1}{2}}, \xi_{k+\frac{1}{2}}, \nu_{k+\frac{1}{2}}, t_{k+\frac{1}{2}}), \quad (12d)$$

where $t_{k+\frac{1}{2}} = t_k + \frac{h}{2}$.

3.3 Control law

Theorem 7. The discrete-time implicit state feedback law

$$u_k = B_d g_d(q_{k+\frac{1}{2}}, \theta_{k+\frac{1}{2}}, \xi_{k+\frac{1}{2}}, \nu_{k+\frac{1}{2}}, t_{k+\frac{1}{2}}) - B_d g(q_{k+\frac{1}{2}}, \theta_{k+\frac{1}{2}}, \xi_{k+\frac{1}{2}}, \nu_{k+\frac{1}{2}}) \quad (13)$$

with stage values computed from

$$q_{k+\frac{1}{2}} = q_k + \frac{h}{2}\xi_{k+\frac{1}{2}} \tag{14a}$$
$$\theta_{k+\frac{1}{2}} = \theta_k + \frac{h}{2}\nu_{k+\frac{1}{2}} \tag{14b}$$
$$\xi_{k+\frac{1}{2}} = \xi_k + \frac{h}{2} f(q_{k+\frac{1}{2}}, \theta_{k+\frac{1}{2}}, \xi_{k+\frac{1}{2}}, \nu_{k+\frac{1}{2}}) \tag{14c}$$
$$\nu_{k+\frac{1}{2}} = \nu_k + \frac{h}{2} g_d(q_{k+\frac{1}{2}}, \theta_{k+\frac{1}{2}}, \xi_{k+\frac{1}{2}}, \nu_{k+\frac{1}{2}}, t_{k+\frac{1}{2}}) \tag{14d}$$

(a) transforms the open-loop discrete-time system (10) to (12). (b) The closed-loop dynamics of the ZOH sampled system (4) corresponds to (12) up to a local truncation error of order $\mathcal{O}(h^3)$.

The system of equations (14) generates a prediction of the states on the subsequent sampling interval with a half implicit Euler step. It can be solved numerically by Newton iteration. The following proof of (a) is more compact compared to Kotyczka and Thoma (2021).

Proof. Consider an open-loop system $\dot{x} = f(x) + gu$ under zero order hold, and a target system $\dot{x} = f_d(x)$ with smooth functions f, f_d. Let $x^0_{k+\frac{1}{2}}$ and $x_{k+\frac{1}{2}}$ be the stage values computed from $x^0_{k+\frac{1}{2}} = x_k + \frac{h}{2}(f(x^0_{k+\frac{1}{2}}) + gu_k)$ and $x_{k+\frac{1}{2}} = x_k + \frac{h}{2} f_d(x_{k+\frac{1}{2}})$. Substitution of $gu_k = f_d(x_{k+\frac{1}{2}}) - f(x_{k+\frac{1}{2}})$ shows that, if the function $\mathrm{id}(\cdot) - \frac{h}{2} f(\cdot)$ is monotonous around x_k (which can be assumed for smooth f and sufficiently small h), that $x_{k+\frac{1}{2}} = x^0_{k+\frac{1}{2}}$. This allows the computation of the stage values based on the target dynamics, which proves (a). (b) follows from second order accuracy of the implicit midpoint rule.

Remark 8. The symplectic control law (13) has the same structure as the continuous-time controller (9) and the quasi-continuous control implementation

$$u_k = B_d g_d(q_k, \theta_k, \xi_k, \nu_k, t_k) - B_d g(q_k, \theta_k, \xi_k, \nu_k), \tag{15}$$

which results from substitution of the sampled states in (9). Equivalently, (15) is obtained by matching of (4d) and (8d) after forward Euler integration.

3.4 Pure position feedback

Often velocities are not directly measured, but determined numerically from position measurements. However, the symplectic controller, respectively the system of equations (14), require the velocity vectors ξ_k and ν_k. We propose their numerical reconstruction from the (filtered) position stage values to arrive at a pure position feedback.

We introduce the filtered stage position values

$$q^f_{k+\frac{1}{2}} = \frac{h}{T+h} q_{k+\frac{1}{2}} + \frac{T}{T+h} q^f_{k-\frac{1}{2}}, \tag{16a}$$
$$\theta^f_{k+\frac{1}{2}} = \frac{h}{T+h} \theta_{k+\frac{1}{2}} + \frac{T}{T+h} \theta^f_{k-\frac{1}{2}}, \tag{16b}$$

where T represents the time constant of a discrete-time first-order lowpass filter, and the reconstructed velocities

$$\tilde{\xi}_k = \frac{q^f_{k+\frac{1}{2}} - q^f_{k-\frac{1}{2}}}{h}, \qquad \tilde{\nu}_k = \frac{\theta^f_{k+\frac{1}{2}} - \theta^f_{k-\frac{1}{2}}}{h}. \tag{17}$$

Corollary 9. The modified system of equations

$$q_{k+\frac{1}{2}} = q_k + \frac{h}{2}\xi_{k+\frac{1}{2}} \tag{18a}$$
$$\theta_{k+\frac{1}{2}} = \theta_k + \frac{h}{2}\nu_{k+\frac{1}{2}} \tag{18b}$$
$$\xi_{k+\frac{1}{2}} = \tilde{\xi}_k + \frac{h}{2} f(q_{k+\frac{1}{2}}, \theta_{k+\frac{1}{2}}, \xi_{k+\frac{1}{2}}, \nu_{k+\frac{1}{2}}) \tag{18c}$$
$$\nu_{k+\frac{1}{2}} = \tilde{\nu}_k + \frac{h}{2} g_d(q_{k+\frac{1}{2}}, \theta_{k+\frac{1}{2}}, \xi_{k+\frac{1}{2}}, \nu_{k+\frac{1}{2}}, t_{k+\frac{1}{2}}) \tag{18d}$$

yields a control law based on only position measurements, including a smoothening velocity approximation to reduce the effect of measurement noise.

With $T \to 0$, the reconstructed velocities tend to $\tilde{\xi}_k = \frac{1}{h}(q_{k+\frac{1}{2}} - q_{k-\frac{1}{2}})$ and $\tilde{\nu}_k = \frac{1}{h}(\theta_{k+\frac{1}{2}} - \theta_{k-\frac{1}{2}})$, which allows for a nice interpretation of the resulting closed-loop dynamics in terms of a generalized Störmer-Verlet scheme on a shifted grid (Kotyczka and Thoma, 2021).

Remark 10. For the implementation it is advisable that at time step t_0, $\tilde{\xi}_0$ and $\tilde{\nu}_0$ are assigned with concrete initial values, e. g., $\tilde{\xi}_0 = \dot{q}(t_0)$ and $\tilde{\nu}_0 = \dot{\theta}(t_0)$, typically zero. For more information we refer to the next section.

3.5 Implementation

The algorithm below describes the control implementation with included velocity reconstruction. If the symplectic controller is implemented based on external velocity signals, only lines 3 and 13 will be required in the for loop.

Algorithm 1. Symplectic controller implementation with pure position feedback (pseudo-code)

Require: t_k, q_k, θ_k, ξ_0, ν_0
Ensure: u_k

```
1:  for k := 0 to N do
2:    if t_k = t_0 then
3:      solve (14) → q_{k+1/2}, θ_{k+1/2}
4:      q^f_{k+1/2} := q_{k+1/2}
5:      θ^f_{k+1/2} := θ_{k+1/2}
6:    else
7:      solve (18) → q_{k+1/2}, θ_{k+1/2}
8:      q^f_{k+1/2} := (16a)
9:      θ^f_{k+1/2} := (16b)
10:   end if
11:   q^f_{k-1/2} := q^f_{k+1/2}
12:   θ^f_{k-1/2} := θ^f_{k+1/2}
13:   u_k := (13)
14: end for
```

4. EXPERIMENTS

The performance of the symplectic control approach, compared to the quasi-continuous implementation, is demonstrated on a real robot system in a two-link scenario.

4.1 Experimental setup

The experimental setup includes a KUKA LWR IV+ robot, which features seven actuated degrees of freedom, and which is equipped with motor position encoders and

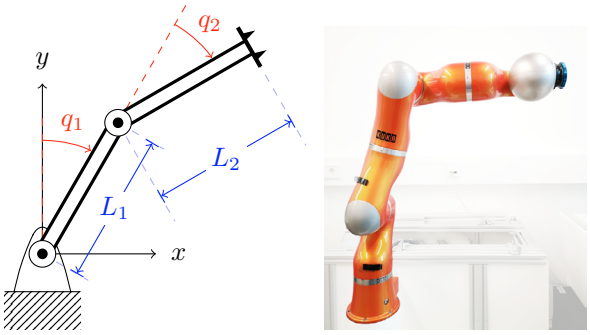

Fig. 3. Two-link robotic arm.

joint torque sensors in each joint. The reader is referred to (Gaz et al., 2016) for exemplary kinematic and dynamic parameters of the robot. The control structure of Fig. 1 is realized with a *Matlab/Simulink* interface. In the following experiments, the Newton method is applied to solve (14) and (18) in case of the symplectic controller.

To implement the proposed control scheme, the feedback of both link and motor position is required. However, as aforementioned, only the latter is directly available. Based on (1c) the link position q can be estimated via

$$q = \theta - K^{-1}\tau \tag{19}$$

using feedback of the available signals θ, τ, and the estimated joint stiffness.

In the experiments the second and fourth link are actuated, while the others are locked. This leads to the two-link model shown in Fig. 3, see the Appendix for details. The Cartesian coordinates of the tool center point (TCP) in the x-y-plane are

$$\phi = \begin{bmatrix} x_{\mathrm{TCP}} \\ y_{\mathrm{TCP}} \end{bmatrix} = \begin{bmatrix} L_1 \sin(q_1) + L_2 \sin(q_1 + q_2) \\ L_1 \cos(q_1) + L_2 \cos(q_1 + q_2) \end{bmatrix}, \tag{20}$$

and the desired task space trajectory is a circle

$$\phi_d(t) = \begin{bmatrix} L + R\cos(\Omega t) \\ L + R\sin(\Omega t) \end{bmatrix} \tag{21}$$

with $L = 0.4\,\mathrm{m}$, $R = 0.0975\,\mathrm{m}$ and $\Omega = 0.8\pi\,\mathrm{rad/s}$.

The inverse kinematics returns the desired link positions $q_d(t)$, and $\theta_d(t) \approx q_d(t)$ is assumed because of the quite large joint stiffnesses. The control gains are chosen as $K_P = \mathrm{diag}\{\kappa, \kappa\}\,\mathrm{Nm/rad}$ and $K_D = \mathrm{diag}\{25, 25\}\,\mathrm{Nms/rad}$, with κ a *closed-loop* stiffness parameter.

4.2 Experimental conditions

In order to compare the performance of the quasi-continuous controller and the symplectic one, we vary the sampling rate $f = \frac{1}{h}$ of the outermost loop and the stiffness κ. In each pass the discrete L^2 norms (RMS values) of position error and the deviation of the input from the nominal trajectory

$$\|e_j\|_h = \left(\frac{1}{N} \sum_{j=0}^{N} |\theta(t_j) - \theta_d(t_j)|^2 \right)^{\frac{1}{2}} \tag{22}$$

and

$$\|u_j\|_h = \left(\frac{1}{N} \sum_{k=0}^{N} |u(t_j) - u_d(t_j)|^2 \right)^{\frac{1}{2}} \tag{23}$$

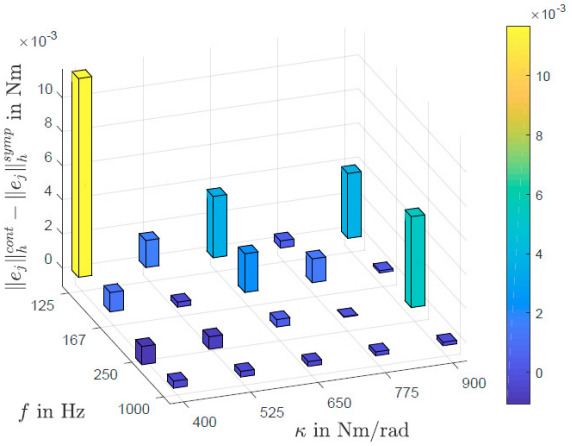

Fig. 4. Difference of position error RMS values between symplectic and quasi-continuous controller.

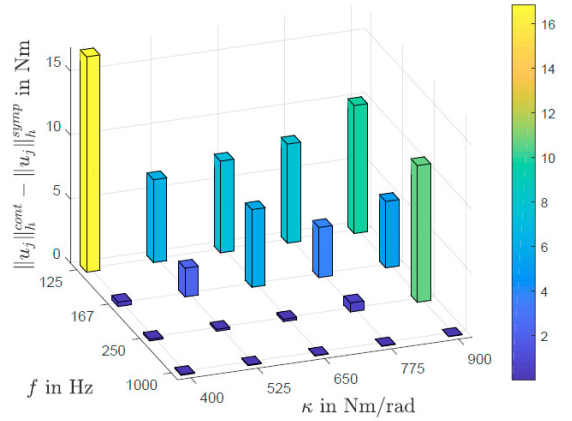

Fig. 5. Difference of RMS values of the feedback components of the input signals.

are determined with $t_j = j \cdot 1\,\mathrm{ms}$. $u_d(t_j)$ represents the ideal feedforward control

$$u_d(t_j) = (M(\theta_d(t_j)) + B_d)\ddot{\theta}_d(t_j) + C(\theta_d(t_j), \dot{\theta}_d(t_j))\dot{\theta}_d(t_j) + \nabla V(\theta_d(t_j)). \tag{24}$$

Experiments are run for $f \in \{1000, 250, 167, 125\}\,\mathrm{Hz}$ and $\kappa \in \{900, 775, 650, 525, 400\}\,\mathrm{Nm/rad}$ for both controllers, providing the norms $\|e_j\|_h^{\mathrm{symp}}$, $\|u_j\|_h^{\mathrm{symp}}$ (symplectic case) and $\|e_j\|_h^{\mathrm{cont}}$, $\|u_j\|_h^{\mathrm{cont}}$ (quasi-continuous case). The symplectic controller implementation receives the same (external) velocity approximations as the quasi-continuous controller. (Pure position feedback is discussed below).

4.3 Results and discussion

The differences in the norms (22) and (23) are displayed in Figs. 4 and 5. In general, the position errors in Fig. 4 suggest the superiority of the symplectic controller for low sampling frequencies and high closed-loop stiffnesses, while for some constellations (e.g., $f = 167\,\mathrm{Hz}$, $\kappa = 900\,\mathrm{Nm/rad}$) this advantage is less pronounced or vanishes. Figure 5 on the norms of the feedback control signal gives a clearer picture: the RMS value (23) (which is related to the control input energy) is considerably higher for the quasi-continuous controller implementation. Three exemplary

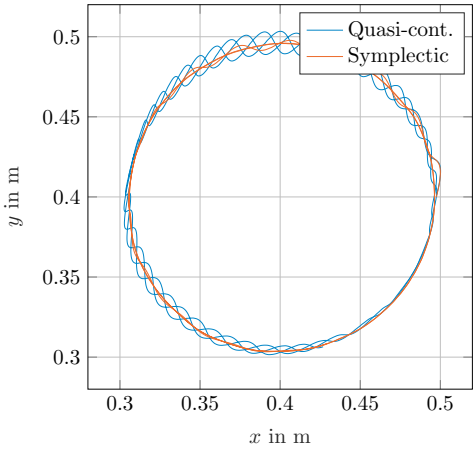

Fig. 6. Trajectories in the x-y-plane for $\kappa = 400\,\mathrm{Nm/rad}$ and $f = 125\,\mathrm{Hz}$.

constellations are taken from Fig. 5 and the values for the feedback control input norms are indicated in Table 1. In the first case, the position error under the symplectic controller is considerably reduced, $\|e_j\|_h^{\mathrm{symp}} < \|e_j\|_h^{\mathrm{cont}}$, see Fig. 6, while $\|e_j\|_h^{\mathrm{symp}} \approx \|e_j\|_h^{\mathrm{cont}}$ in the two other cases. For the first case, the feedback control signals are compared in Figs. 7 and 8.

Table 1. Feedback control input RMS values for selected constellations.

f, κ	$\|u_j\|_h^{\mathrm{cont}}$	$\|u_j\|_h^{\mathrm{symp}}$
125 Hz, 400 Nm/rad	22.3 Nm	5.43 Nm
167 Hz, 525 Nm/rad	6.48 Nm	4.23 Nm
250 Hz, 775 Nm/rad	5.18 Nm	4.42 Nm

In order to estimate the potential increase of assignable stiffness κ with the symplectic approach in contrast to the quasi-continuous one, the values in the right column of Table 1 are taken as reference, and the stiffness imposed by the quasi-continuous controller is successively reduced until $\|u_j\|_h^{\mathrm{cont}}$ becomes comparable [4] to $\|u_j\|_h^{\mathrm{symp}}$. The results of these experiments are summarized in Table 2: the symplectic controller allows an increase of stiffness by 4% at $f = 250\,\mathrm{Hz}$, by 14% at 167 Hz and by 29% at 125 Hz.

Table 2. Assignable stiffnesses at comparable RMS values of the feedback control input

f	$\kappa, \|u_j\|_h^{\mathrm{cont}}$	$\kappa, \|u_j\|_h^{\mathrm{symp}}$
125 Hz	310 Nm/rad, 5.47 Nm	400 Nm/rad, 5.43 Nm
167 Hz	460 Nm/rad, 4.31 Nm	525 Nm/rad, 4.23 Nm
250 Hz	740 Nm/rad, 4.56 Nm	775 Nm/rad, 4.42 Nm

4.4 Experiments with pure position feedback

The robot is again controlled with $\kappa = 400\,\mathrm{Nm/rad}$ and at $f = 125\,\mathrm{Hz}$. The pure position feedback is implemented according to Algorithm 1 with two different time constants, $T = \frac{1}{20\pi}$ s and $T = \frac{1}{200\pi}$ s.

Remark 11. A first-order lowpass filter with $T = \frac{1}{20\pi}$ s is applied in the computation of velocities in the "conventional" setup (see Fig. 1).

Since both time constants T lead to satisfactory tracking performance, we focus on the input behaviour shown in Fig. 9 and 10. The figures support the statement that the pure position feedback does not significantly impair the quality of the original symplectic controller, but the choice of the filter time constant is of central importance.

[4] A deviation of $\leq 4\,\%$ is considered as comparable here.

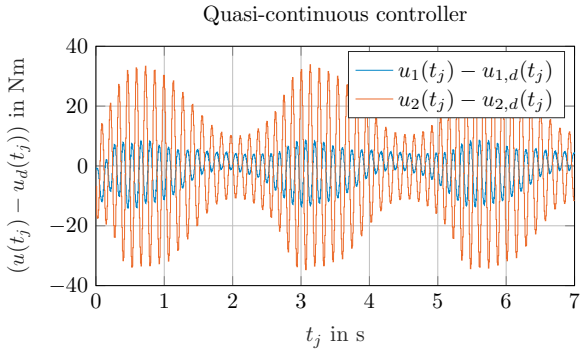

Fig. 7. Feedback control signals at $\kappa = 400\,\mathrm{Nm/rad}$ and $f = 125\,\mathrm{Hz}$ for the quasi-continuous controller.

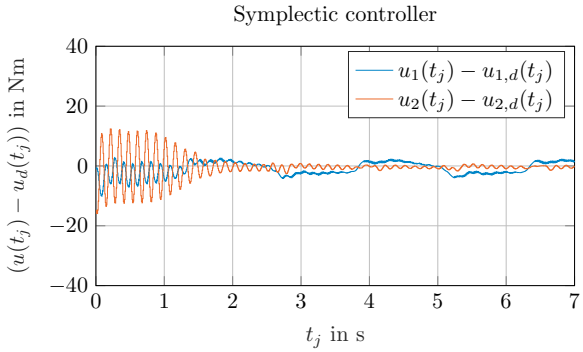

Fig. 8. Feedback control signals at $\kappa = 400\,\mathrm{Nm/rad}$ and $f = 125\,\mathrm{Hz}$ for the symplectic controller.

5. CONCLUSIONS

We presented paper the symplectic discrete-time control design for serial elastic manipulators, including a pure position feedback variant containing a first-order lowpass filter. The effectiveness of the resulting control implementation scheme based on the implicit midpoint rule was illustrated in several experiments for a two-link scenario.

The second order control implementation has proven not only advantageous concerning the considerably higher assignable closed-loop stiffness at lower sampling rates, but also in terms of the reduced norm of the control input signal, which can be attributed to the half-step prediction of the state variables. Thereby, the structure of the control law remained unaltered compared to the continuous-time control design.

Being a model-based approach, even stronger improvements can be expected (which is supported by simulation results) if the uncertainty in the parameters of the system model for position control (yellow box in Fig. 1, Appendix) can be reduced. The systematic choice of filter parameters for pure position feedback, as well as an efficient numerical implementation of the prediction step, are important issues to be considered for the extension to seven degrees of freedom on KUKA LWR IV+. Moreover, we are currently working on a symplectic impedance control approach and the possibilities of external force feedback.

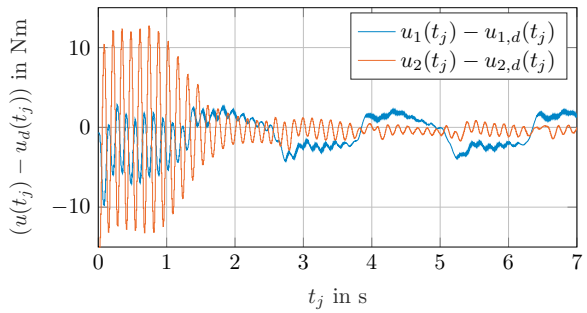

Fig. 9. Feedback control input signal at $\kappa = 400\,\mathrm{Nm/rad}$ and $f = 125\,\mathrm{Hz}$ with pure position feedback and $T = \frac{1}{20\pi}$ s. Comparable to Fig. 8.

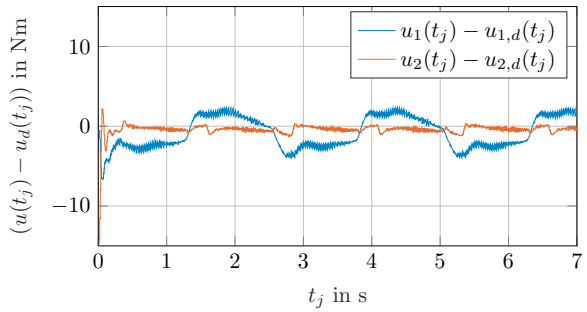

Fig. 10. Improvement of the control signal by an adapted filter time constant $T = \frac{1}{200\pi}$ s.

APPENDIX

The robot model of Fig. 3 has the kinetic energy

$$T = \frac{1}{2}\dot{q}^T M(q)\dot{q} + \frac{1}{2}\dot{\theta}^T B_d \dot{\theta} \tag{25}$$

with inertia matrix

$$M(q_2) = \begin{bmatrix} c_1 + c_2 + 2c_3\cos(q_2) & c_2 + c_3\cos(q_2) \\ c_2 + c_3\cos(q_2) & c_2 \end{bmatrix} \tag{26}$$

and the potential energy

$$U(q,\theta) = \frac{1}{2}(\theta - q)^T K(\theta - q) + V(q) \tag{27}$$

with gravity potential

$$V(q) = c_4 g\cos(q_1) + c_5 g\cos(q_1 + q_2). \tag{28}$$

The constants $c_1, \ldots, c_5$ include the manipulator masses m_i, the inertias J_i w. r. t. the centers of gravity, the total lengths L_i and the distances l_i from the joints to the centers of gravity:

$$c_1 = J_1 + m_1 l_1^2 + m_2 L_1^2, \quad c_2 = J_2 + m_2 l_2^2, \tag{29}$$

$$c_3 = m_2 L_1 l_2, \quad c_4 = m_1 l_1 + m_2 L_1, \quad c_5 = m_2 l_2. \tag{30}$$

REFERENCES

Ackermann, J. (1985). *Sampled-Data Control Systems*. Springer.

Albu-Schäffer, A., Ott, C., and Hirzinger, G. (2007). A unified passivity-based control framework for position, torque and impedance control of flexible joint robots. *Int. J. Robot. Res.*, 26(1), 23–39.

Aoues, S., Matignon, D., and Alazard, D. (2015). Control of a flexible spacecraft using discrete IDA-PBC design. *IFAC-PapersOnLine*, 48(13), 188–193.

Bloch, A.M., Leok, M., Marsden, J.E., and Zenkov, D.V. (2006). Controlled Lagrangians and potential shaping for stabilization of discrete mechanical systems. In *45th IEEE CDC*, 3333–3338.

Brogliato, B., Ortega, R., and Lozano, R. (1995). Global tracking controllers for flexible-joint manipulators: a comparative study. *Automatica*, 31(7), 941–956.

Chandrasekaran, B. and Conrad, J.M. (2015). Human-robot collaboration: A survey. In *IEEE SoutheastCon 2015*.

Chen, Y. (1987). Frequency response of discrete-time robot systems – Limitations of PD controllers and improvements by lag-lead compensation. In *IEEE ICRA*, 464–472.

de Wit, C.C., Siciliano, B., and Bastin, G. (1996). *Theory of Robot Control*. Springer.

Gaz, C., Flacco, F., and Luca, A.D. (2016). Extracting feasible robot parameters from dynamic coefficients using nonlinear optimization methods. In *IEEE ICRA*, 2075–2081.

Hairer, E., Lubich, C., and Wanner, G. (2006). *Geometric numerical integration: Structure-preserving algorithms for ordinary differential equations*. Springer.

Hassanzadeh, I., Kharrati, H., and Bonab, J.R. (2008). Model following adaptive control for a robot with flexible joints. In *IEEE Canadian Conf. Electrical and Computer Eng.*, 1467–1472.

Khosla, P. (1987). Choosing sampling rates for robot control. In *IEEE ICRA*, 169–174.

Kotyczka, P. and Lefèvre, L. (2019). Discrete-time port-Hamiltonian systems: A definition based on symplectic integration. *Syst. Control Lett.*, 133, 104530.

Kotyczka, P. and Lefèvre, L. (2020). Discrete-time control design based on symplectic integration: Linear systems. *IFAC-PapersOnLine*, 7563–7568.

Kotyczka, P., Martens, C., and Lefèvre, L. (2021). High order discrete-time control implementation based on Gauss-Legendre collocation. In *7th IFAC Workshop LHMNC, Berlin*.

Kotyczka, P. and Thoma, T. (2021). Symplectic discrete-time energy-based control for nonlinear mechanical systems. *Automatica (to appear), arXiv preprint, arxiv.org/abs/2104.14153*.

Loría, A. and Avila-Becerril, S. (2014). Output-feedback global tracking control of robot manipulators with flexible joints. In *Amer. Contr. Conf.*, 4032–4037.

Lozano, R. and Brogliato, B. (1992). Adaptive control of robot manipulators with flexible joints. *IEEE T. Automat. Contr.*, 37(2), 174–181.

Monaco, S. and Normand-Cyrot, D. (2007). Advanced tools for nonlinear sampled-data systems' analysis and control. *Eur. J. Control*, 13(2-3), 221–241.

Moreschini, A., Mattioni, M., Monaco, S., and Normand-Cyrot, D. (2019). Discrete port-controlled Hamiltonian dynamics and average passivation. In *58th IEEE CDC*, 1430–1435.

Nakamura, T., Saga, N., Nakazawa, M., and Kawamura, T. (2003). Development of a soft manipulator using a smart flexible joint for safe contact with humans. In *IEEE/ASME Int. Conf. Advanced Intelligent Mechatronics*, 441–446.

Nicosia, S. and Tomei, P. (1992). A method to design adaptive controllers for flexible joint robots. In *IEEE ICRA*, 701–706.

Oberer-Treitz, S., Dietz, T., and Verl, A. (2013). Safety in industrial applications: From fixed fences to direct interaction. In *IEEE ISR 2013*.

Ortega, R., Kelly, R., and Loria, A. (1995). A class of output feedback globally stabilizing controllers for flexible joints robots. *IEEE T. Robotic. Autom.*, 11(5), 766–770.

Ott, C., Albu-Schäffer, A., Kugi, A., and Hirzinger, G. (2008). On the passivity-based impedance control of flexible joint robots. *IEEE T. Robot.*, 24(2), 416–429.

Ozgoli, S. and Taghirad, H.D. (2008). A survey on the control of flexible joint robots. *Asian J. Control*, 8(4), 332–344.

Paden, B. and Panja, R. (1988). Globally asymptotically stable 'PD+' controller for robot manipulators. *Int. J. Control*, 47(6), 1697–1712.

Spong, M.W. (1987). Modeling and control of elastic joint robots. *Journal of Dynamic Systems, Measurement, and Control*, 109(4), 310–318.

Spong, M.W. (1990). *Control of Flexible Joint Robots: A Survey*. University of Illinois, Coordinated Science Laboratory.

Tang, W., Chen, G., and Lu, R. (2001). A modified fuzzy PI controller for a flexible-joint robot arm with uncertainties. *Fuzzy Set. Syst.*, 118(1), 109–119.

A.5 Optimal trajectory control of geometrically exact strings with space-time finite elements

CRediT author statement:

Tobias Thoma:	Conceptualization, Acuration of Experimental Data, Methodology, Software, Visualization, Writing - Original Draft
Paul Kotyczka:	Supervision, Writing - Original Draft

Optimal Trajectory Control of Geometrically Exact Strings with Space-Time Finite Elements

Tobias Thoma[1] and Paul Kotyczka[1]

Abstract— **In this contribution, we present a variational space-time formulation which generates an optimal feed-forward controller for geometrically exact strings. More concretely, the optimization problem is solved with an indirect approach, and the space-time finite element method translates the problem to a set of algebraic equations. Thereby, only the positional field and the corresponding adjoint variable field are approximated by continuous shape functions, which makes the discretization of a velocity field unnecessary. In addition, the variational formulation can be solved using commercial or open source finite element packages. The entire approach can also be interpreted as a multiple-shooting method for solving the optimality conditions based on the semi-discrete problem. The performance of our approach is demonstrated by a numerical test.**

I. Introduction

Increasing efficiency of mechatronic devices is often achieved through lightweight design using flexible mechanical structures like beams, strings or plates, and so on. This leads to a more complex modeling procedure often relying on the theory of nonlinear continuum mechanics. Due to the limited number of actuators the considered systems are highly under-actuated. This makes their analysis and control design challenging. A common strategy to handle such systems is a two degree of freedom control structure containing a feed-forward and a feed-back part, see [1], [2] for recent examples. While a simple feed-back controller reacts to unexpected disturbances, an advanced feed-forward part is responsible for highly accurate tracking of a given reference trajectory. In this contribution, we will only focus on the feed-forward part for reference tracking.

Starting in 1995, Fliess et al. [3] coined the concept of flatness, thus achieving a new milestone for the feed-forward control design of nonlinear systems. Flat systems offer the possibility of a purely algebraic inversion-based control design [4], [5]. The concept of differential flatness has been extended for infinite-dimensional systems including several mechanical structures, e.g., [6]. Knüppel and Woittennek [7] designed a feed-forward controller for a nonlinear string based on the theory of flatness and the method of characteristics. In the case of non-flat systems the feed-forward control design is more difficult and we have to distinguish between minimum and non-minimum phase systems [8]. Since these system classes contain an internal dynamics their inversion usually involves solving a two-point boundary value problem. Chen and Paden [9] presented a stable inversion of nonlinear non-minimum phase systems to generate a bounded solution for the system state and consequently the control input to realize the desired output trajectory with pre- and post-actuation phases. Taylor and Li [10] introduced finite difference methods for the stable inversion of nonlinear systems. In order to obtain a stable inversion without pre- and post-actuation phase, Graichen et al. [11] modified the boundary value problem. Besides inversion-based feed-forward control one can also design an optimal trajectory tracking controller, see [12] for a survey on numerical methods for optimal control.

Blajer and Kołodziejczyk [13] introduced the servo-constraint framework forming a set of differential algebraic equations for under-actuated mechanical systems. Their work had a huge influence on the multibody system dynamics community and motivated several research articles [14]. In general, these articles focus either on flat, minimum or non-minimum phase systems. E.g., Otto and Seifried [15] applied the servo-constraint framework to a flat crane system for real-time trajectory control. Otto and Seifried [16] demonstrated the challenges of servo-constraints for systems with a high differential index. Ströhle and Betsch [17] solved the inverse dynamics of geometrically exact strings using servo-constraints and a space-time finite element discretization. Brüls et al. [18] extended the approach of Chen and Paden [9] to the servo-constraint framework. In order to simplify the control design for non-minimum phase systems, Drücker and Seifried [19] approximated the original boundary value problem. Bastos et al. [20] formulated an optimization problem using servo-constraints for solving the inverse dynamics. Bastos et al. [21] also showed that their optimization problem converges to the original two-point boundary value problem of Brüls et al. [18] as the pre- and post-actuation phase goes to infinity. An analysis of alternative cost functionals is given in [22].

To the best of our knowledge, flatness-based approaches have commonly been used for the control of strings. These were mostly based on either infinite-dimensional or lumped mass systems, e.g., [23], [7], [17]. The spatial Galerkin approximation of a geometrically exact string can generate a non-minimum phase system with many degrees of freedom, for which the mentioned approaches of inversion-based feed-forward control design remain elaborate and non-trivial tasks.

The intention of our contribution is to show the design of a feed-forward controller, which

- can be applied for large scale structural mechanical (non-minimum phase) systems,
- does not require the explicit analysis of a semi-discrete

[1]Technical University of Munich, TUM School of Engineering and Design, Chair of Automatic Control, 85748 Germany (e-mail: {tobias.thoma, kotyczka}@tum.de)

system and its internal dynamics,
- can be easily implemented with commercial or open source finite element packages.

We achieve this by formulating an optimization problem to track the desired reference trajectory on a sufficiently large time interval (containing pre- and post-actuation), expressing the necessary stationarity conditions in variational form in space and time, and coding them in a finite element software. Using space-time finite elements, the optimal feed-forward controller is obtained from the solution of a set of algebraic equations. Due to the special form of our variational formulation an explicit discretization of the velocities is not required. A similar approach for the linear wave equation is given in [24].

The paper is organized as follows. In Section II, we recall the theory of continuum mechanics for geometrically exact strings and a corresponding Galerkin approximation with finite elements. Afterwards, we define the overall problem and focus on the feed-forward control design in Section III. This includes the variational formulation and its discretization. In Section IV, we test our approach with a numerical example and Section V concludes the contribution with an outlook.

II. Geometrically exact strings

In this section, we recall the basic equations of geometrically exact strings and their spatial finite element approximation as a starting point for the formulation of our approach. The interested reader is referred to [25], [26] for more information.

A. Problem description

In the following, we consider the one-dimensional reference configuration $\Omega_0 = [0, L] \subset \mathbb{R}^d,\ d = 1, 2, 3$. The position of each particle in the reference configuration is described by the arc length coordinate $s = X_1 \in \mathbb{R}$. The momentum balance of a string is given by

$$\rho(s)A(s)\partial_t^2 r(s,t) = \partial_s n(s,t) + b(s,t) \quad \text{in } \Omega_0, \tag{1}$$

where the position vector $r(s,t)$ describes the motion or actual configuration of the string, see Figure 1. As usual $\rho(s)$ represents the density, $A(s)$ the cross-sectional area, $b(s,t)$ body forces, and $n(s,t)$ the normal force.

Assumption 1: In the present work, we use the simple nonlinear hyperelastic constitutive equation

$$n(s,t) = EA(1 - ||\partial_s r(s,t)||^{-1})\partial_s r(s,t), \tag{2}$$

where E represents the Young's modulus. More precise constitutive laws are given in the literature, see [17].

In order to complete the system description, we apply the boundary conditions

$$\begin{aligned} n(0,t) &= -u(t), \\ n(L,t) &= 0, \end{aligned} \tag{3}$$

where $u(t)$ denotes the control input or actuating force vector. This force should transfer the string from an initial configuration at time t_i,

$$\begin{aligned} r(s,t_i) &= r_i(s), \\ \partial_t r(s,t_i) &= v_i(s), \end{aligned} \tag{4}$$

to a final one at the end time t_e,

$$\begin{aligned} r(s,t_e) &= r_e(s), \\ \partial_t r(s,t_e) &= v_e(s), \end{aligned} \tag{5}$$

whereby the end of the string

$$y(t) = r(L,t) \tag{6}$$

should follow a desired trajectory $y_d(t)$ as closely as possible. Before we continue with this task in Section III, we show how to set up the finite-dimensional state space model.

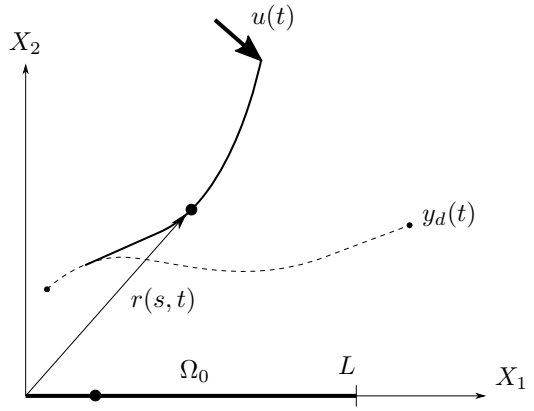

Fig. 1. Reference and actual configuration on $\mathbb{R}^2$.

B. Weak formulation

For ease of notation, we introduce

$$\langle a, b \rangle_M = \int_M a \odot b \, \mathrm{d}s$$

for the integration of products of scalar and vector valued functions over some domain M. As a next step, we recall an appropriate weak form of equation (1). By testing (1) and integrating by parts, one can see that any sufficiently regular solution of (1) under the boundary conditions (3) is characterized by the variational single-field (displacement) formulation

$$\langle \rho A \partial_t^2 r, w \rangle_{\Omega_0} = -\langle n, \partial_s w \rangle_{\Omega_0} + \langle b, w \rangle_{\Omega_0} + uw|_{s=0}, \tag{7}$$

$\forall w \in H^1(\Omega_0),\ t \geq 0$.

C. Spatial discretization

In order to obtain a spatial approximation of above weak formulation, we have to find the approximation $r_h \in V_h \subset H^1(\Omega_0)$ solving the discretized weak form

$$\langle \rho A \partial_t^2 r_h, w_h \rangle_{\Omega_0} = -\langle n, \partial_s w_h \rangle_{\Omega_0} + \langle b, w_h \rangle_{\Omega_0} + uw_h|_{s=0}, \tag{8}$$

$\forall w_h \in V_h$, and $t \geq 0$, where w_h represents the discretized test function and V_h an appropriate finite dimensional subspace, e.g. a standard finite element space. Accordingly,

this discretization process leads to a system of ordinary differential equations of the form[1]

$$\mathrm{M}\ddot{\mathrm{r}} = -\mathrm{k}(\mathrm{r}) + \mathrm{b} + \mathrm{G}\mathrm{u}, \tag{9}$$

where r and $\dot{\mathrm{r}}$ denote the vector representations of the discretized functions. Projecting the initial conditions (4) and final ones (5) on these vector representations, gives us

$$\begin{array}{lll} \mathrm{r}(t_i) & = \mathrm{r}_i, & \mathrm{r}(t_e) = \mathrm{r}_e, \\ \dot{\mathrm{r}}(t_i) & = \mathrm{v}_i, & \dot{\mathrm{r}}(t_e) = \mathrm{v}_e. \end{array} \tag{10}$$

In order to complete the state space representation (9) with regard to the above task, we use the corresponding output

$$\mathrm{y} = r_h(L,t) = \mathrm{C}\mathrm{r}. \tag{11}$$

Remark 1: In order to solve an initial boundary value problem, an appropriate time-stepping scheme can be used to integrate the semi-discrete equation (9) in time. In the following, we will call this process a time-marching simulation. More information regarding this can be found in the Appendix.

III. Optimal trajectory feed-forward control design

In this section, we start with the cost functional to obtain an optimal feed-forward controller for the semi-discrete model, and cast it in terms of inner products on a space-time domain. We derive the corresponding variational identities, which, with appropriate Galerkin approximation in time, can be immediately implemented as a space-time finite element problem in available software.

Problem 1: Among all vectors $\mathrm{r}(t)$, $\mathrm{u}(t)$ that fulfill (9) and the boundary conditions (10) find those that minimize the cost function

$$\tilde{J} = \int_{t_i}^{t_e} \left(\frac{1}{2}\mathrm{u}^\top \mathrm{u} + \frac{\alpha}{2}(\mathrm{C}\mathrm{r} - \mathrm{y}_d)^\top (\mathrm{C}\mathrm{r} - \mathrm{y}_d) \right) \mathrm{d}t \tag{12}$$

with a factor $\alpha \in \mathbb{R}^{>0}$ penalizing the trajectory error compared to a quadratic input regularization term.

A. Lagrange functional

We now consider a rectangular space-time domain $\Omega = \Omega_0 \times T$, where $T = [t_i, t_e]$ is a sufficiently large time interval for possible phases of pre- and post-actuation, see Figure 2. To account for the system dynamics, we can define the Lagrange functional

$$\begin{aligned} J \quad &= \tfrac{1}{2}\langle u, u\rangle_{\Gamma_u} + \tfrac{\alpha}{2}\langle r_h - y_d, r_h - y_d\rangle_{\Gamma_y} \\ &\quad -\langle \partial_s w_h, n\rangle_\Omega + \langle w_h, b - \rho A \partial_t^2 r_h\rangle_\Omega + \langle w_h, u\rangle_{\Gamma_u} \end{aligned} \tag{13}$$

containing the Lagrange multiplier $w_h \in V_h(\Omega_0) \otimes H^1(T)$.

[1]The nonlinearity in $\mathrm{k}(\mathrm{r})$ results from the nonlinear character of (2).

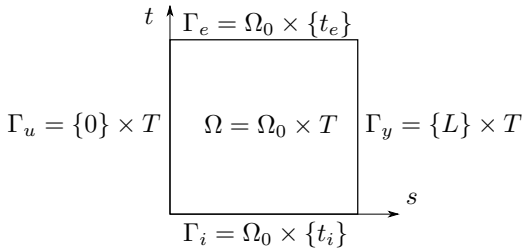

Fig. 2. Space-time domain.

B. Variational identities

As a next step, we derive the variational identities which will be approximated in the following section.

Lemma 1: Let (r_h, u, w_h) be a sufficiently regular solution for Problem 1 minimizing (13). Then the variational identities

$$\begin{aligned} &\langle \delta u, u + w_h\rangle_{\Gamma_u} = 0, \\ &\langle \partial_t \delta w_h, \rho A \partial_t r_h\rangle_\Omega - \langle \partial_s \delta w_h, n\rangle_\Omega + \langle \delta w_h, b\rangle_\Omega \\ &\qquad + \langle \delta w_h, v_i\rangle_{\Gamma_i} - \langle \delta w_h, v_e\rangle_{\Gamma_e} + \langle \delta w_h, u\rangle_{\Gamma_u} = 0, \\ &\langle \partial_t \delta r_h, \rho A \partial_t w_h\rangle_\Omega - \langle \partial_s \delta r_h, \nabla_{\partial_s r} n \cdot \partial_s w_h\rangle_\Omega \\ &\qquad + \alpha \langle \delta r_h, r_h - y_d\rangle_{\Gamma_y} = 0, \end{aligned} \tag{14}$$

hold for all regular test functions $\delta r_h \in \mathcal{R}$, $\delta w_h \in \mathcal{W}$, and $\delta u \in \mathcal{U}$ with

$$\mathcal{W} = V_h(\Omega_0) \otimes H^1(T), \tag{15}$$

$$\mathcal{R} = \{\delta r_h \in \mathcal{W} \mid \delta r_h(s, t_i) = 0,\ \delta r_h(s, t_e) = 0\}, \tag{16}$$

$$\mathcal{U} = H^1(T). \tag{17}$$

Proof: By considering the variational derivative of (13) and setting it to zero, one can see that

$$\begin{aligned} \delta J \quad &= \langle \delta u, u + w_h\rangle_{\Gamma_u} \\ &\quad -\langle \partial_s \delta w_h, n\rangle_\Omega + \langle \delta w_h, b\rangle_\Omega - \underbrace{\langle \delta w_h, \rho A \partial_t^2 r_h\rangle_\Omega}_{(*)} \\ &\quad -\langle \partial_s \delta r_h, \nabla_{\partial_s r} n \cdot \partial_s w_h\rangle_\Omega - \underbrace{\langle \partial_t^2 \delta r_h, \rho A w_h\rangle_\Omega}_{(**)} \\ &\quad +\alpha \langle \delta r_h, r_h - y_d\rangle_{\Gamma_y} + \langle \delta w_h, u\rangle_{\Gamma_u} = 0. \end{aligned} \tag{18}$$

Integration by parts of $(*)$ leads to

$$\begin{aligned} (*) \quad &= -\langle \partial_t \delta w_h, \rho A \partial_t r_h\rangle_\Omega \\ &\qquad -\langle \delta w_h, \rho A v_i\rangle_{\Gamma_i} + \langle \delta w_h, \rho A v_e\rangle_{\Gamma_e}, \end{aligned} \tag{19}$$

where the corresponding velocity boundary conditions are already substituted. Integration by parts of $(**)$ gives us

$$\begin{aligned} (**) \quad &= -\langle \partial_t \delta r_h, \rho A \partial_t w_h\rangle_\Omega \\ &\qquad -\langle \partial_t \delta r_h, \rho A w_h\rangle_{\Gamma_i} + \langle \partial_t \delta r_h, \rho w_h\rangle_{\Gamma_e}. \end{aligned} \tag{20}$$

Due to the fixed boundary conditions (10), δr_h can not be varied at the boundaries Γ_i, Γ_e, which makes the boundary terms in (20) vanish. ■

C. Time discretization

For the discretization in time, we likewise use a Galerkin approximation of the variational identities (14). As indicated in the introduction, we use standard finite element spaces for the approximation.

Proposition 1: By defining

$$\mathcal{W}_t \subset \mathcal{W},\ \mathcal{R}_t \subset \mathcal{R},\ \text{and}\ \mathcal{U}_t \subset \mathcal{U}$$

as appropriate finite dimensional subspaces, we can search for an approximation $(u_t, w_{h_t}) \in \mathcal{U}_t \times \mathcal{W}_t$, and

$$r_{h_t} \in \{r_{h_t} \in \mathcal{W}_t \mid r_{h_t}(s,t_i) = r_i,\ r_{h_t}(s,t_e) = r_e\}$$

for the solution of our problem satisfying the discretized identities

$$\begin{aligned}
&\langle \delta u_t, u_t + w_{h_t}\rangle_{\Gamma_u} = 0,\\
&\langle \partial_t \delta w_{h_t}, \rho A \partial_t r_{h_t}\rangle_\Omega - \langle \partial_s \delta w_{h_t}, n\rangle_\Omega + \langle \delta w_{h_t}, b\rangle_\Omega\\
&\qquad + \langle \delta w_{h_t}, v_i\rangle_{\Gamma_i} - \langle \delta w_{h_t}, v_e\rangle_{\Gamma_e} + \langle \delta w_{h_t}, u_t\rangle_{\Gamma_u} = 0,\\
&\langle \partial_t \delta r_{h_t}, \rho A \partial_t w_{h_t}\rangle_\Omega - \langle \partial_s \delta r_{h_t}, \nabla_{\partial_s r} n \cdot \partial_s w_{h_t}\rangle_\Omega\\
&\qquad + \alpha \langle \delta r_{h_t}, r_{h_t} - y_d\rangle_{\Gamma_y} = 0,
\end{aligned} \tag{21}$$

for all $(\delta u_t, \delta r_{h_t}, \delta w_{h_t}) \in \mathcal{U}_t \times \mathcal{R}_t \times \mathcal{W}_t$.

Remark 2: Testing (21) with $\delta u_t = \delta w_{h_t}|_{\Gamma_u} \in \mathcal{W}_t|_{\Gamma_u}$ allows us to eliminate the first line of (21) and use $\langle \delta w_{h_t}, u_t\rangle_{\Gamma_u} = -\langle \delta w_{h_t}, w_{h_t}\rangle_{\Gamma_u}$ in the second line of (21). This reduces the amount of equations for the discretization process.

Since we use bilinear basis functions of s and t, our approximated computational domain represents a structured mesh with rectangular shaped space-time finite elements. The mesh is spanned by n_s cells in s-direction and n_t cells in t-direction, leading to $n_s \times n_t$ space-time finite elements.

D. Discussion

Our result from the space-time finite element perspective can be related to works based on semi-discrete models and the time integration with special time finite elements. Since we assume that the space of w_h consists of tensor products of bilinear functions of s and t, e.g. $w_h(s,t) = \phi(s)\mathrm{w}(t)$, the above Lagrange functional can be rewritten as

$$\begin{aligned}
J \quad &= \tfrac{1}{2}\langle \mathrm{u}, \mathrm{u}\rangle_T + \tfrac{\alpha}{2}\langle \mathrm{Cr} - \mathrm{y}, \mathrm{Cr} - \mathrm{y}\rangle_T\\
&\quad + \langle \mathrm{w}, -\mathrm{M}\ddot{\mathrm{r}} - \mathrm{k}(\mathrm{r}) + \mathrm{b} + \mathrm{Gu}\rangle_T,
\end{aligned} \tag{22}$$

which can also be found in the work of Altmann and Heiland [22]. Using the Euler-Lagrange equation, we can derive the optimality conditions

$$\begin{aligned}
\mathrm{u} \quad &= -\mathrm{G}^\top \mathrm{w},\\
\mathrm{M}\ddot{\mathrm{r}} \quad &= -\mathrm{k}(\mathrm{r}) + \mathrm{b} + \mathrm{Gu},\\
\mathrm{M}\ddot{\mathrm{w}} \quad &= -\nabla_{\mathrm{r}}\mathrm{k}(\mathrm{r})\mathrm{w} + (\mathrm{Cr} - \mathrm{y}_d)\alpha.
\end{aligned} \tag{23}$$

In case of

$$\mathcal{W}_t = [V_h(\Omega_0) \otimes P_1(T)] \cap H^1(\Omega)$$

the approximation of the variational identities[2] corresponds to a multiple-shooting method [12], where the optimality conditions (23) are integrated via a special (unbiased displacement-continuous, velocity-discontinuous) time finite element scheme [27].

[2] P_1 denotes the standard finite element space of continuous first-order Lagrange polynomials.

IV. Numerical test

To demonstrate the performance of the above control design approach, we now provide some numerical results.

A. Model scenario

We consider a planar motion of a geometrically exact string under gravity. The suspended rope performs a finite-time transition between two stationary set-points, with the end of the string following the desired trajectory

$$y_d(t) = \begin{bmatrix}1\\1\end{bmatrix}\psi(t) \tag{24}$$

with

$$\psi(t) = \begin{cases} 0, & t \le \Delta t,\\ 3\left(\frac{t-\Delta t}{\Delta t}\right)^2 - 2\left(\frac{t-\Delta t}{\Delta t}\right)^3, & \Delta t < t \le 2\Delta t,\\ 1, & t > 2\Delta t. \end{cases} \tag{25}$$

Remark 3: Since (1) has a hyperbolic character the traveling time of information depends on the wave propagation speed. Therefore, $y(t)$ requires a pre- and post actuation phase Δt larger than the traveling time of a wave between $s = 0$ and $s = L$ for steering the string from one steady-state to another one. This is especially relevant for flatness based control [7]. A pre- and post-actuation phase in $y_d(t)$ allows us to approximate the inverse solution similar to [21]. Consequently, $y(t)$ follows $y_d(t)$ almost exactly, see also Figure 5.

The initial set point at time $t_i = 0$ results from solving the equilibrium problem of (9) where $V_h = P_1(\Omega_0) \cap H^1(\Omega_0)$ and $r(0,t) \equiv 0$. Therefore, $n_s = 10$ equidistant finite elements were used. The final set-point at time $t_e = 6$ corresponds to the initial one except that the positional arguments are shifted by one in both directions. The remaining parameters[3] of the experiment are given in Table I.

TABLE I
PARAMETERS

L	ρ	EA	g	Δt	α
1	1	1	9.81	2	100

B. Details on the computational approximation process

Since we use a finite element method for the space-time discretization, the computational domain is partitioned into 10×100 uniform rectangles. The trial functions of (21) are generated via continuous Lagrangian shape functions of first order what leads to the approximation spaces

$$\mathcal{W}_t = [P_1(\Omega_0) \otimes P_1(T)] \cap H^1(\Omega), \qquad \mathcal{U}_t = \mathcal{W}_t|_{\Gamma_u}.$$

The following computational results are generated with the finite element framework FEniCSx [28], [29], [30], [31].

[3] Since this is a purely academic example, no units are used.

C. Numerical results

Solving (21) according to the above details, we generate several illustrations. E.g., Figure 3 shows the position field $r(s,t)$ in X_1-direction and the finite element mesh. The components of the corresponding input force vector $u(t)$ are given in Figure 4. To verify our results we apply the generated input $u(t)$ to a time-marching simulation. It uses an implicit midpoint rule for the time integration and the time step size $\tau = 0.06$. Further information on the time-marching simulation is given in the Appendix. In Figure 5, the resulting output $y(t)$ in X_1-direction is presented[4]. In order get an impression of the overall motion, Figure 6 shows several snapshots of the string configuration which also result from the time-marching simulation.

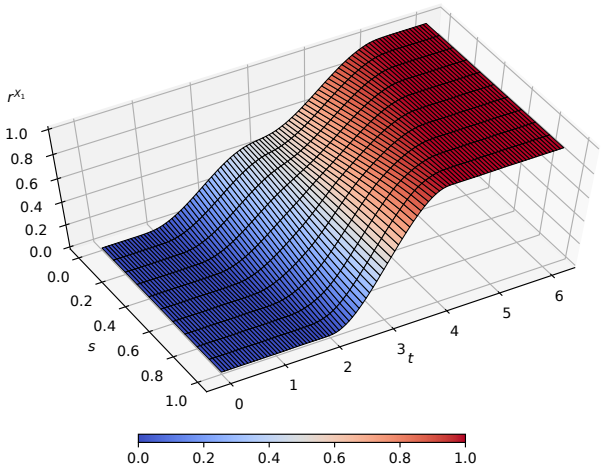

Fig. 3. Numerical solution of $r(s,t)$ in X_1-direction.

V. Conclusion

We presented how to generate an optimal trajectory feed-forward controller for geometrically exact strings exploiting a space-time variational formulation of the problem. The big advantage of this approach, which is related to corresponding formulations for semi-discretized models and the solution of their two-point boundary value problems, is the ease of implementation in commercial or free finite element software, in conjunction with the efficient solution of the resulting algebraic system of equations.

In future research, we might extend the control design to three-dimensional systems. This goes hand in hand with a more complex implementation using tensor products if the favored finite element toolbox is not compatible with four-dimensional meshes. Moreover, the challenges or advantages of unstructured space-time finite element meshes or other Galerkin approximation methods have not been discussed yet. Additionally, we want to extend the feed-forward control design to other cost functionals. Consequently, and depending on its real-time capability, the presented control design might also be relevant for model predictive control.

[4]Figure 4 and 5 also contain the solutions for lower values of α to illustrate the increased deviation from the desired trajectory if it is less penalized in the quadratic cost functional.

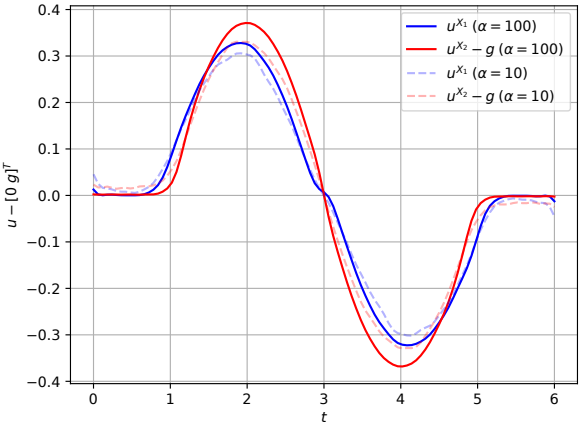

Fig. 4. Numerical solution of $u(t)$. In order to present the input force in X_1-direction and the one in X_2-direction in the same diagram, we subtract the gravitational portion.

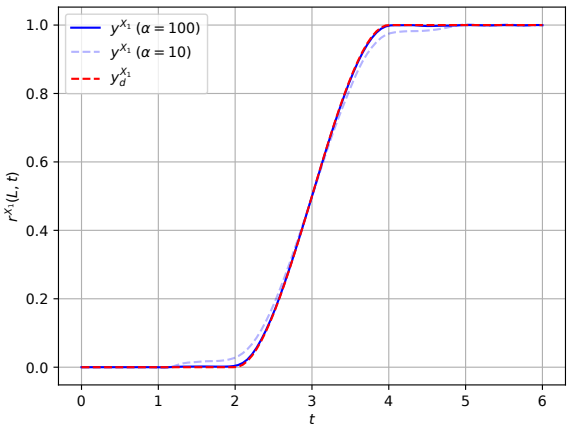

Fig. 5. Actual output $y(t)$ compared with $y_d(t)$. In the case of a large α, $y(t)$ is close to $y_d(t)$. The results in X_2-direction are similar and omitted for the sake of clarity.

Appendix

In this contribution, the numerical time integration of (9) is called a time-marching simulation; e.g., in Section IV we applied an implicit midpoint rule. Therefore, we introduce the velocity $\mathrm{v} = \dot{\mathrm{r}}$ to rewrite (9) as a first order system $\dot{\mathrm{x}} = \mathrm{f}(\mathrm{x},\mathrm{u})$ with $\mathrm{x}^\top = [\mathrm{r}^\top\ \mathrm{v}^\top]$; and define

$$d_\tau \mathrm{x} = \tau^{-1}(\mathrm{x}^{n+1} - \mathrm{x}^n), \quad \text{and} \quad \mathrm{x}^{n+\frac{1}{2}} = 2^{-1}(\mathrm{x}^{n+1} + \mathrm{x}^n),$$

where τ is a fixed time step size and $t^n = n\tau$, $n \geq 0$ the discrete time step. We now use

$$d_\tau \mathrm{x} = \mathrm{f}(\mathrm{x}^{n+\frac{1}{2}}, \mathrm{u}^{n+\frac{1}{2}})$$

to obtain $\mathrm{x}^{n+1} \approx \mathrm{x}(t^{n+1})$ at the next time step t^{n+1}.

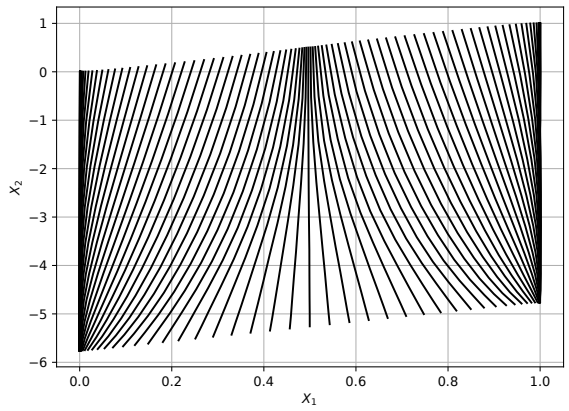

Fig. 6. Snapshots at different time steps starting from the left with the initial string configuration at time $t = t_i$ and ending in the final one ($t = t_e$) on the right.

ACKNOWLEDGMENT

The authors would like to thank Tengman Wang, Levent Ögretmen, and Philipp L. Kinon for insightful discussions. The support by the DFH-UFA French-German doctoral college "Port-Hamiltonian Systems: Modeling, Numerics and Control" is gratefully acknowledged.

REFERENCES

[1] M. Wang and P. Kotyczka, "Trajectory control of an elastic beam based on port-Hamiltonian numerical models," *at - Automatisierungstechnik*, vol. 69, no. 6, pp. 457–471, 2021.

[2] M. Morlock, M. Burkhardt, R. Seifried, and P. Eberhard, "End-effector trajectory tracking of flexible link parallel robots using servo constraints," *Multibody System Dynamics*, vol. 56, no. 1, pp. 1–28, 2022.

[3] M. Fliess, J. Lévine, P. Martin, and P. Rouchon, "Flatness and defect of non-linear systems: Introductory theory and examples," *International Journal of Control*, vol. 61, no. 6, pp. 1327–1361, 1995.

[4] R. Rothfuß, J. Rudolph, and M. Zeitz, "Flachheit: Ein neuer Zugang zur Steuerung und Regelung nichtlinearer Systeme," *auto*, vol. 45, no. 11, pp. 517–525, 1997.

[5] V. Hagenmeyer and M. Zeitz, "Flachheitsbasierter Entwurf von linearen und nichtlinearen Vorsteuerungen (Flatness-based design of linear and nonlinear feedforward controls)," *at - Automatisierungstechnik*, vol. 52, no. 1, pp. 3–12, 2004.

[6] N. Petit and P. Rouchon, "Flatness of heavy chain systems," *SIAM Journal on Control and Optimization*, vol. 40, no. 2, pp. 475–495, 2001.

[7] T. Knüppel and F. Woittennek, "Flatness based control design for a nonlinear heavy chain model," *IFAC Proceedings Volumes*, vol. 43, no. 14, pp. 701–706, 2010.

[8] H. Khalil, *Nonlinear Control*, ser. Always Learning. Pearson, 2014.

[9] D. Chen and B. Paden, "Stable inversion of nonlinear non-minimum phase systems," *International Journal of Control*, vol. 64, no. 1, pp. 81–97, 1996.

[10] D. Taylor and S. Li, "Stable inversion of continuous-time nonlinear systems by finite-difference methods," *IEEE Transactions on Automatic Control*, vol. 47, no. 3, pp. 537–542, 2002.

[11] K. Graichen, V. Hagenmeyer, and M. Zeitz, "A new approach to inversion-based feedforward control design for nonlinear systems," *Automatica*, vol. 41, no. 12, pp. 2033–2041, 2005.

[12] A. Rao, "A survey of numerical methods for optimal control," *Advances in the Astronautical Sciences*, vol. 135, 2010.

[13] W. Blajer and K. Kołodziejczyk, "A geometric approach to solving problems of control constraints: Theory and a dae framework," *Multibody System Dynamics*, vol. 11, no. 4, pp. 343–364, 2004.

[14] S. Drücker and R. Seifried, "Trajectory-tracking control from a multibody system dynamics perspective," *Multibody System Dynamics*, vol. 58, no. 3–4, pp. 341–363, 2023.

[15] S. Otto and R. Seifried, "Real-time trajectory control of an overhead crane using servo-constraints," *Multibody System Dynamics*, vol. 42, no. 1, pp. 1–17, 2017.

[16] S. Otto and R. Seifried, *Open-Loop Control of Underactuated Mechanical Systems Using Servo-Constraints: Analysis and Some Examples*. Springer International Publishing, 2018, pp. 81–122.

[17] T. Ströhle and P. Betsch, "A simultaneous space-time discretization approach to the inverse dynamics of geometrically exact strings," *International Journal for Numerical Methods in Engineering*, vol. 123, no. 11, pp. 2573–2609, 2022.

[18] O. Brüls, G. J. Bastos, and R. Seifried, "A stable inversion method for feedforward control of constrained flexible multibody systems," *Journal of Computational and Nonlinear Dynamics*, vol. 9, no. 1, 2013.

[19] S. Drücker and R. Seifried, "Application of stable inversion to flexible manipulators modeled by the absolute nodal coordinate formulation," *GAMM-Mitteilungen*, vol. 46, no. 1, 2023.

[20] G. Bastos, R. Seifried, and O. Brüls, "Inverse dynamics of serial and parallel underactuated multibody systems using a dae optimal control approach," *Multibody System Dynamics*, vol. 30, no. 3, pp. 359–376, 2013.

[21] G. Bastos, R. Seifried, and O. Brüls, "Analysis of stable model inversion methods for constrained underactuated mechanical systems," *Mechanism and Machine Theory*, vol. 111, pp. 99–117, 2017.

[22] R. Altmann and J. Heiland, "Simulation of multibody systems with servo constraints through optimal control," *Multibody System Dynamics*, vol. 40, no. 1, pp. 75–98, 2016.

[23] R. M. Murray, "Trajectory generation for a towed cable system using differential flatness," *IFAC Proceedings Volumes*, vol. 29, no. 1, pp. 2792–2797, 1996.

[24] U. Langer, R. Löscher, O. Steinbach, and H. Yang, "Robust finite element solvers for distributed hyperbolic optimal control problems," *Computers amp; Mathematics with Applications*, vol. 180, pp. 166–190, 2025.

[25] S. S. Antman, *Nonlinear Problems of Elasticity*. Springer New York, 1995.

[26] J. Bonet and R. D. Wood, *Nonlinear Continuum Mechanics for Finite Element Analysis*. Cambridge University Press, 2008.

[27] O. A. Bauchau, "The finite element method in time for multibody dynamics," *Journal of Computational and Nonlinear Dynamics*, vol. 19, no. 7, 2024.

[28] I. A. Baratta, J. P. Dean, J. S. Dokken, M. Habera, J. S. Hale, C. N. Richardson, M. E. Rognes, M. W. Scroggs, N. Sime, and G. N. Wells, "Dolfinx: The next generation fenics problem solving environment," 2023.

[29] M. W. Scroggs, I. A. Baratta, C. N. Richardson, and G. N. Wells, "Basix: A runtime finite element basis evaluation library," *Journal of Open Source Software*, vol. 7, no. 73, p. 3982, 2022.

[30] M. W. Scroggs, J. S. Dokken, C. N. Richardson, and G. N. Wells, "Construction of arbitrary order finite element degree-of-freedom maps on polygonal and polyhedral cell meshes," *ACM Transactions on Mathematical Software*, vol. 48, no. 2, pp. 1–23, 2022.

[31] M. S. Alnæs, A. Logg, K. B. Ølgaard, M. E. Rognes, and G. N. Wells, "Unified form language: A domain-specific language for weak formulations of partial differential equations," *ACM Transactions on Mathematical Software*, vol. 40, no. 2, pp. 1–37, 2014.